63-4-1

RADC—TDR—63—127

Copy No. 17 of 50 Copies

March 12, 1963

PSEUDO RANDOM ARRAY INVESTIGATION

by

J. W. Sherman M. I. Skolnik

Final Report

Contract AF 30(602)–2626

ECI ONIC UNICATIONS INC.

HOME OFFICE—ST. PETERSBURG, FLORIDA

Prepared
for
Rome Air Development Center
Air Force Systems Command
United States Air Force
Griffiss Air Force Base
New York

RESEARCH DIVISION
1830 YORK ROAD
TIMONIUM, MARYLAND

PATENT NOTICE

When Government drawings, specifications, or other data are used for any purpose other than in connection with a definitely related Government procurement operation, the United States Government thereby incurs no responsibility nor any obligation whatsoever and the fact that the Government may have formulated, furnished, or in any way supplied the said drawings, specifications or other data is not to be regarded by implication or otherwise as in any manner licensing the holder or any other person or corporation, or conveying any rights or permission to manufacture, use, or sell any patented invention that may in any way be related thereto.

ASTIA NOTICE

Qualified requestors may obtain copies of this report from the ASTIA Document Service Center, Arlington Hall Station, Arlington 12, Virginia. ASTIA Services for the Department of Defense contractors are available through the "Field of Interest Register" on a "need-to-know" certified by the cognizant military agency of their project or contract.

OTS NOTICE

This report has been released to the Office of Technical Services, U.S. Department of Commerce, Washington 25, D.C., for sale to the general public.

RADC—TDR—63—127

March 12, 1963

PSEUDO RANDOM ARRAY INVESTIGATION

by

J. W. Sherman

M. I. Skolnik

Final Report

Contract AF 30(602)—2626

Project No. 4506

Task No. 450604

HOME OFFICE—ST. PETERSBURG, FLORIDA

Prepared
for
Rome Air Development Center
Air Force Systems Command
United States Air Force
Griffiss Air Force Base
New York

RESEARCH DIVISION
1830 YORK ROAD
TIMONIUM, MARYLAND

FOREWORD

Increased requirements of modern radars in the areas of transmitted power, scanning ability and resolution have led to the utilization of arrays of radiating elements as antennas. However, due to the high performance in angular resolution and gain, arrays envisaged have become exceedingly large, containing many elements and associated circuitry. To reduce the costs of these arrays, methods of retaining radar performances with a minimum number of radiating elements have become essential. The number of elements in a conventional (half-wavelength) equally spaced array can be substantially reduced if unequal spacing is employed between elements.

This effort was initiated to investigate a firm mathematical approach to the non-uniform spacing problem. The approach was to be of a statistical nature and applicable to large (10,000 to 50,000 element) planar arrays The technical development of this effort was to provide element selection rules which would be applicable to thinning (as much as 90%) conventional planar arrays and yet maintain the antenna performances associated with conventional arrays of the same physical dimensions.

The contractor was successful in establishing a statistical approach to the spacing problem. He was successful in describing an array in statistical terms which allowed for a firm mathematical solution of element positions. Model arrays with 30%, 50%, 70%, and 90% thinning were analyzed and it is concluded that the statistical approach will provide a thinned-out array capable of achieving side lobes in the order of -24 db for a 10,000 element conventional array.

The contractor also offers a straight-forward technique for designing thinned arrays with acceptable sidelobes. This approach takes advantage of the natural thinning involved when an array is composed of concentric rings with equal spacings and equiangular radials. Further, density taper was employed on a ring array and the computed results were in close agreement with the theoretical main beam and side lobe performance. The contractor discusses another approach whereby a technique called Dynamic Programming provides a computer solution to the non-uniform array solution. The technique was employed on linear arrays and the results are very encouraging and should be further investigated.

The usefulness of this effort is represented by the fact that thinned out arrays can now be designed by other than "trial and error" methods Guide lines and design criteria are made available whereby the theory of non-uniformly spaced arrays is placed on a rather firm mathematical foundation. It is felt that this study is beneficial in that now thinned arrays can be designed to meet low side lobes, and main beam and scanning performances with some degree of assurance. This can represent a substantial economic savings to the USAF since a reduced number of radiating elements relieves some of the complexity and costs of large

conventional arrays. The mathematical foundation developed in this study will help in bringing a degree of predictability to the limitation and advantages of thinned out arrays.

John A. Potenza
RADC Project Engineer

ACKNOWLEDGEMENTS

The following have made major contributions to this report and to the success of this project.

B. Z. Hollman	Sections 3 and 6
L. C. Kefauver	Section 5
T. A. Kehoe	Section 9
M. J. King	Section 7
G. Nemhauser*	Section 5
F. C. Ogg*	Section 3
R. F. Packard	Sections 4 and 9
J. D. Rodgers	Section 9
W. A. Visher	Section 9
G. Washnitzer*	Section 7

The Rome Air Development Center Contract Technical Monitor was John Potenza.

J. W. Sherman
M. I. Skolnik

*Consultants

ABSTRACT

This final report describes an investigation of thinned array antennas with unequally spaced elements. Several approaches to array design have been explored and guide lines established for designing arrays. The design techniques reported here include statistically designed density-tapered arrays, ring arrays, and the application of dynamic programming to array theory. The statistical analysis of arrays, the investigation of arrays from an energy concept and number theory have been used to predict average and peak sidelobe levels of antenna arrays in which elements have been removed. The techniques of thinning arrays 50, 70, and 90 percent have been verified by pattern measurements of several model antennas.

TABLE OF CONTENTS

TABLE OF CONTENTS (Continued)

LIST OF ILLUSTRATIONS

LIST OF ILLUSTRATIONS (Cont'd)

LIST OF ILLUSTRATIONS (Cont'd)

LIST OF ILLUSTRATIONS (Cont'd)

LIST OF TABLES

1. INTRODUCTION AND SUMMARY

This technical report describes a study and investigation of the design of thinned array antennas with unequal spacings between elements. The purpose of this investigation was to provide a better understanding of the application of unequally spaced arrays in antenna technology and to establish a set of design guide-lines. The investigation was directed primarily to the thinning-out of large conventional planar arrays with 10,000 or more elements with up to 90% of the elements removed.

Several thinning techniques were investigated. The technique of major interest was the probabilistic or statistical approach discussed in Section 3 whereby the amplitude taper of a conventional antenna was used as the probability density function for determining whether or not a particular element was to be removed. This is especially applicable to large planar arrays. The necessary design computations are readily programmed for digital computers. The results show this to be a satisfactory design procedure and that it is possible to predict the average pattern behavior from a knowledge of the amplitude distribution used as the model.

A deterministic density-tapered approach was also considered in which elements are spaced within a circular aperture at the intersection of radial lines and concentric rings. The results presented in Section 4 are comparable to those achieved with the statistical designs.

Section 5 describes a slightly different approach to design based on the optimization technique called dynamic programming. This is a computer procedure widely used in Operations Research for efficiently searching for an optimum solution. It is applied here to linear arrays of 25 elements. The results obtained were found to be better than those achieved with other techniques and were quite encouraging.

Various other techniques were explored. These are summarized in Section 6. Some seem to offer some promise but others were found to lead to no success.

An application of a theorem from number theory is described in Section 7 for obtaining an analytical expression for an upper bound to the sidelobe level. Although it is an interesting result its applicability seems limited.

Section 8 derives some relationships describing the properties of unequally spaced arrays from an energy point of view.

The theoretical pattern computations obtained by the statistical procedures of Section 3 were experimentally verified using the ECI "Holey Plate" array modeling technique as described in Section 9.

Design guide-lines for the statistical approach, thinning by ring arrays, and dynamic programming are given in their respective sections.

Section 2, however, summarizes the general guide lines for unequally spaced arrays and the areas of applicability of each.

The results presented here indicate that the unequal spacing of array elements is a good procedure for achieving low sidelobe levels in practical arrays with large numbers of elements and where it is not convenient to employ an amplitude taper.

2. GENERAL DESIGN GUIDE-LINES

2.1 Introduction

In the sections of this report that describe specific design techniques (Sections 3, 4, and 5) a brief resume of the design guide lines applicable to each technique is given. This section summarizes the guide lines applicable to the general design of arrays with unequally spaced elements.

It can be shown using either sampling theory or Fourier series analysis that in a filled array with elements equally spaced a half-wavelength apart, there are sufficient degrees of freedom (amplitude and phase at each element) to satisfy the constraints (independent values of the radiation pattern) to perform satisfactory pattern synthesis over the visible region of angular coverage. That is, it is possible to synthesize a pattern to match a desired pattern (in the least mean square sense) by specifying the amplitude and phase at each of the half-wavelength spaced elements. When elements are removed from a filled array of fixed size, there are fewer degrees of freedom but the number of constraints remains unchanged. Thus the resulting radiation pattern cannot be as well controlled.

In many situations it is not necessary to completely control the shape of the radiation pattern so that it may not be necessary to utilize a filled array. The shape of the main beam is controlled primarily by the outer dimensions of the aperture and is little affected by the actual distribution or number of elements. The sidelobe level is, however, heavily influenced by the number of elements contained within the aperture and their distribution. Many antenna specifications simply require that the sidelobe level be below a certain level without further specifying the detailed character of the sidelobes. This is the kind of requirement that can be aptly met by judicious removal of elements.

When contemplating the use of a thinned array it should be kept in mind that the antenna gain and effective receiving area are proportional to the number of elements remaining.

2.2 Applications of Thinned, Unequally Spaced Arrays

The actual design of a particular thinned array and the technique employed will depend in part on the use to which it is put. Some of the possible applications of a thinned array are:

Pattern synthesis In many applications it is necessary to obtain sidelobes lower than the -13.2 db value that is characteristic of a uniform rectangular aperture of equally spaced elements. A well known technique for reducing the sidelobes is to apply an amplitude taper across the aperture. This solution is not always acceptable in a transmitting application where each element has its own transmitter that must be operated at full power for maximum efficiency. The statistical

technique described in Section 3 is well suited for achieving acceptable radiation patterns with a thinned array. In addition to eliminating the need for an amplitude taper, this technique reduces the total number of elements by about half. For this reason, it is also of value in receiving arrays.

Narrow-beam patterns Thinning an array permits the realization of narrow beamwidths with reduced number of elements and with more or less uniform sidelobes. The sidelobe level depends on the number of elements remaining. In general greater numbers of elements would be removed for this application than for the pattern synthesis application mentioned above. Removal of 90% or more of the elements might be typical. Although the beamwidth depends only on the aperture size and not the number of elements remaining, the gain and effective area are dependent on the number of elements. Thus when considering the question of resolution, the signal-to-noise ratio must also be included.

Broadband operation Equally spaced arrays are inherently narrowband if grating lobes can not be tolerated. An array with half-wavelength spacing at the lowest frequency will have greater than half-wavelength spacing at the upper end of the band and may therefore be limited in performance. Thinned arrays with pseudo random spacings offers a means for operating arrays over a wide band of frequencies without significant pattern deterioration, if properly designed.

Wide angle scan An array with unform element spacings greater than half-wavelength can be scanned only over a limited angular sector before grating lobes appear. The same number of unequally spaced elements can provide a much larger angle of scan without the appearance of large spurious lobes. This is related to the problem of broadband operation and is solved in a similar manner.

The thinned unequally spaced array is a useful design procedure that supplements conventional array techniques by performing functions not practical or convenient with other procedures.

2.3 Application of Specific Techniques

This report considers three major techniques for the design of thinned unequally spaced arrays; namely, statistical density taper, ring arrays, and dynamic programming. The first two apply primarily to planar apertures. Dynamic programming is well suited to a linear antenna but has not yet been applied to planar apertures. Each technique has its area of application for which it is best suited.

If the array contains a large number of elements the statistical density taper of Section 3 can be readily employed to obtain the element configuration. It is not practical in most cases to compute the element spacings by hand without the aid of a computer, but it can

be readily programmed for a digital computer if desired. The work involved in computing the radiation pattern is generally too much to be hand calculated conveniently. Some machine technique or model pattern measurement must generally be employed. It is important to examine the resulting radiation pattern of a statistical array in order to insure that the randomly selected element locations give the desired results.

In using the pseudo random, or statistical density-taper, procedure a density taper must be selected which is modeled after a suitable amplitude taper A_n that produces a radiation pattern in a conventional array with sidelobes below the specified value. The statistical sidelobe level (Equation 6) also depends on the form of A_n and should be checked to see if its value is consistent with the desired design level. If not, a different taper is selected.

The average gain of this array is equal to the average number of elements remaining $\overline{N_E}$ (Equation 7). The average sidelobe level of a thinned array also approaches $\overline{N_E}$ (Equation A. 18) when the fraction of elements removed is large. The peak lobe is found to be from 3 db to 9 db greater than the average. There is generally no problem with second order beam suppression (grating lobes) in the statistical array radiation pattern. By properly selecting the spacing quantization the array can be scanned $\pm 90^{\circ}$ with negligible pattern deterioration.

The ring array technique of Section 4 is also useful for the design of large thinned arrays. The results achieved are comparable to those obtained statistically. The design procedures are described in Section 4. Radiation patterns for ring arrays are not as predictable as the average pattern of a large statistical array, but it is possible to develop a collection of empirical cases which offer guidance in attempting a new design. The ring array may be designed without the need of a computer or extensive calculations. Furthermore, the radiation pattern is easier to compute than that of a statistical array.

Dynamic programming, as described in Section 5, has been primarily applied to linear arrays. It is especially useful where it is necessary to minimize the sidelobe level over some specified angular region. The radiation patterns achieved by dynamic programming are optimum in this sense and produce superior results. A general purpose digital computer is necessary for determining the optimum spacings with dynamic programming.

In addition to these techniques for designing a thinned array with unequal spacings, it is possible to design a thinned array with equal spacings between elements. Grating lobes are produced but in some instances these can actually be of benefit, providing the resulting angular ambiguities can be resolved.[27]

3. STATISTICALLY DESIGNED DENSITY-TAPERED ARRAYS

Summary

This section discusses the design of "thinned" planar array antennas in which the density of elements located within the aperture is made proportional to the amplitude of the aperture illumination of a conventional "filled" array. Density tapering permits good sidelobe performance from arrays of equally radiating elements. The selection of the element locations to provide the desired density taper is performed statistically by utilizing the amplitude taper as the probability density function for specifying the location of elements. The statistical design procedures and the theoretical prediction of performance are given. The application to a 50 wavelength diameter planar aperture is discussed and the results compared to conventional amplitude-taper designs. Examples of computed patterns are shown for density tapers modeled after 25, 30, 35, and 40 db circular Taylor distributions. The properties of a planar array of 10,000 elements were examined for "natural" thinning and for 70% and 90% of the elements removed. The sidelobes are determined more by the number of remaining elements than by the model amplitude taper. Statistically designed density-tapered arrays are useful when the number of elements is large and when it is not practical to employ an amplitude-taper to achieve low sidelobes.

3.1 Introduction

The design of "thinned" planar array antennas by statistical means allows the density of elements located within the aperture to be made proportional to the amplitude of the aperture illumination of a conventional "filled" array. (A "thinned" array is one that contains less elements than a "filled" array of equally spaced elements located a half wavelength apart.) The selection of the element locations to provide the desired density taper is performed statistically by utilizing the amplitude taper as the probability density function for specifying the location of the elements. In a "thinned" array all the elements are assumed to radiate equal power if a transmitting array, or equal amplitude weighting if a receiving array. For convenience the elements are taken to be isotropic radiators. It is further assumed that the element spacings of a "thinned" array are not equal. This rules out interferometer antennas with their characteristic radiation pattern consisting of grating lobes, or secondary principal maxima.

An unequally spaced, thinned array may be used to (1) achieve a narrow main lobe with reduced number of elements (2) achieve a wide scan angle or operate over a broad frequency band without the appearance of grating lobes, or (3) achieve desirable radiation patterns without amplitude taper across the aperture. It is the last mentioned application which is of major interest in this section.

3.2 Description

The usual method for designing antennas to achieve low side lobes is to taper the amplitude of the aperture illumination so that the received (or radiated) energy is greater at the center than at the edges. There are a number of synthesis techniques[1-5] that have been described in the literature for determining the proper amplitude illumination across the aperture to obtain a specified far field radiation pattern. The design of antennas with an amplitude taper for the purpose of achieving a desired sidelobe level is well understood.

It is also possible to design array antennas for low sidelobes by employing a density taper (also called space taper) instead of an amplitude taper. The signal at each element of the array is of equal amplitude but the spacings between adjacent elements differ. Thus the density of equal-amplitude elements vary as a function of location within the aperture. By analogy to the amplitude taper, the equal-amplitude elements will be, in general, more dense at the center of the aperture than at the edges.

A density taper has advantages over an amplitude taper in certain applications. Transmitting arrays, for example, with individual power amplifiers at each element are easier to design and build and more efficient to operate if each amplifier delivers full rated power. If an amplitude taper were used it would mean that all tubes would not operate at full power or power must be wasted in attenuation, or alternatively, the tubes must be of different size. The density-tapered array does not suffer any of these inconveniences and permits the system designer to employ equal-power amplifiers at each element and still achieve low sidelobes.

Receiving antennas might also benefit from density tapering instead of amplitude tapering. The attenuation necessary at each receiving element can increase the effective noise temperature and might be detrimental to a low-noise antenna system. Also, fewer total elements are needed for density-tapered than for amplitude-tapered arrays.

The theory of the design of density-tapered arrays is not on as firm a foundation as that of amplitude-tapered arrays. For example, the design techniques of Dolph[3] and Taylor[4] which are based on the properties of polynomials and which are widely used for amplitude-tapered antennas are not applicable to unequally spaced arrays. What theory[6-8] that does exist for unequally spaced arrays has not been easy to apply when the array contains more than a small number of elements.

Several design procedures[9-11] have been described in the literature which give radiation patterns with more or less reasonable sidelobe behavior without significant deterioration in the shape of the main beam. These techniques are somewhat empirical in nature. One

such design technique is to approximate the amplitude taper of the conventional array with the density taper of the unequally spaced array. That is, the density of equal-amplitude elements in some region of the aperture is made proportional to the amplitude that some equivalent amplitude-tapered array would have at the same location within the aperture. By approximating the density-tapered aperture illumination to the desired amplitude-tapered illumination it is hoped that the radiation pattern of the density tapered array will be a reasonable approximation to the desired radiation pattern. Although no precise theoretical justification has been offered for this approach, it is capable of producing acceptable results in practice, especially when the number of antenna elements is large.

There are two basic methods for matching a density taper to an amplitude taper. In one technique the density is matched deterministically to the desired amplitude taper by trial and error placement of the elements[12, 13] or by certain approximation techniques applied to the integral of the aperture illumination.[14-17] The other design technique, and the one which is the subject of this section, is a statistical method which utilizes the desired amplitude illumination as a probability density function for determining whether or not an element should be located at a particular point within the aperture. This technique which is well suited for programming on a digital computer has been discussed by Allen[18] and by Rabinowitz and Kolar.[19] Allen attributes its origin to J.R. Cogdell of Lincoln Laboratory. The basic idea of thinning array antennas probably was inspired by the original work of Ruze[2] on the effects of random errors in antennas.

A computer method for designing statistical density-tapered arrays is described in this paper and the results for 10,000 element, one-degree beamwidth array antennas are given for various degrees of thinning and design sidelobe levels. The computed results are compared to the theoretical predictions.

Unequally spaced arrays designed statistically must be described in statistical terms. Appendix I derives the important properties of such arrays. Before considering the application of this technique, the major results derived in Appendix I will be summarized.

If elements are removed from an N-element "filled" array, the field-intensity in the far field may be written

$$E(\theta, \phi) = \sum_{n=1}^{N} F_n \exp j\psi_n \ , \qquad (1)$$

where θ, ϕ are the angular coordinates describing the field, ψ_n is the phase of the signal at the n^{th} element, and F_n is either zero or unity according to whether the n^{th} element is removed or left in place. In a

statistically designed array F_n is selected randomly and independently from element to element so that its ensemble average is $\overline{F}_n = kA_n$, where k is a factor less than unity to account for the degree of thinning, and A_n is the normalized amplitude of the excitation that would be applied to the n^{th} element of a conventional amplitude-tapered antenna whose field-intensity is

$$E_o(\theta, \phi) = \sum_{n=1}^{N} A_n \exp j\psi_n \tag{2}$$

When k = 1, the array is said to be "naturally" thinned.

The average field-intensity (ensemble average over many selections) is

$$\overline{E(\theta, \phi)} = k E_o(\theta, \phi) \tag{3}$$

which is similar to that of the model amplitude-tapered array. The average power pattern, or radiation pattern, is

$$\overline{|E(\theta, \phi)|^2} = k^2 |E_o(\theta, \phi)|^2 + \sum_{n=1}^{N} kA_n(1 - kA_n) \tag{4}$$

The first term of the radiation pattern is proportional to the radiation pattern of the model amplitude-tapered array. It is identically equal to it when k = 1, corresponding to a naturally thinned array. The second term is independent of angle. Thus the average statistical sidelobes which dominate the pattern outside the vicinity of the main beam and the near-in sidelobes may be written

$$\overline{SL} = \sum_{n=1}^{N} kA_n(1 - kA_n) \tag{5}$$

The gain is equal to the number of elements remaining. Therefore the average gain is

$$\overline{G} = \overline{N}_R = k \sum_{n=1}^{N} A_n \tag{6}$$

3.3 Application

The statistical-design procedure consists of first selecting a suitable model amplitude taper. Amplitude tapers which give low

sidelobes generally have a maximum at the center of the aperture and decrease in amplitude towards the edges. The Taylor distributions[21, 22] for circular apertures are applied here as models for statistical density-taper designs.

The individual elements are assumed to be located only at the intersections of a rectangular grid within a circular aperture Figure 1. The spacing of the grid is determined by how far in angle the beam is to be scanned without the appearance of undesirable grating lobes. It is assumed that the beam must scan the full hemisphere so that the spacing quantization is a half wavelength. A rectangular coordinate system is shown in Figure 1. Although the resulting apertures are circular, the rectangular coordinate system has the advantage that is is easier to provide steering commands to the individual phase shifters at each element in a practical array-antenna system. Also, in a practical array-antenna system it is easier to provide steering commands to the individual phase shifters at each element if located on a rectangular grid. The circular aperture was selected as the basic geometry to study since it results in patterns with a high degree of circular symmetry. In the examples to follow, the original aperture was a 50λ by 50λ square (λ = wavelength) with a grid separation of half-wavelength. This square aperture, if completely filled, would contain 10,201 elements and produce a half power beamwidth of approximately one degree. The electric field intensity, $E(\theta, \phi)$ of a statistically designed array of isotropic elements located on a rectangular grid is

$$E(\theta,\phi) = \sum_{m=0}^{M-1} \sum_{n=0}^{N-1} F_{mn} \exp\left\{j2\pi d\left[m(\sin\theta\cos\phi - \sin\theta_o\cos\phi_o) + n(\sin\theta\sin\phi - \sin\theta_o\sin\phi_o)\right]\right\} \quad (7)$$

where θ, ϕ are the angular coordinates, as shown in Figure 1, (θ_o, ϕ_o) is the angular position to which the beam is steered, M and N are the number of rows and columns, respectively, and F_{mn} takes on the values 0 or 1 according to a probability density function derived from the specified amplitude taper of the model array. The field is summed with respect to one corner of the rectangular array. For convenience in computing the patterns and in visualizing the results, Equation 7 can be simplified if the beam is always steered in the plane that the pattern is being measured. Thus ϕ is set equal to ϕ_o and the variation in the θ plane is examined. With this simplification and a basic grid separation of a half-wavelength, Equation 7 becomes

$$E(\theta,\phi_o) = \sum_{m=0}^{M-1} \sum_{n=0}^{N-1} F_{mn} \exp\left[j\pi u(m\cos\phi_o + n\sin\phi_o)\right] \quad (8)$$

where $u = \sin\theta - \sin\theta_o$. For a circular aperture, $F_{mn} = 0$ in the region

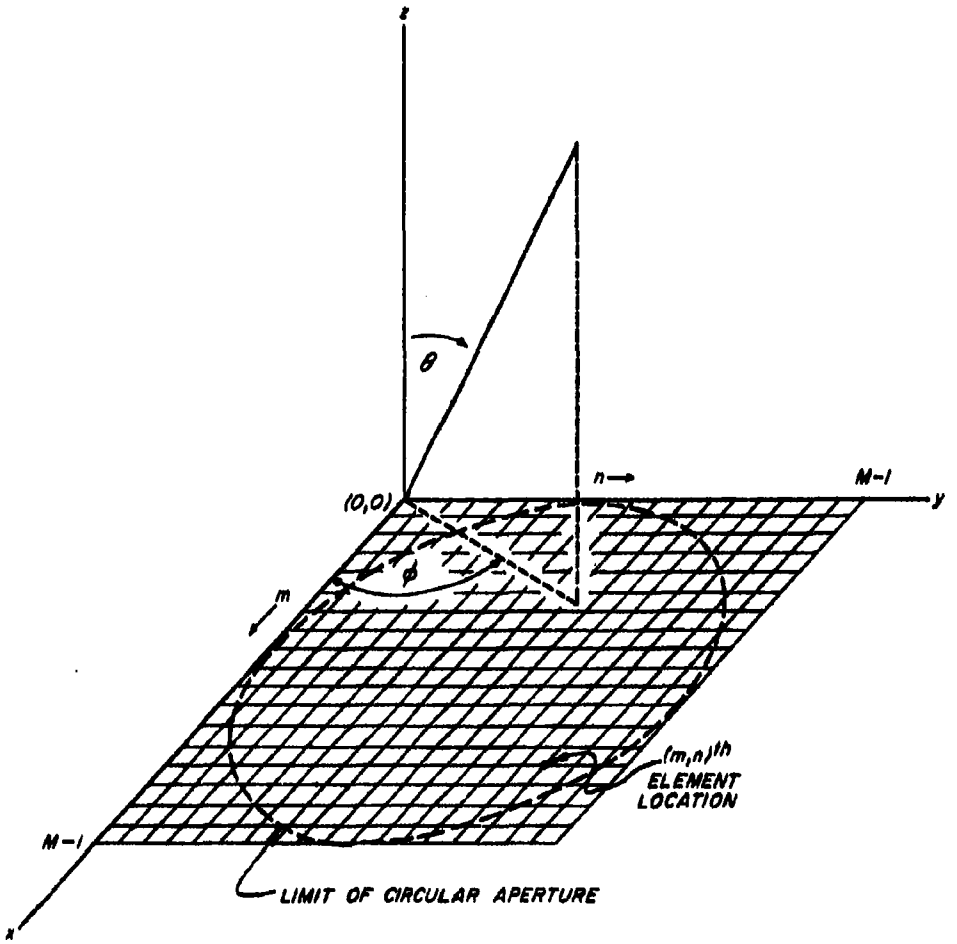

FIG. 1 -GEOMETRY OF AN M BY M ELEMENT ARRAY ARRANGED ON A RECTANGULAR GRID. ANGULAR COORDINATES ARE ALSO SHOWN.

of the rectangular grid outside the 50λ diameter circle.

The Taylor circular aperture distributions specify the amplitude of the aperture illumination as a function of the radial displacement of the element. The aperture illumination function, A_{mn}, must be normalized so that its maximum (which usually occurs at the center) is unity. This makes A_{mn} a probability density function. The actual probability density function used to determine whether or not an element is located at m, n is given by kA_{mn}, where k is a constant which depends on the amount of elements removed. "Natural" thinning corresponds to k = 1. Table I presents the percentage of elements removed for natural thinning assuming various Taylor distributions. The percentage removed is based on a "filled" square aperture of half-wavelength spacing. Also shown (in parentheses) is the percentage removed if computed relative to a circular aperture of the same diameter (50λ). In all that follows, the quoted percentage removed is based on a square aperture even though the "thinned" aperture is circular. This follows previous practice of other authors. The radiation patterns of the Taylor distributions for the 25, 30, and 35 db sidelobe designs have a value of $\bar{n} = 3$, where $\bar{n}$ is the number of equal amplitude sidelobes adjacent to the main beam.[21] For the 40 db design $\bar{n} = 4$.

If it is desired to remove more elements than given by natural thinning (max $A_{mn} = 1$), the values of A_{mn} may be multiplied by a factor k less than unity. For example, with the 25 db Taylor design, 70 percent removal corresponds to k = 0.658 and 90 percent removal corresponds to k = 0.219. The appropriate values of k are also shown in Table I. The factor k corresponds to the probability that an element is located at the center of the array.

The computations for the 50λ by 50λ array were programmed on the IBM 7090 computer and were performed by the IBM Service Bureau in Houston, Texas. The values of A_{mn} used for the model array were obtained by interpolation of the Hansen tables[22] for the various Taylor distributions considered. The statistical quantities F_{mn} were determined by generating for each (m, n) a random number between 0 and 1. An element was located at the grid position (m, n) if the random number was less than or equal to the value of kA_{mn} at that point. For example, suppose that at a point (m, n) the value of the normalized distribution $kA_{mn} = 0.765$. Then if the random number generated were 0.623 the element would be located at the point in question, and if it were 0.766 it would be absent. In addition to this criterion, elements were not placed at those positions of the grid which lay outside a circular aperture. Thus the corners of the grid are automatically eliminated. This means that for a square grid, $(\pi/4)M^2$ of the element positions are available, where M is the number of elements on one side of the square

3.4 Results

Figures 2 through 5 give the computed patterns of the statistically-designed space-tapered arrays using as a model the Taylor circular aperture distribution for 25, 30, 35 and 40 db sidelobes, respectively. Only the u region extending from 0 to 1.0 is shown. The pattern is symmetrical about $u = 0$ and because the basic grid quantization is a half wavelength, it is also symmetrical about $u = \pm 1$. Thus the principal plane pattern plotted over the region $0 \leq u \leq 1$ describes the behavior over the region $-2 \leq u \leq 2$, (If the antenna beam is steered to $\pm 90^{\circ}$, the pattern must be examined out to $u = 2$. If the beam is not steered the pattern beyond $u = 1$ is of no importance.) Also shown on these patterns is the predicted average sidelobe level due to the statistical removal of elements (Equation 5).

It can be seen from an examination of these figures that the near-in sidelobes are determined by the Taylor design for the 25 and 30 db cases. The near-in sidelobes of the 35 db and 40 db designs do not behave as predicted by the model pattern but are determined more by the statistical pattern. In all four cases the sidelobes in the region removed from the main beam depend on the statistical pattern, (Equation 5) rather than the model pattern (first term of Equation 4).

Figure 6a is a repeat of Figure 3 for the 30 db statistical design but with the pattern superimposed of the model array designed with an amplitude taper. The main beam and the near-in sidelobe behavior of the two patterns are similar, but the sidelobe level of the statistical design is higher than the Taylor design over a large part of the angular region. This difference is not too important for practical arrays for two reasons. First, the sidelobes of the statistical designs with natural thinning are sufficiently low for most purposes. Second, the sidelobes of a practical array with an amplitude taper are generally not as low as indicated by the theoretical pattern because of the ever present random errors in the aperture distribution which result in a higher sidelobe level than predicted.[2]

The Taylor distribution of Figure 6a was designed to have the first three sidelobes adjacent to the main beam equal to the design value of 30 db. It is seen that only the first lobe has this value. This discrepancy might be a result of the fact that the Taylor distribution applies to a continuous aperture but was applied to a discrete (array) aperture.

The orthogonal principal plane pattern ($\phi = 90$) for the statistical density-tapered design of Figure 3 and Figure 6a is shown in Figure 6b. This differs in detail from the $\phi = 0^{\circ}$ pattern because the statistical nature of the design does not result in perfect angular symmetry. The two patterns of Figure 6 give a qualitative indication of the variation that can be expected with the statistical density-taper designs for principal plane patterns.

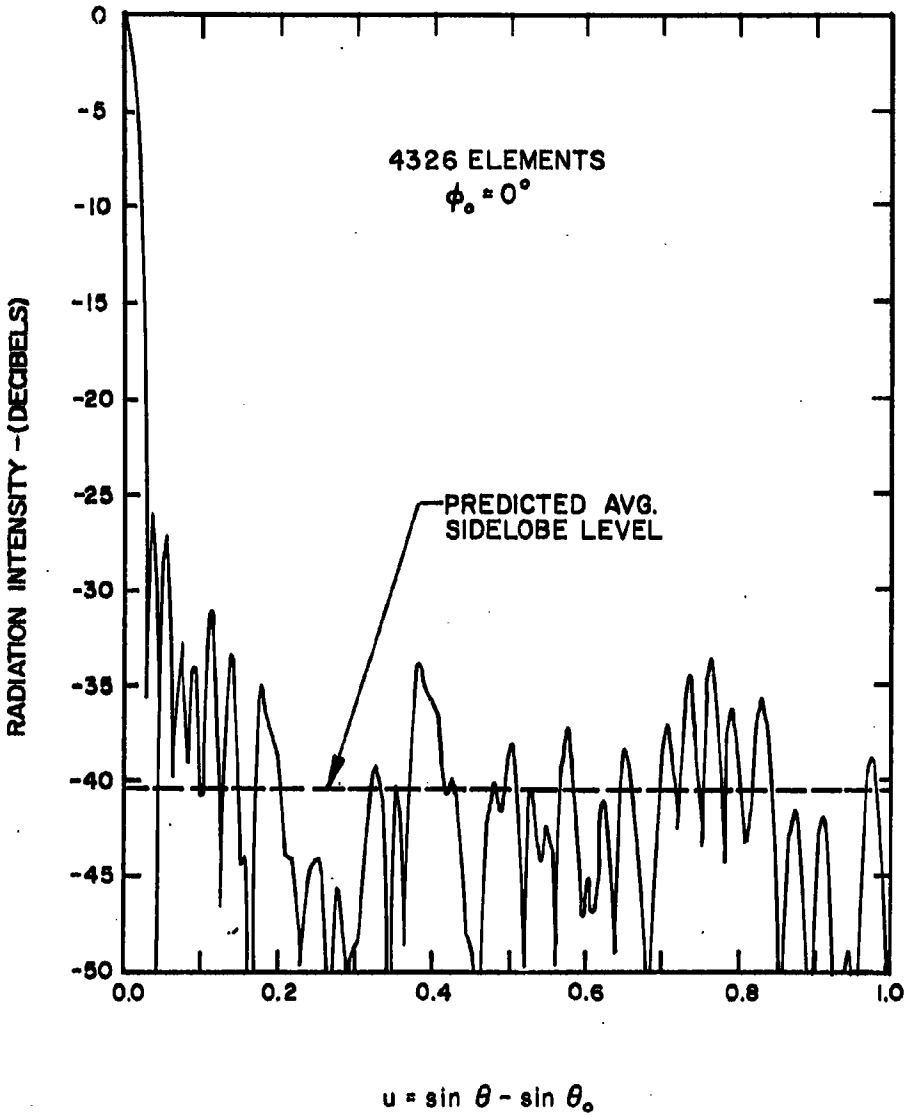

FIG. 2 - COMPUTED RADIATION PATTERN OF A STATISTICALLY DESIGNED ARRAY USING THE 25db TAYLOR CIRCULAR APERTURE DISTRIBUTION.

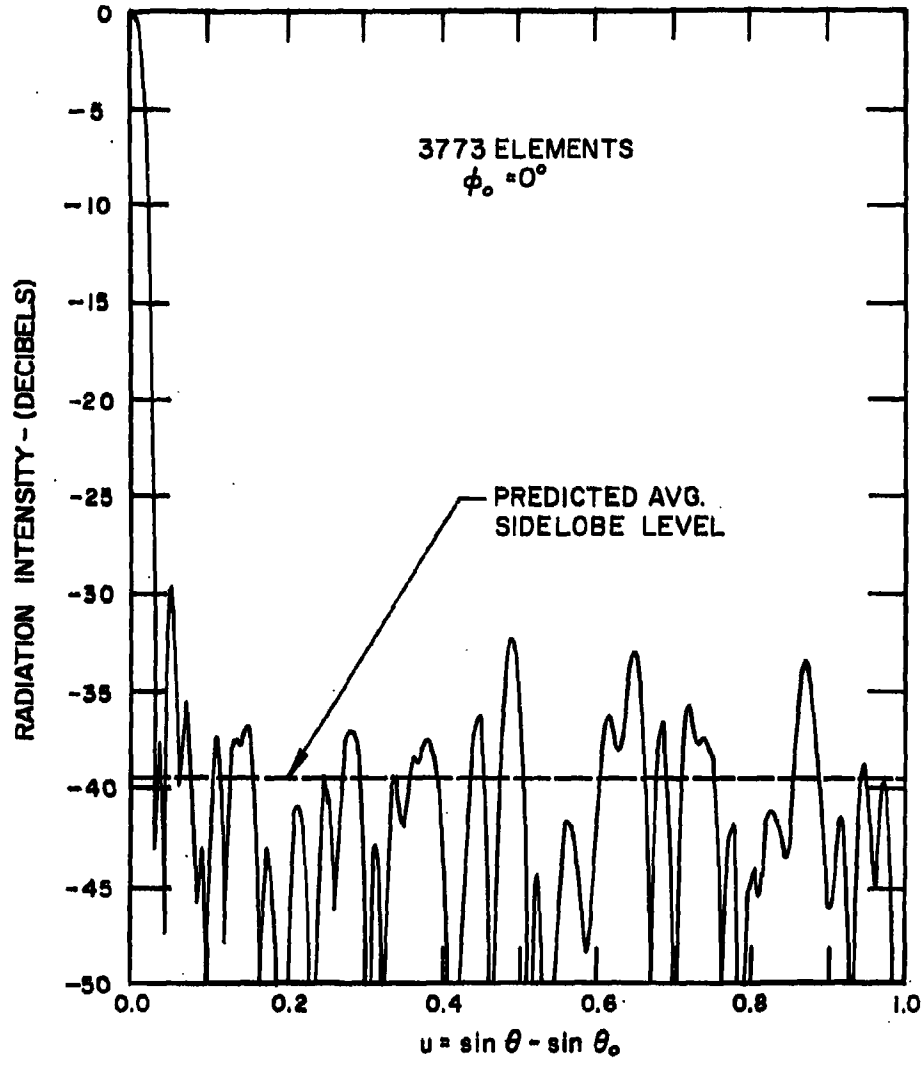

FIG. 3 - COMPUTED RADIATION PATTERN OF A STATISTICALLY DESIGNED ARRAY USING THE 30db TAYLOR CIRCULAR APERTURE DISTRIBUTION.

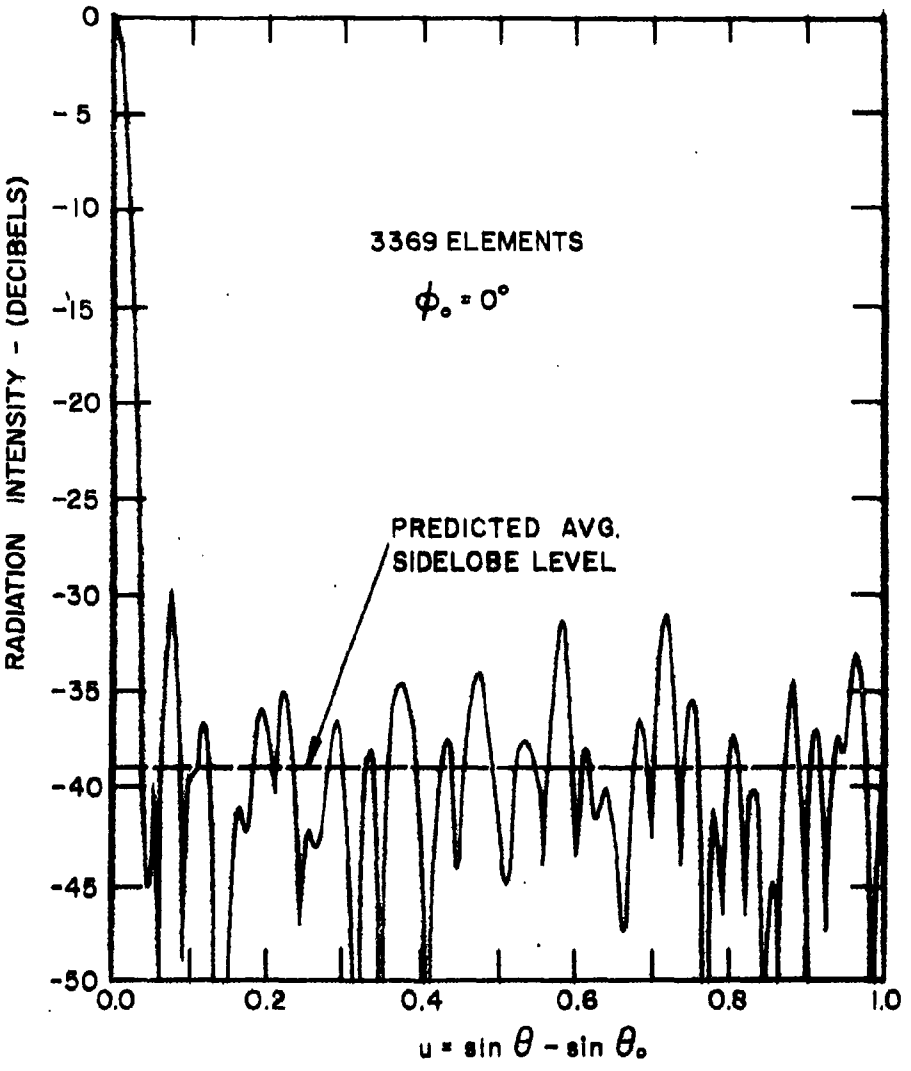

FIG. 4 - COMPUTED RADIATION PATTERN OF A STATISTICALLY DESIGNED ARRAY USING THE 35 db TAYLOR CIRCULAR APERTURE DISTRIBUTION.

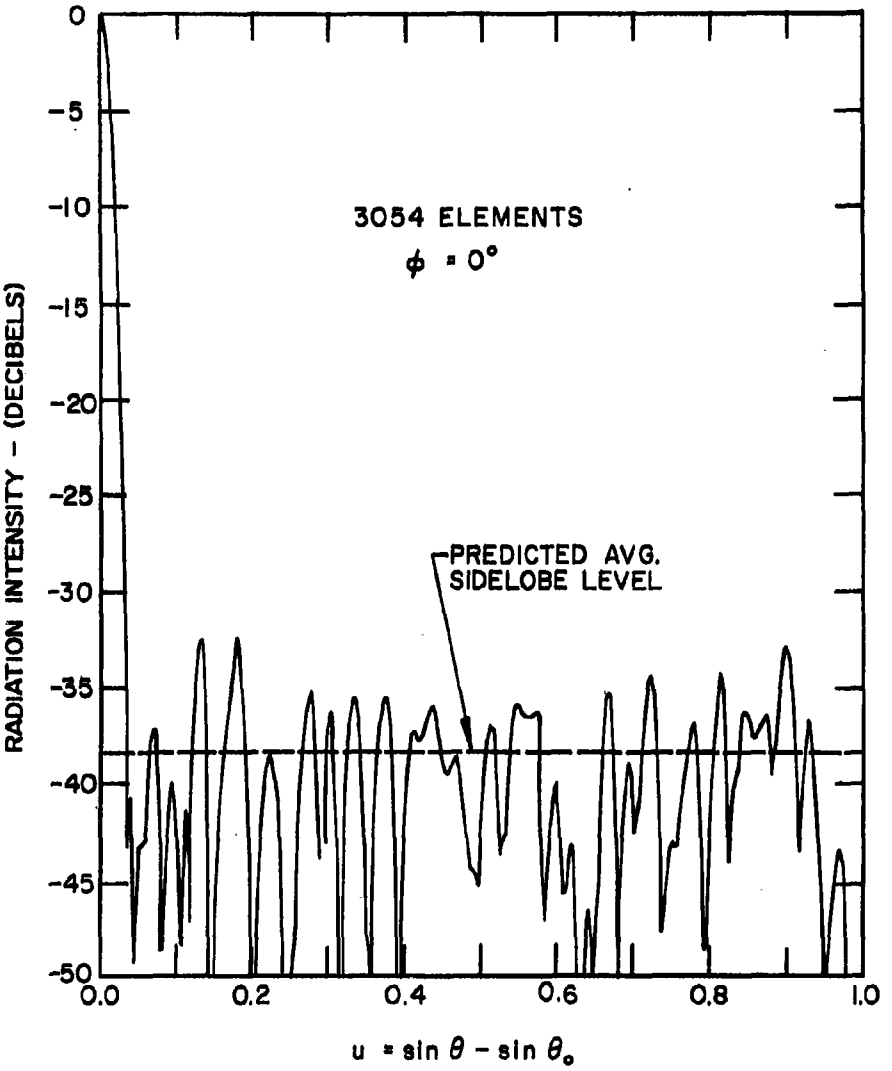

FIG. 5 - COMPUTED RADIATION PATTERN OF A STATISTICALLY DESIGNED ARRAY USING THE 40db TAYLOR CIRCULAR APERTURE DISTRIBUTION.

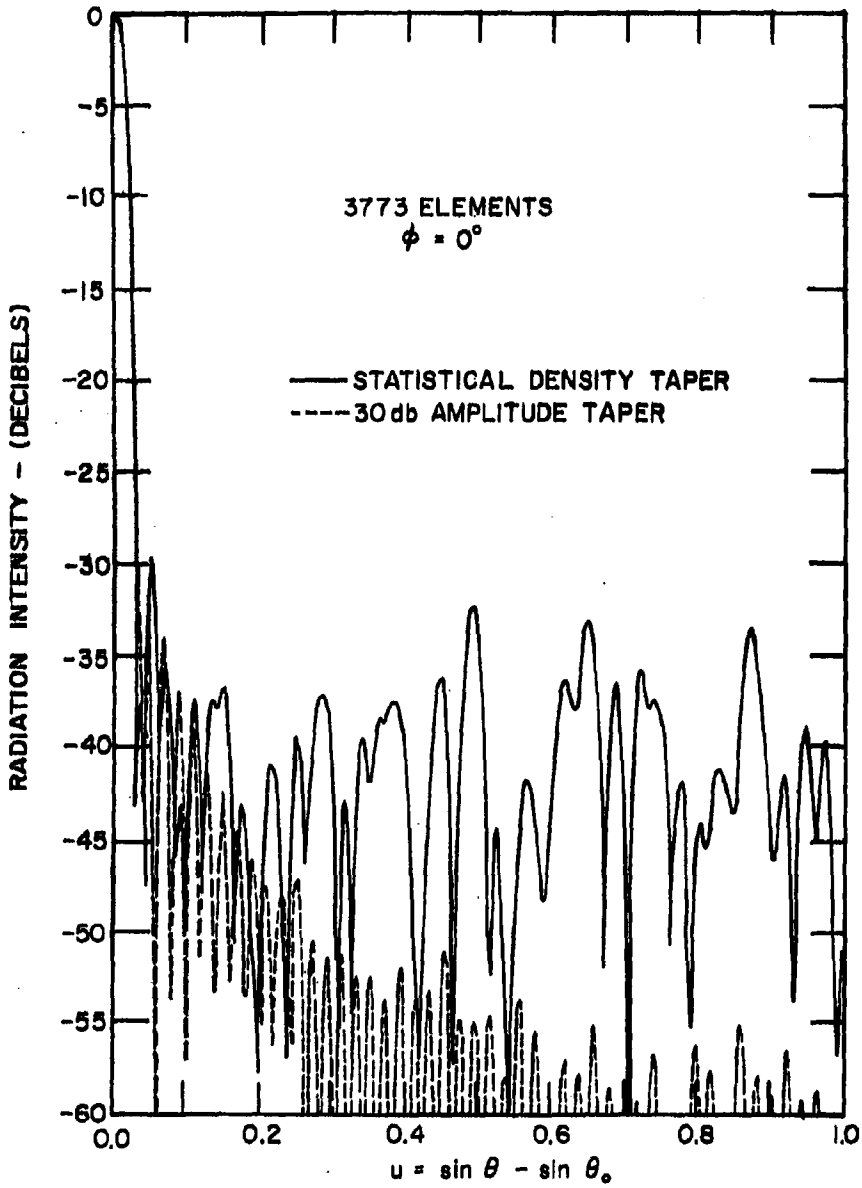

FIG. 6a - STATISTICAL DENSITY-TAPER RADIATION PATTERN IS THE SAME AS THAT OF FIG.3. THE AMPLITUDE-TAPER RADIATION PATTERN IS THAT OF THE 30db TAYLOR DESIGN

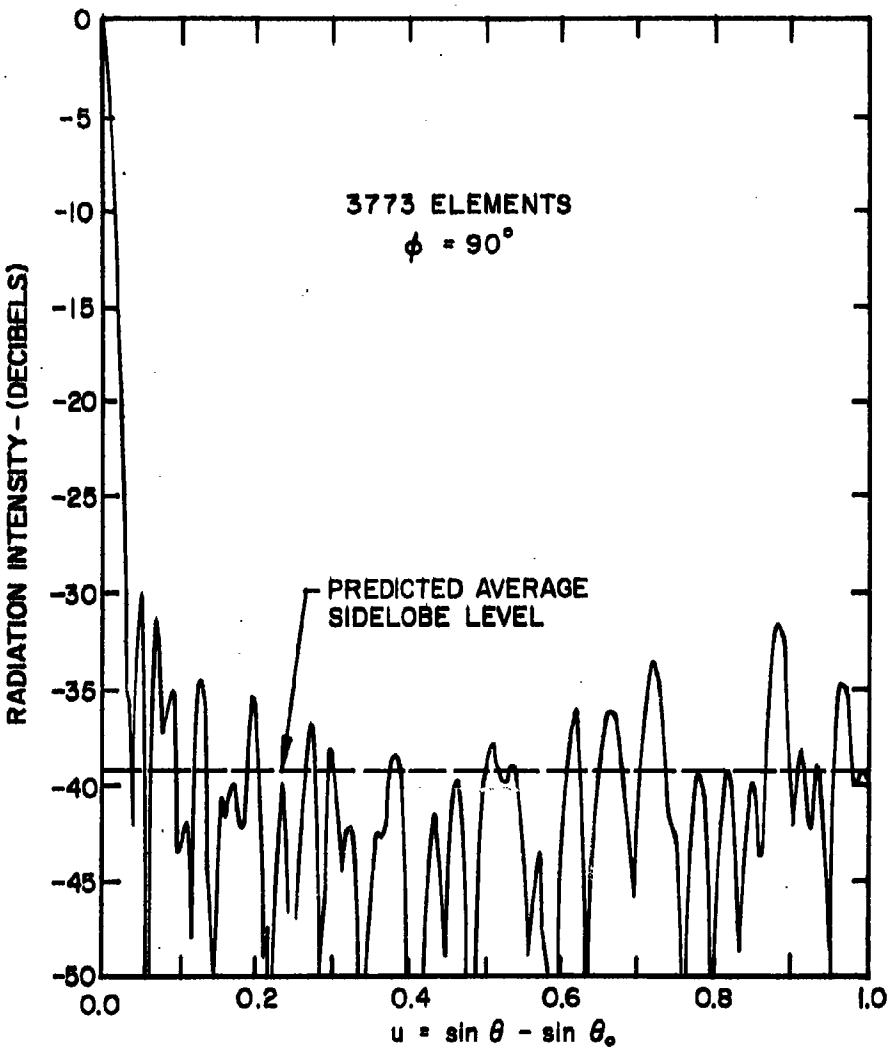

FIG. 6b - 30db STATISTICAL DENSITY-TAPER AS IN FIG. 3 BUT FOR THE ORTHOGONAL PRINCIPAL PLANE (ϕ = 90°)

The examples of Figures 2 through 6 were for natural thinning. The patterns for the 30 db design with fewer elements than obtained with natural thinning are shown in Figure 7 (70% element removal) and Figure 8 (90% element removal). In both cases the sidelobe behavior is determined by the statistical removal of elements and not by the design used as the model. All of the examples examined indicate that the shape of the main beam is relatively unaffected by the removal of elements.

The effects of thinning the 25 db and 35 db circular Taylor distributions have also been computed. Figures 9 and 10 are, for the 25 db distribution shown for natural thinning in Figure 2, thinned 70% and 90%, respectively. When the naturally thinned 35 db distribution of Figure 4 is thinned 70% and 90% the patterns appear as in Figures 11 and 12, respectively.

The placement of elements within the aperture is shown in Figure 13 for the 30 db natural thinning (pattern given by Figure 3). Figure 14 is the aperture element distribution for the 25 db design with 90% of the elements removed (pattern given by Figure 10).

The computed patterns of the naturally thinned and the 90% thinned designs were experimentally measured using the ECI array modeling technique known as the "holey plate."[24] Figures 13 and 14 represent the scale model aperture that was used.

3.5 Discussion

The results obtained for the design of 50 wavelength diameter circular apertures thinned by the technique of statistical density-tapering are summarized in Table II. The values listed should be considered as approximate only, since they were obtained by examining in each case the principal plane radiation patterns of only one set of statistically determined element locations. These results, nevertheless, are consistent with the theoretical predictions as derived in Appendix I.

It is seen that the sidelobes outside of the first few adjacent to the main beam are more influenced by the degree of thinning than by the particular amplitude taper used as the model for the probability density function. The major portion of the radiation pattern is governed by the statistical sidelobes whose average value was given by Equation 5. The peak statistical sidelobes in the examples considered are from 3 to 9 db higher.

Equation 5 shows that the statistical sidelobes of a thinned array are determined by the model aperture amplitude distribution A_n and by k, the factor which determines the number of elements removed. The near-in sidelobes are also determined by A_n. An interesting synthesis problem is to determine k and A_n such that the peak sidelobes are a specified (statistical) value over the entire angular region. It is not sufficient to merely require that the statistical sidelobes be a

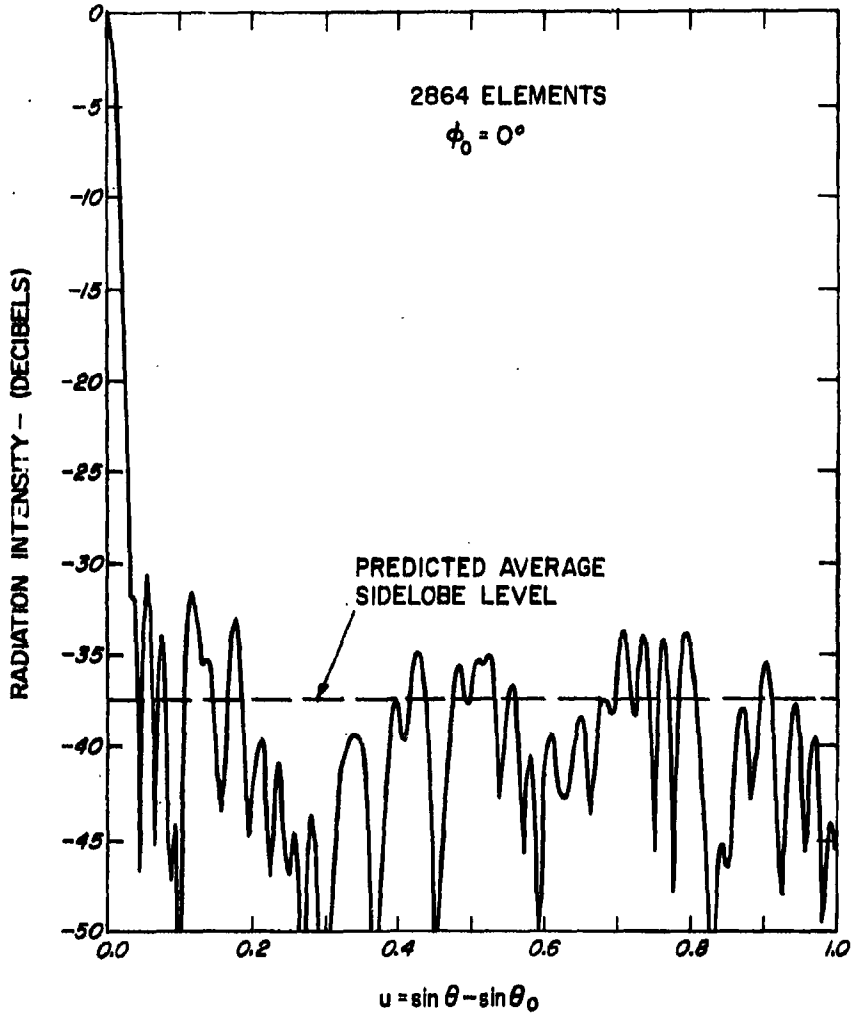

FIG. 7 – COMPUTED RADIATION PATTERN OF A STATISTICALLY DESIGNED ARRAY USING THE 30 db TAYLOR DISTRIBUTION (AS IN FIG. 3) AS THE PROBABILITY DENSITY FUNCTION BUT WITH APPROXIMATELY 70% OF THE ELEMENTS REMOVED. N_R=2864 ELEMENTS

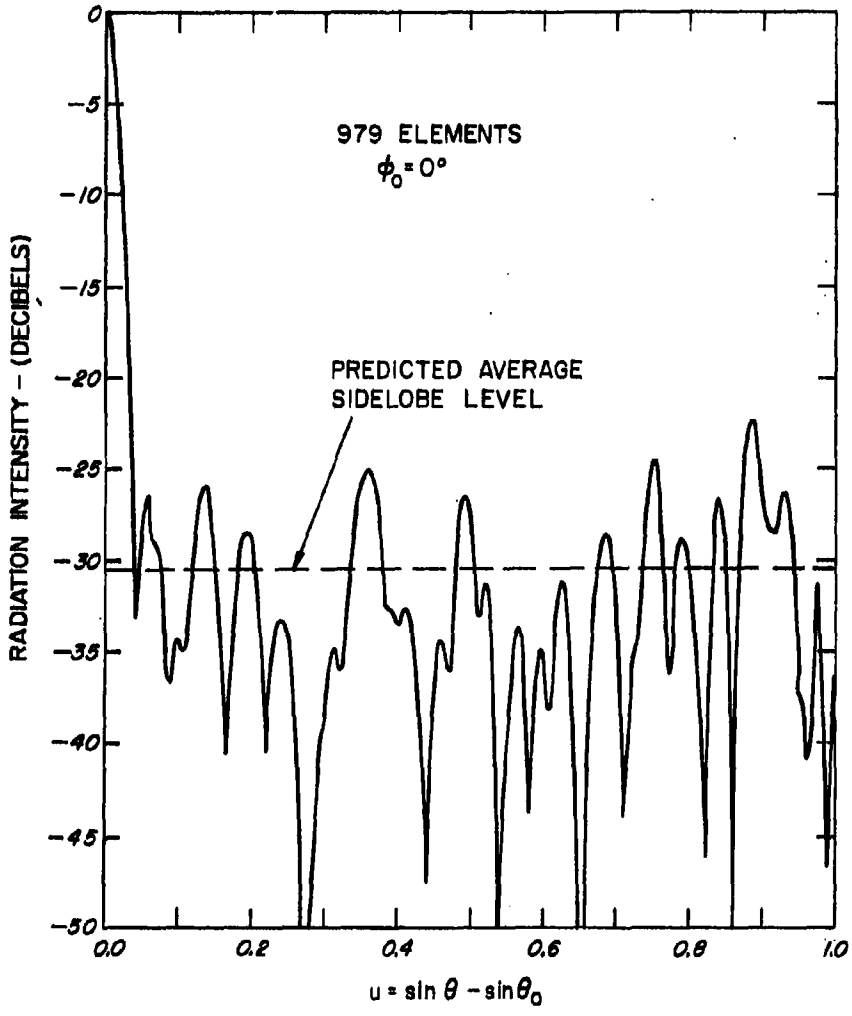

FIG. 8 – 30db STATISTICAL DENSITY TAPER AS IN FIG. 3, BUT DESIGNED FOR APPROXIMATELY 90% REMOVAL OF ELEMENTS. $N_R = 979$ ELEMENTS.

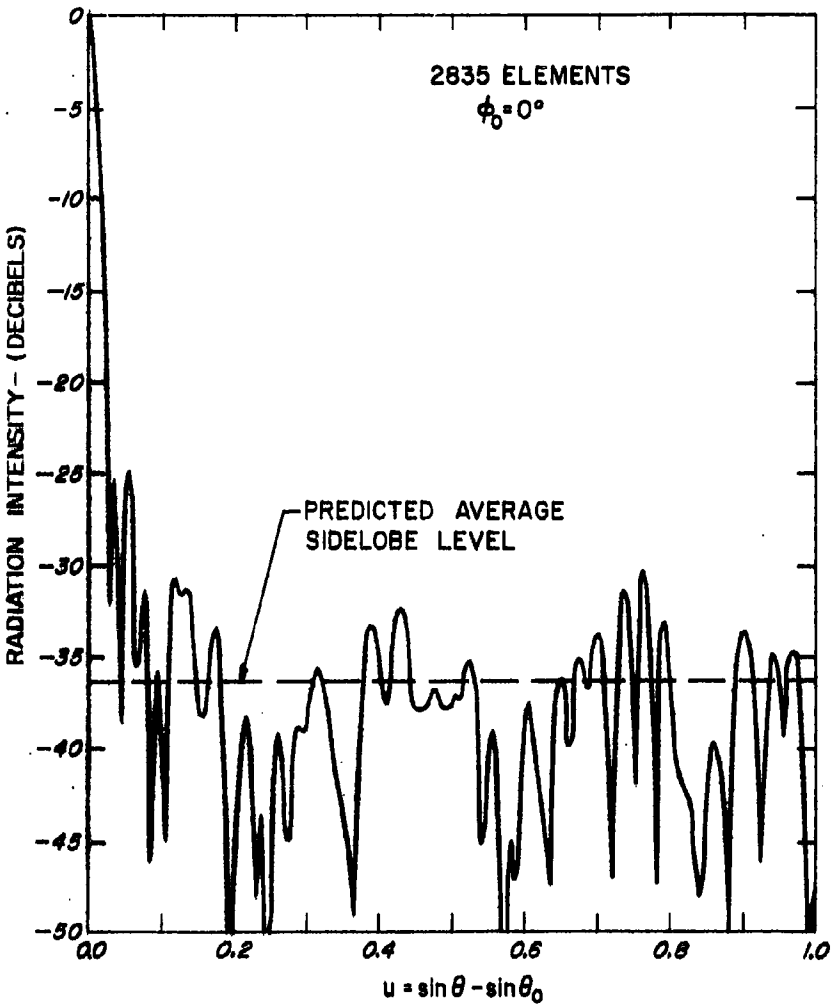

FIG. 9 - COMPUTED RADIATION PATTERN OF A STATISTICALLY DESIGNED ARRAY USING THE 25 db TAYLOR DISTRIBUTION (AS IN FIG. 2) AS THE PROBABILITY DENSITY FUNCTION BUT WITH APPROXIMATELY 70% OF THE ELEMENTS REMOVED. N_R=2835 ELEMENTS

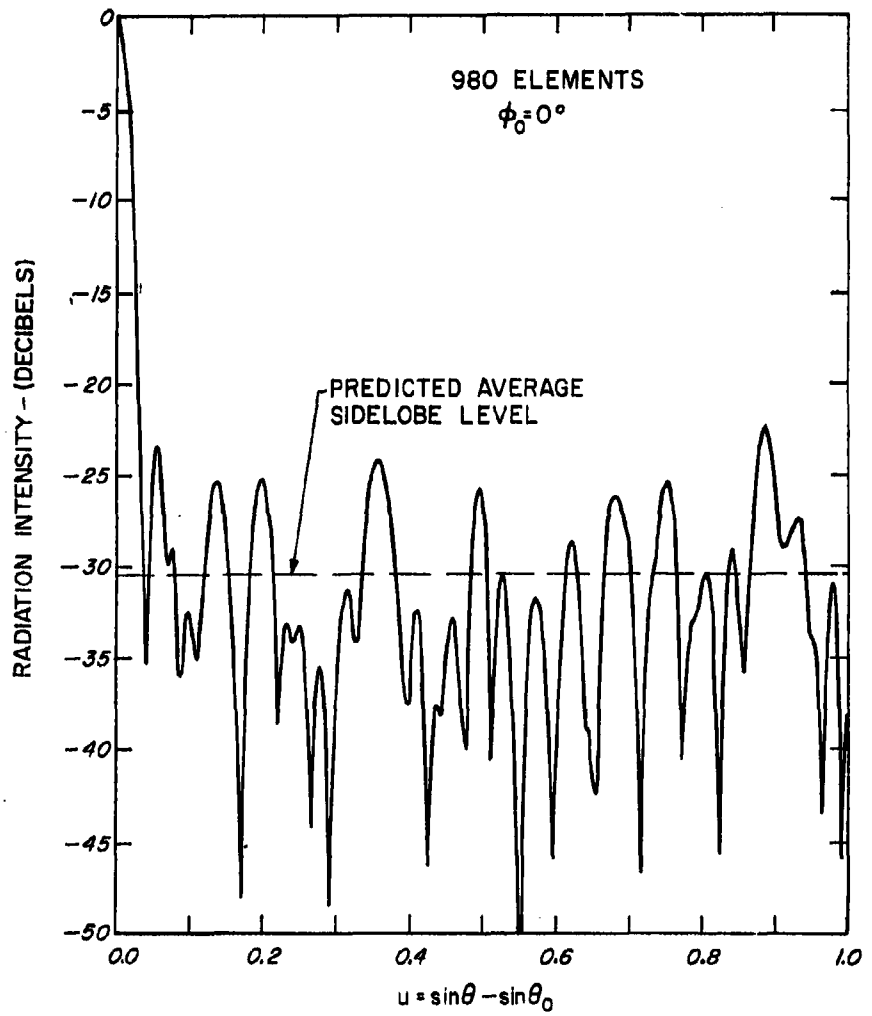

FIG. 10 - COMPUTED RADIATION PATTERN OF A STATISTICALLY DESIGNED ARRAY USING THE 25 db TAYLOR DISTRIBUTION (AS IN FIG. 2) AS THE PROBABILITY DENSITY FUNCTION BUT WITH APPROXIMATELY 90% OF THE ELEMENTS REMOVED.
N_R=980 ELEMENTS

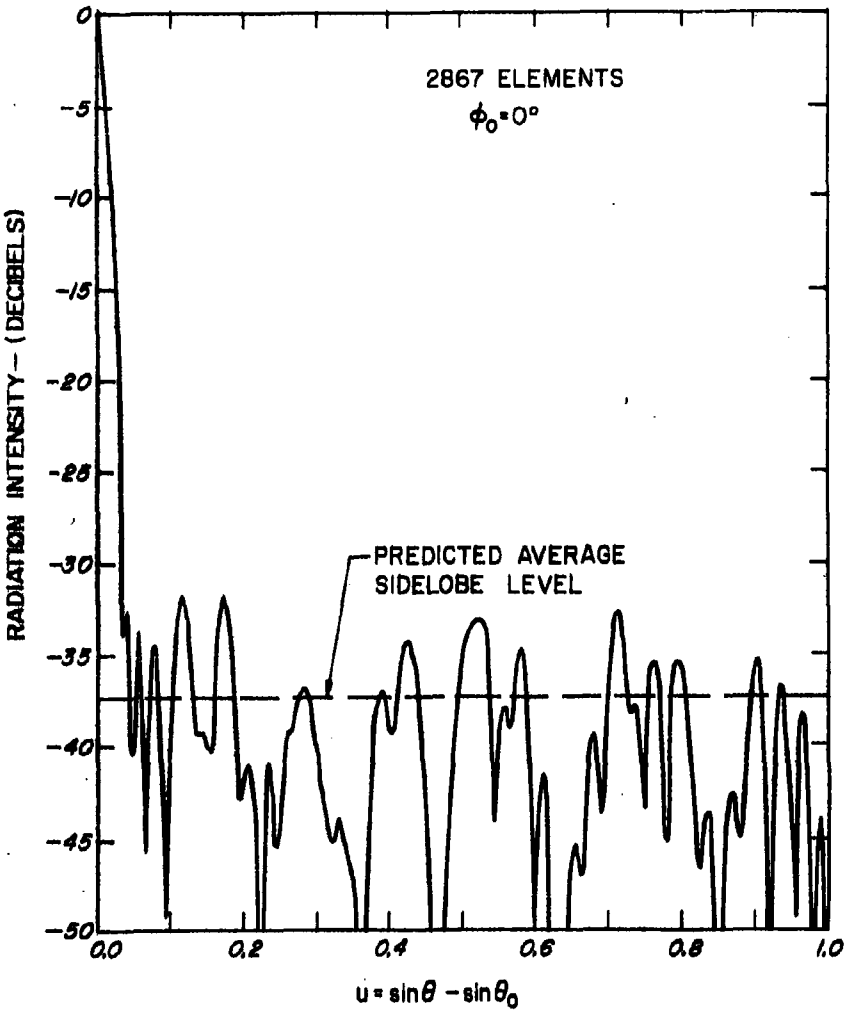

FIG. 11 – COMPUTED RADIATION PATTERN OF A STATISTICALLY DESIGNED ARRAY USING THE 35 db TAYLOR DISTRIBUTION (AS IN FIG. 4) AS THE PROBABILITY DENSITY FUNCTION BUT WITH APPROXIMATELY 70% OF THE ELEMENTS REMOVED. $N_R = 2867$ ELEMENTS

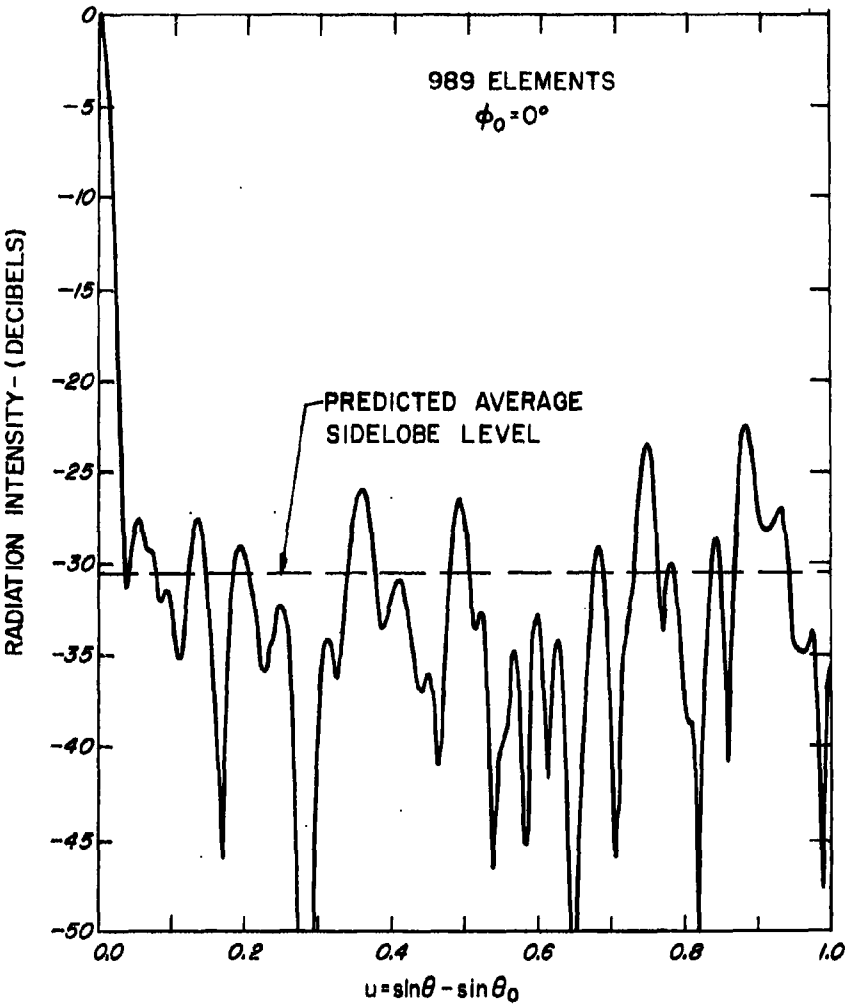

FIG. 12 - COMPUTED RADIATION PATTERN OF A STATISTICALLY DESIGNED ARRAY USING THE 35 db TAYLOR DISTRIBUTION (AS IN FIG. 4) AS THE PROBABILITY DENSITY FUNCTION BUT WITH APPROXIMATELY 90% OF THE ELEMENTS REMOVED. $N_R = 989$ ELEMENTS

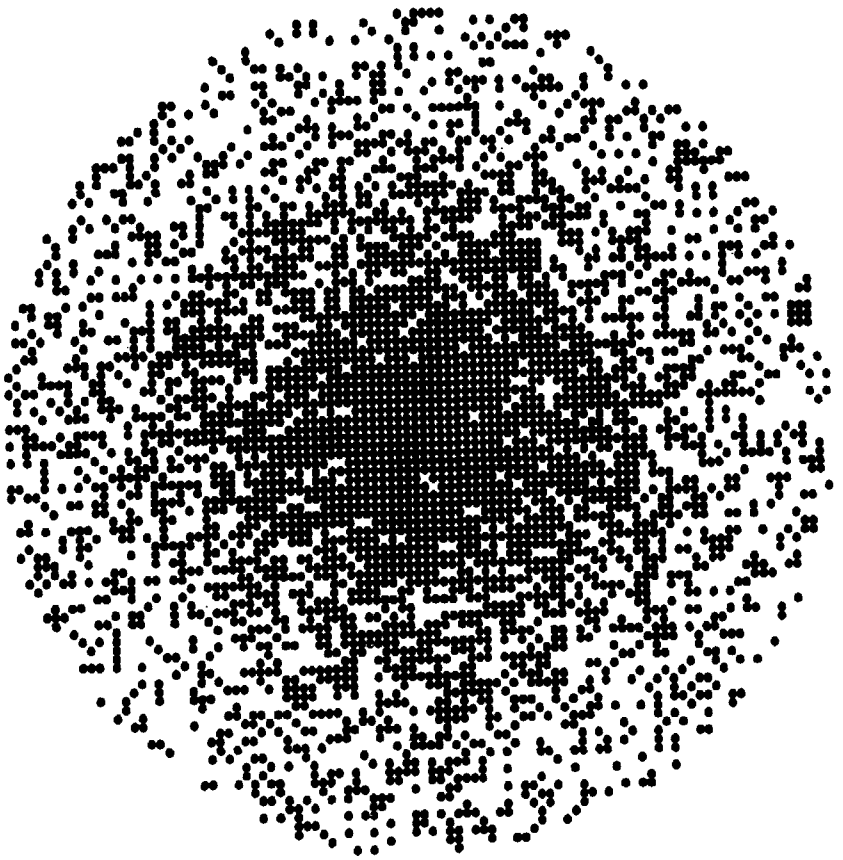

FIG. 13 - ACTUAL LOCATIONS OF ELEMENTS DETERMINED STATISTICALLY FOR THE NATURALLY THINNED 30 db DENSITY-TAPER ARRAY WHOSE PATTERN IS SHOWN IN FIG. 3.

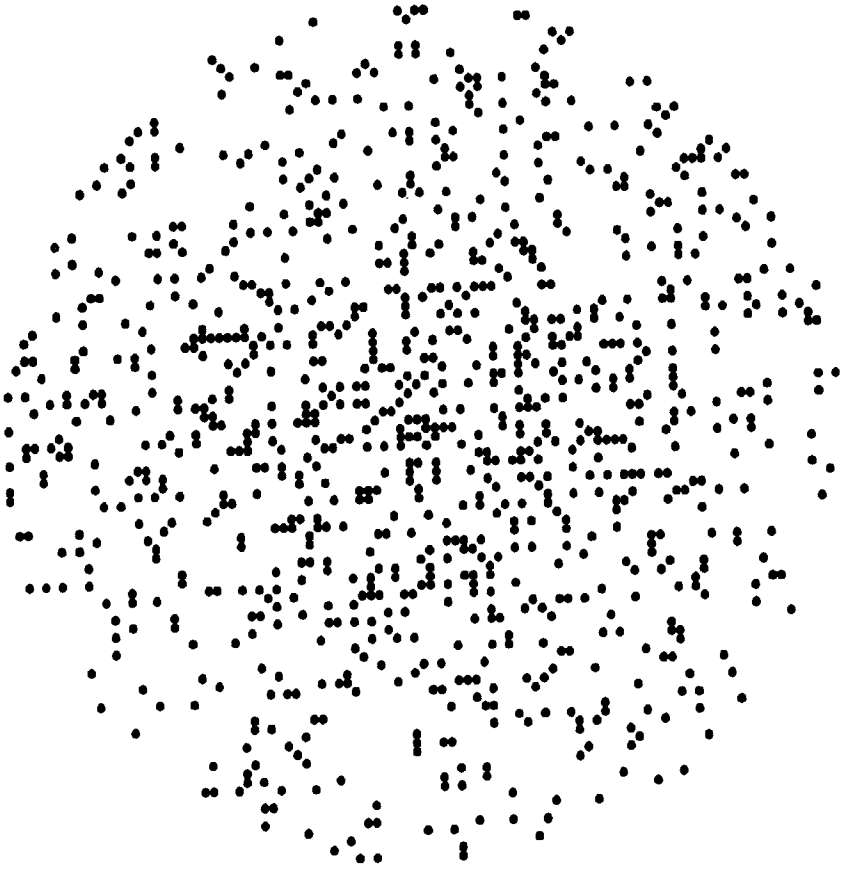

FIG. 14 - ACTUAL LOCATION OF ELEMENTS DETERMINED STATISTICALLY FOR THE 25 db DENSITY-TAPER ARRAY WITH 90% OF THE ELEMENTS REMOVED. CORRESPONDING RADIATION PATTERN IS SHOWN IN FIG. 8.

minimum since this occurs for the trivial cases of $kA_n = 0$ and $kA_n = 1$ over the entire aperture. The former corresponds to no aperture distribution (no antenna) and the latter corresponds to the uniform distribution of equally-spaced elements which produce high near-in sidelobes (and no thinning). From this it is concluded that those portions of the aperture distribution near the maximum and those near zero contribute little to the statistical sidelobe level. Those values of A_n in the vicinity of $A_n = 0.5$ contribute most. Thus a model amplitude distribution should be chosen which gives the designed near-in sidelobe level and which has most of the energy either near $A_n = 1$ or $A_n = 0$.

The principal plane patterns are statistically independent, so that the variation between $\phi_o = 0^o$ and $\phi_o = 90^o$ gives some idea of the variation. However, the two principal plane patterns (Figures 3 and 6b) for the 30 db naturally thinned density-tapered array are not a sufficient number of trials for statistical purposes. In addition to Figure 8, there are five additional cases for the 30 db, 90% thinned, density-tapered array, i.e., the $\phi_o = 90^o$ case for Figure 8, plus two additional independently determined arrays with principal plane patterns for each. The "best" of this group of six patterns is shown in Figure 15. All sidelobes are below -24 db, and it is interesting to note that from Figure 60 in the discussion of arrays from an energy viewpoint this is the peak sidelobe expected on the basis of two dimensional sine waves for the sidelobe pattern. The actual variation of the peak sidelobes for these arrays was for peaks from -21.5 db to -24.0 db with an average of -22.4 db. The average sidelobe level without the -24 db case is -22 db, and the next best pattern is an array whose peak sidelobe was -22.9 db. Thus it is believed that the pattern of the array in Figure 15 is an exception to typical patterns that can be achieved using the statistical approach to array design.

The statistical density-taper does not give satisfactory results if the number of elements is too small. Applied to a 25 element linear array 50 wavelengths long, this technique did not produce satisfactory results. From other work[25] the expected peak sidelobes should have been in the vicinity of -8 to -9 db. Therefore a 10 db Taylor amplitude distribution was used as the model for the probability density function.[26] With nine trials, the average number of elements was approximately 25, the expected design value, but the variance was large. The number of elements in the nine trials varied, and the patterns for the extreme cases are sketched in Figure 16 (17 elements) and Figure 17 (37 elements). Figure 18 is a statistically designed array which contains 25 elements. More important, the peak sidelobes in the cases examined were of the order of -5 to -6 db, considerably higher than those obtained with other design methods.

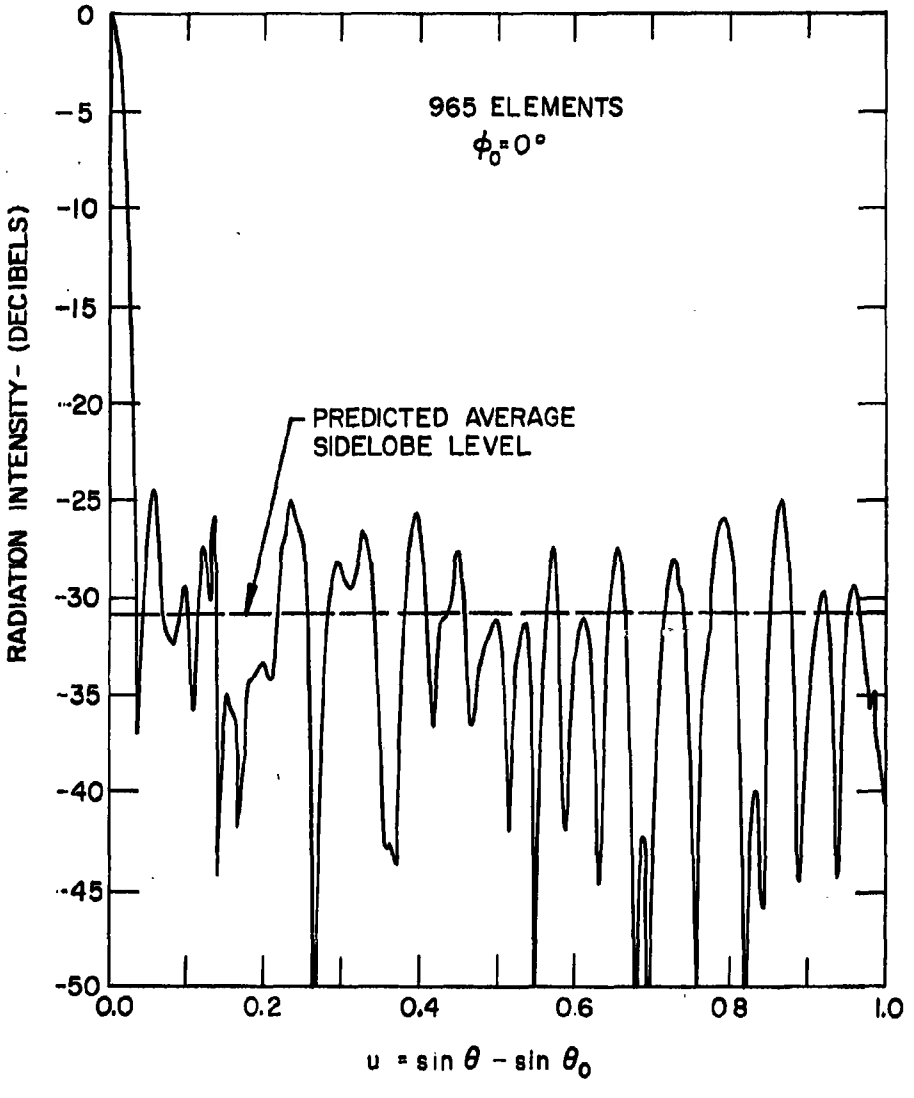

FIG.15 – SAME AS FIG.8 BUT ANOTHER INDEPENDENT DESIGN FOR APPROXIMATELY 90% ELEMENT REMOVAL. $N_R = 965$ ELEMENTS

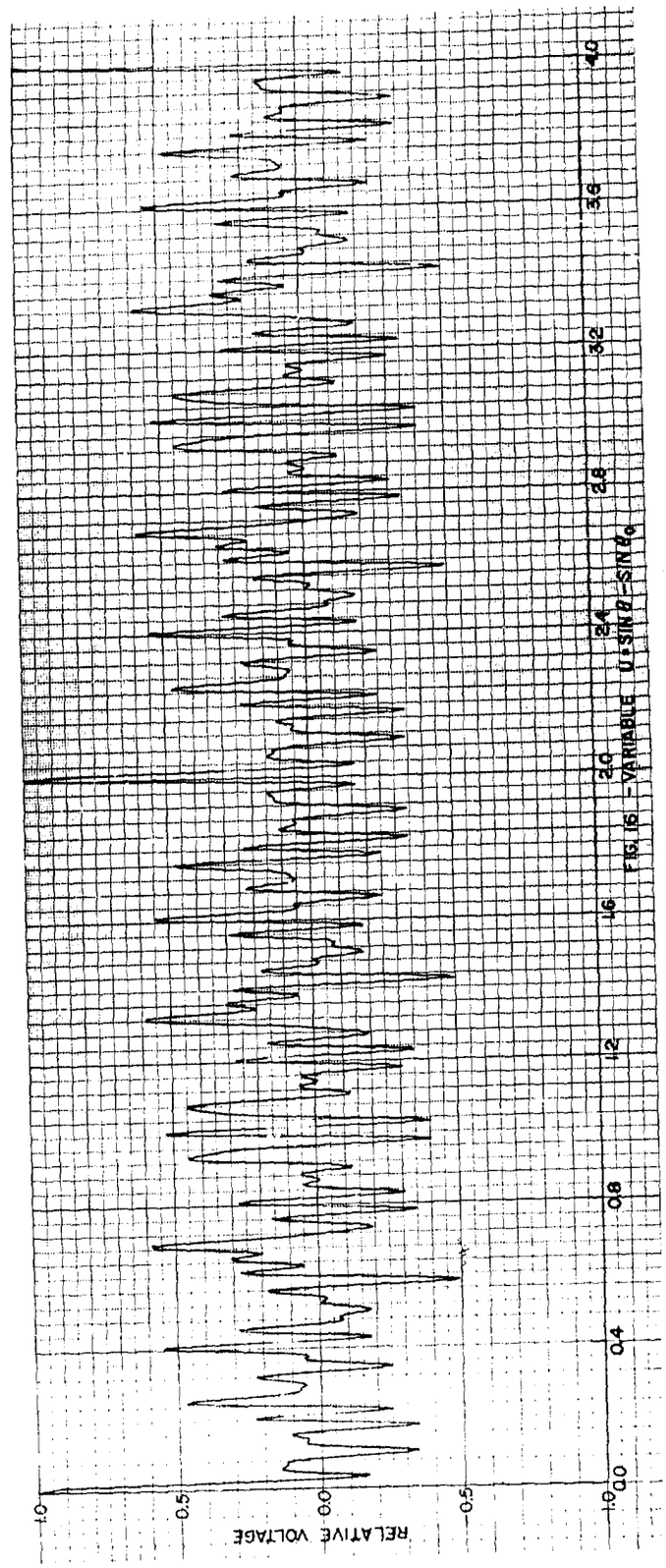
RELATIVE VOLTAGE
-1.0
-0.5
0.0
0.5
1.0
0.0
0.4
0.8
1.2
1.6
2.0
2.4
2.8
3.2
3.6
4.0
FIG. 16 - VARIABLE U•SIN θ - SIN θo

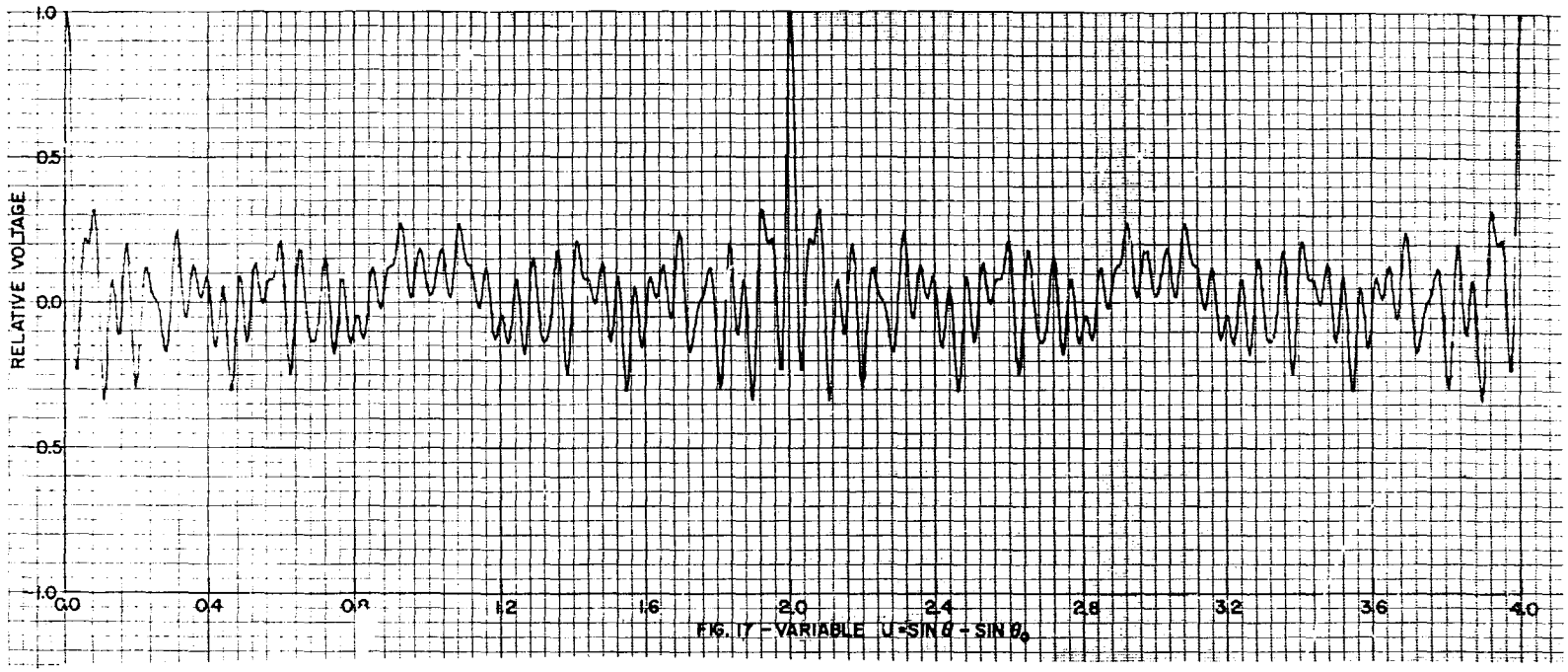

FIG. 17 - VARIABLE $U = \sin\theta - \sin\theta_0$

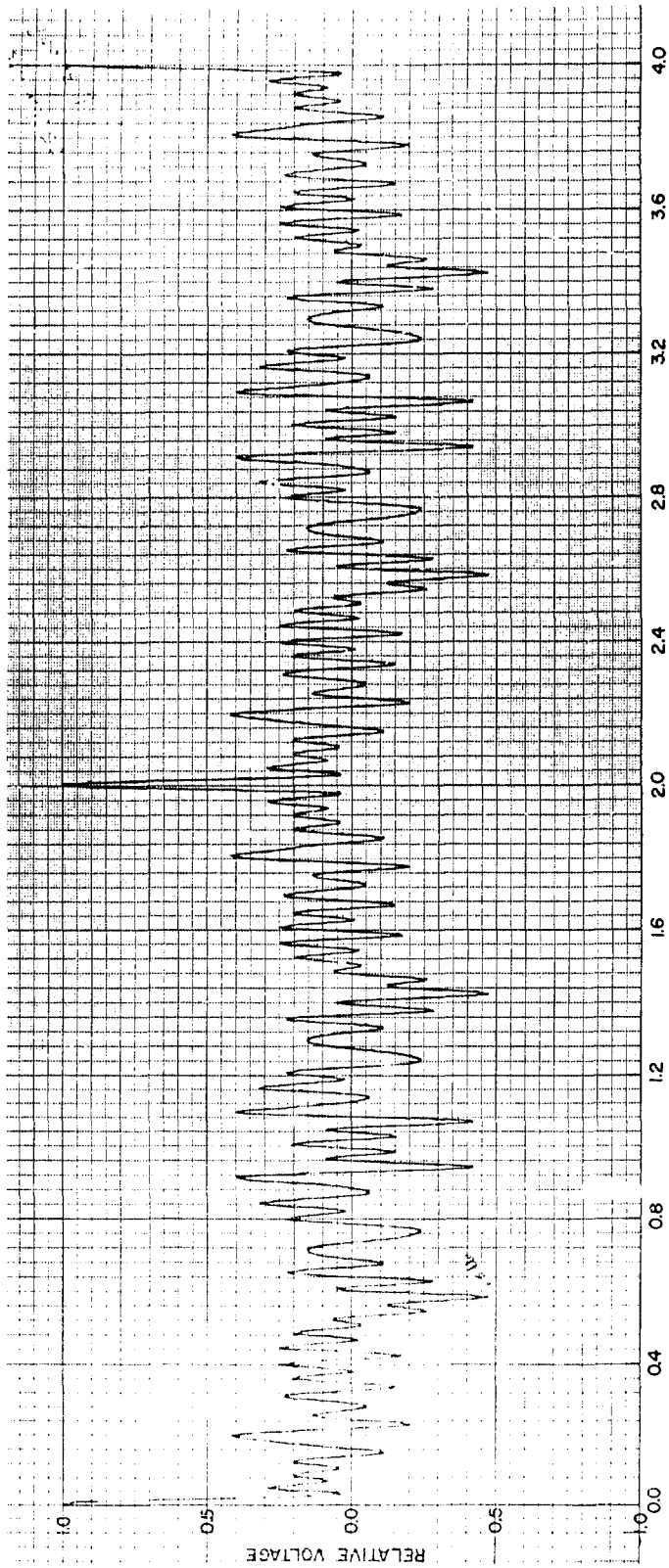

FIG. 18 - VARIABLE $U = \sin\theta - \sin\theta_0$

3.6 Guide Lines

The statistically designed, density-tapered planar arrays reported here depended primarily upon the IBM 7090 computer for determining the element locations. It is not the purpose of this set of guide lines to consider the writing of such a computer program, but instead to point out the overall capabilities of such a technique.

This study included the investigation of thinning large planar arrays (10,000 to 50,000 elements) 30, 50, 70, and 90 percent. Table I indicates the amount of natural thinning for a 10,201 element array using several circular Taylor distributions as a model. The 25 db distribution thins this array more than 50% and the 40 db distribution thins nearly 70%. Thus, if it were required that the array be thinned only 30% it does not seem practical to achieve -25 db (or less) peak sidelobes with the class of model distributions investigated. In natural thinning the probability that an element is located at the center of the array is one, and is less than one for all other regions of the array. If less thinning than the natural amount is required, then the probability is greater than one for the element at the array center. This is the reason 30% thinning has not been achieved using statistical density-tapering techniques for a 10,201 element array.

It has been established that natural thinning in the 10,201 element array will give the model sidelobe level for density-tapering using the 25 and 30 db circular distributions. Furthermore, these arrays may be thinned 70% and achieve the model sidelobe levels. However, it is not possible to achieve the model sidelobe levels under any conditions for the 35 and 40 db cases. This is because the sidelobe levels in density-tapered arrays may be predicted in terms of a statistical average which is beginning to dominate the sidelobe pattern. It is observed from Table II that if the difference between the Taylor design sidelobe level and the predicted statistical average is less than + 7 db, then the sidelobe peaks will not achieve the level of the model distribution. This is an empirical result, and has no firm theoretical basis. It is indicated in Section 8 that a 6 db difference could be expected theoretically between the RMS sidelobe average and the peak sidelobe if the sidelobe region was considered to be a two dimensional sine wave.

All discussion has been concerned with natural thinning in an array of approximately 10,000 elements. If more thinning is required then the probability that an element is in a particular location in the naturally thinned array is multiplied by the constant k in Table I. Thus, varying degrees of thinning may be accomplished. But consideration must always be paid to the statistical average. For example observe that for 90% thinning there is no distribution (25, 30, or 35 db) which has advantage over the other in terms of sidelobes. Compare Figures 8, 10, and 12. This is because their statistical averages are practically the same, and it is this average which dominates the patterns.

These results can be extended to a 50,000 element array by observing that the predicted statistical average sidelobe level is multiplied by N'/N, where N' is the number of elements in the new array. Thus for a 50,000 element array this ratio is 4.90 or 6.9 db. Hence, -6.9 db may be added to this column in Table II. It should therefore be possible to achieve peak sidelobes of around -38 db with a naturally thinned 50,000 element array using this distribution as a model. Reducing the elements 70% should permit sidelobes of around -37 db, and 90% would allow -30 db sidelobes.

3.7 Conclusions

The pseudo random or statistical density-taper array has been shown to be a satisfactory technique for achieving radiation patterns with good sidelobe behavior without the necessity of an amplitude taper across the aperture. The ability to achieve low sidelobes with all elements radiating equal power is an important consequence of this design procedure. The necessary computations for determining element locations can be readily programmed for modern digital computers. Sufficient elements must be employed to obtain good statistical averages and good patterns. Natural thinning results in radiation patterns comparable to that obtained with practical amplitude-tapered aperture distributions. Since the gain of the array is approximately equal to the number of elements remaining, too severe a thinning may not be wise unless the resulting gain reduction can be tolerated.

It is suggested that this technique be considered for the design of large array antennas where good sidelobes are important and where it is not convenient to use an amplitude taper across the aperture.

Design Sidelobe Level Decibels	Percent Elements Removed for Natural Thinning		k (70% thinning)	k (90% thinning)
	w.r.t. Square Aperture	w.r.t. Circular Aperture		
25	54.4	(42)	0.660	0.220
30	60.3	(49.5)	0.795	0.262
35	64.7	(55)	0.850	0.286
40	68.6	(60)	0.955	0.318

TABLE I

Properties Of Taylor Distributions Used In Statistical Array Design

Taylor Design Sidelobe Level (db)	Thinning	Maximum of the 1st Three Sidelobes (db)	Maximum of the Remaining Sidelobes (db)	Predicted Statistical Av. Sidelobe (db)	No. of Elements		Half-power Beamwidth Δu	
					Predicted average	Actual	Taylor dist.	Actual
-25	Natural	-26.0	-31.2	-40.5	4560	4326	0.023	0.022
-30		-29.5	-32.0	-39.6	3970	3773	0.024	0.025
-35		-30.0	-31.2	-39.0	3530	3369	0.025	0.028
-40		-32.0	-32.5	-38.4	3140	3054	0.026	0.028
-25	70%	-25.0	-30.0	-36.8	3000	2835	0.023	0.024
-30		-30.5	-34.0	-37.1	3000	2864	0.024	0.028
-35		-32.0	-33.0	-37.5	3000	2867	0.025	0.028
-25	90%	-23.7	-22.6	-30.4	1000	980	0.023	0.024
-30		-25.5	-22.0	-30.5	1000	979	0.024	0.028
-35		-27.0	-22.0	-30.6	1000	989	0.025	0.028

TABLE II

Summary Of Results

4. THINNING PLANAR ARRAY ANTENNAS WITH RING ARRAYS

Summary

A study has been made of severely thinning planar arrays by removing a large fraction of the elements, but keeping the main lobe width relatively unchanged and maintaining reasonably good sidelobe levels. The amplitude of the signal at each element is assumed constant (no amplitude taper). Peak sidelobes of the order of -24 db are obtained with a 10,000 element array thinned 90 percent (1000 elements remaining). Several approaches have been taken in designing the element configuration to achieve these sidelobes, but all use concentric ring arrays where the elements are placed at the intersection of rings with radials. The behavior of the pattern when the beam is steered off broadside has also been investigated and a slight deterioration of peak sidelobes has been noted.

4.1 The Ring Array Antenna

Consider an array composed of isotropic elements located on concentric rings in such a fashion that there are M rings and N elements per ring (N x M = total number of elements). Equal amplitude signals are assumed at each isotropic element. Let the elements be placed at the intersection of the concentric rings and the radials as sketched in Figure 19. Assuming N to be an even number, the radiation pattern is identical every $360^\circ/N$. This is of advantage since the complete radiation pattern of the array is described by examining only the limited sector $0 \le \phi \le 360^\circ/N$. Also, the symmetry of this arrangement tends to spread the radiated energy more or less uniformly in the ϕ angle. The more radials used (and hence the more elements on each ring) the less the radiation field depends upon ϕ.

Define the principal plane to be that plane passing through element 1, and the z axis. Let the array be steered to some position θ_o, ϕ_o by the insertion of the proper phase at each element. The radiation pattern for this condition may be shown to be

$$E(\theta,\phi) = \frac{1}{MN}\sum_{m=1}^{M}\sum_{n=1}^{N} \exp\left[jkr_m\left\{\sin\theta\cos(\phi_n-\phi) - \sin\theta_o\cos(\phi_n-\phi_o)\right\}\right] \tag{9}$$

where $k = \frac{2\pi}{\lambda}$, λ = wavelength, r_m = radius of m^{th} ring, and $\phi_n = \frac{360^\circ}{N}(n-1)$. This expression can be simplified when the radiation pattern is examined only in the plane in which the beam is steered; that is, when $\phi = \phi_o$. With this assumption and writing $u = \sin\theta - \sin\theta_o$. Equation 10 may be written

$$E(u,\phi_o) = \frac{2}{MN}\sum_{m=1}^{M}\sum_{n=1}^{N/2} \cos\left[kur_m\cos(\phi_n-\phi_o)\right] \tag{10}$$

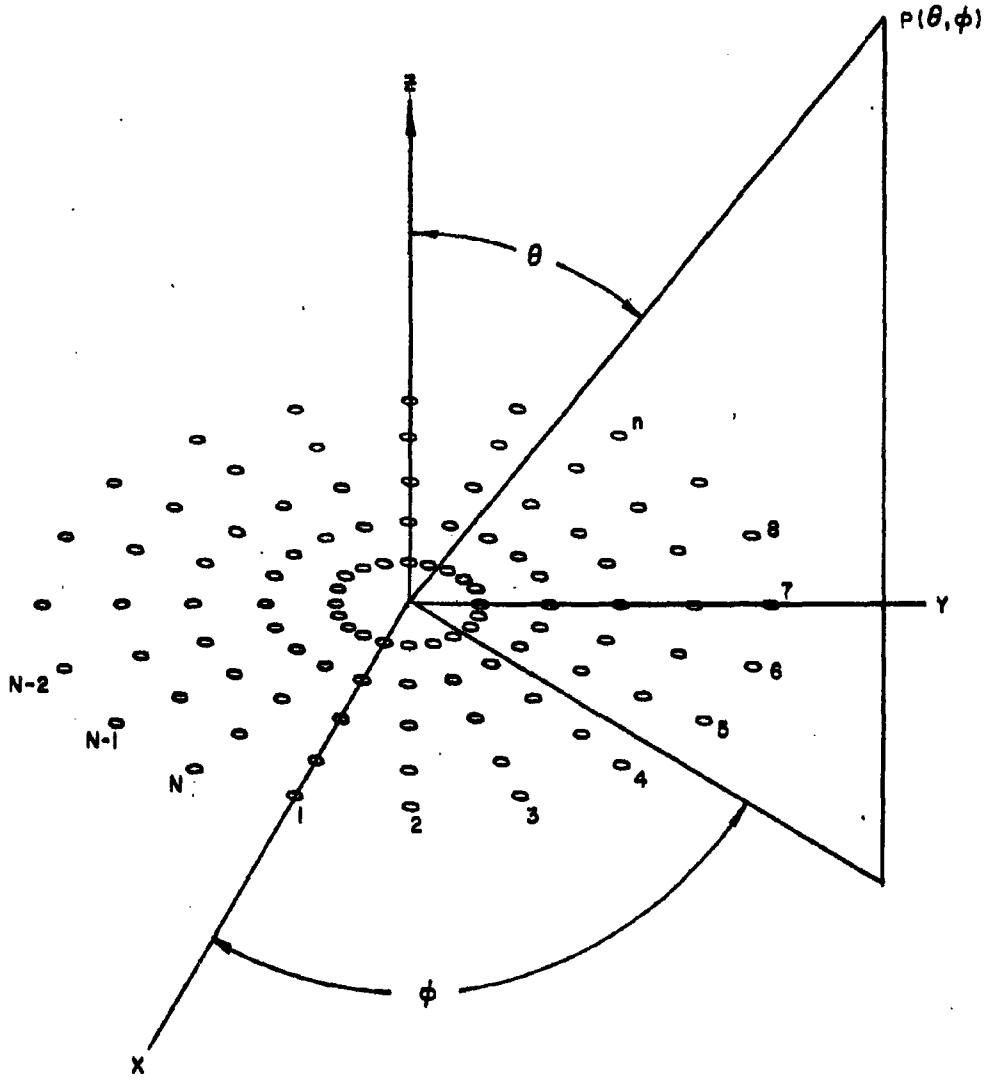

FIG. 19 -ARRAY CONFIGURATION AND COORDINATES

A circular array composed of isotropic elements spaced half a wavelength apart and having a one degree beamwidth requires a diameter of 56 wavelengths. Such an array would require 12,769 elements if arranged on a 113 by 113 rectangular grid. It is the purpose of this study to consider the effects of reducing the total number of elements from 12,769 to approximately 1,000 elements. This corresponds to thinning the array by 92.2%.

4.2 The Uniform Ring Array

Consider a uniform ring array composed of concentric rings with equal spacing between the rings and equi-angular radials. It is required to place 1,000 elements in a 56λ diameter circle and maintain at least a half wavelength spacing between all elements. If 36 elements are located symmetrically on each ring then 28 rings result in a total of 1,008 elements. The choice of 36 elements per ring was based on two factors. First, the radiation pattern will repeat every 10°, so that only a small portion of the total radiation pattern must be investigated in order to have it described fully. Second, the half wavelength condition will not allow rings near the array center so that for 36 elements per ring the minimum radius is three wavelengths. Thus, a compromise is made between the minimum allowed ring radius and the number of elements per ring.

For the rings spaced with equal separation the number of elements as a function of distance from the array center is roughly proportional to the radius, whereas the physical area is proportional to the radius squared. Thus there is a natural density taper of elements within the array which is inversely proportional to the radial distance, r. This density taper should help reduce the 17.6 db first sidelobe found with a conventional circular antenna array when each element radiates identical energy.

For the 56λ diameter array composed of 28 rings, the separation between rings was 28/31 wavelength. The inner most ring had a diameter of 4(28/31) wavelengths. With equal spacing between rings Equation 10 can be conveniently reduced to a single summation by using Lagrange's Identity.[33]

The radiation intensity $|E|^2$ for the uniform ring array just described was determined for ϕ_o equal to 0° and 5° and is shown in Figures 20 and 21. Table III gives the null half-width (distance between main beam maximum and first null), 3 db half-width, and the peak sidelobe in several regions of u for these patterns as well as all other patterns discussed here. These values may be compared to a uniformly radiating circular aperture which would have a null half-width $u_n = 0.022$, a 3 db half-width of $u_{3db} = 0.009$, and a peak sidelobe of 17.6 db adjacent to the main beam. Comparing Figures 20 and 21 it is seen that the overall level of sidelobes in the plane between the radials is considerably lower, but the peak sidelobe value is not changed significantly. If the

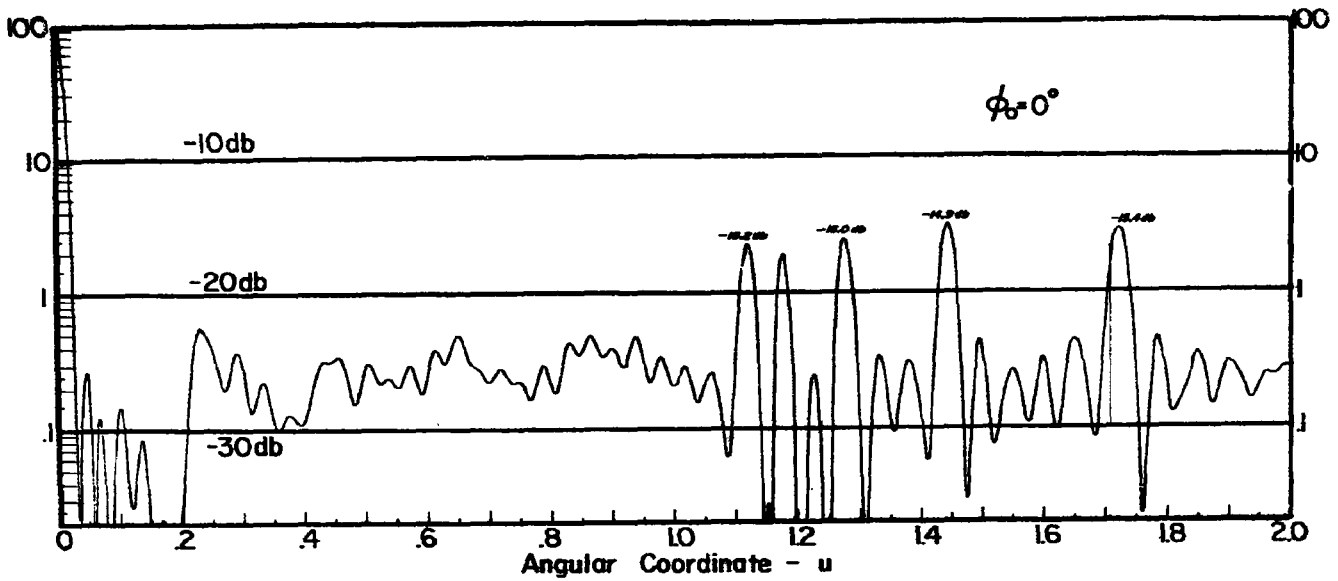

FIG.20-PATTERN OF EQUALLY SPACED RINGS (ϕ_o=0°)

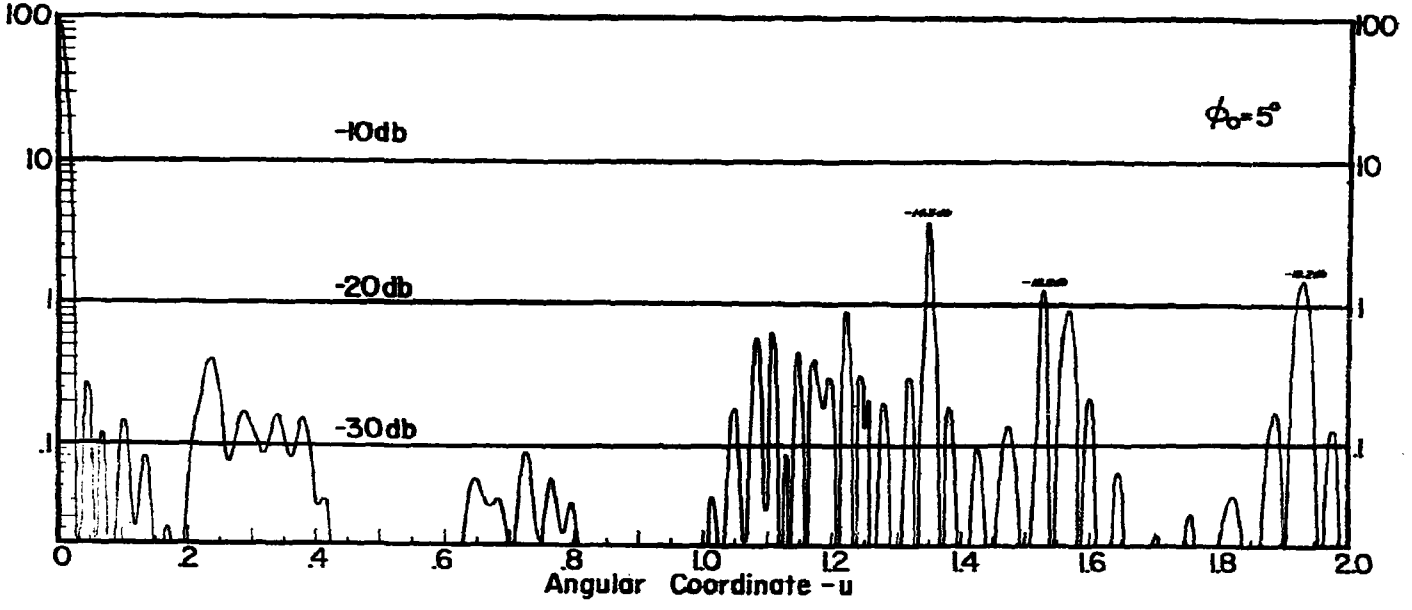

FIG.21-PATTERN OF EQUALLY SPACED RINGS (ϕ_o=5°)

array is steered in either the $\phi = 0^{\circ}$ or 5° plane, the sidelobes in the region $u > 1$ will apear. The higher sidelobes occurring for $u > 1$ are undesirable and the remaining discussion will be concerned with reducing the high sidelobes in this region.

4.3 Space Tapering Ring Arrays

In order to further reduce the peak sidelobes encountered in the pattern of the uniform ring array, the technique of space tapering[12, 14, 16] was investigated. Space tapering or density tapering consists of spacing the rings so that the density of rings has the same variation as the amplitude variation across the aperture of a conventionally designed array. In this study the various circular distributions of Taylor,[21] as computed by Hansen,[22] have been utilized as models for the density distribution.

A brief description of how the radius of each ring is determined is necessary. A cumulative distribution of the amplitude taper of interest is sketched as a function of radius (abscissa) of the ring array. By dividing the cumulative distribution into M equal parts (M being the number of rings), the radii of the rings are found by projection from the cumulative distribution to the abscissa.[14] There are several practical conditions that must be considered. First, it is desired that the element separations be at least a half wavelength. Second, the ring array has a "built-in" space taper varying approximately as $1/r$. To compare the effect of ignoring the $\lambda/2$ minimum separation in a ring array, patterns were computed for a 35 db Taylor distribution with and without this condition. These patterns are sketched in Figures 22 and 23. In both cases the natural $1/r$ taper of the array has been ignored. The $\lambda/2$ condition which has been imposed in Figure 22 introduces a hole of 3λ radius at the center of the array. In Figure 23, where no such condition was applied, the beam is broadened considerably due to the large density of elements at the center. The actual radii of the rings for all cases are given in Table IV.

Figure 24 seeks to illustrate the effect of accounting for the $1/r$ natural space taper. This is a sketch of the same 35 db Taylor distribution used in Figure 22 with compensation made for the natural radial taper. The sidelobes adjacent to the main beam are considerably lower than the two previous cases. This is to be expected although the first sidelobe is only 32 db down with the next two 35 db below the main beam. There is no significant difference in the level of peak sidelobes when the ring array is not steered ($0 < u < 1$). An interesting consequence of imposing these conditions is that if the $\lambda/2$ condition is ignored, but correction is made for the $1/r$ taper then all elements naturally space themselves at least $\lambda/2$ apart for the 35 db distribution.

Upon comparing these three patterns several conclusions may be reached. The very broad main beam of Figure 23 signifies that it is unwise to pack too many elements near the center. The imposing

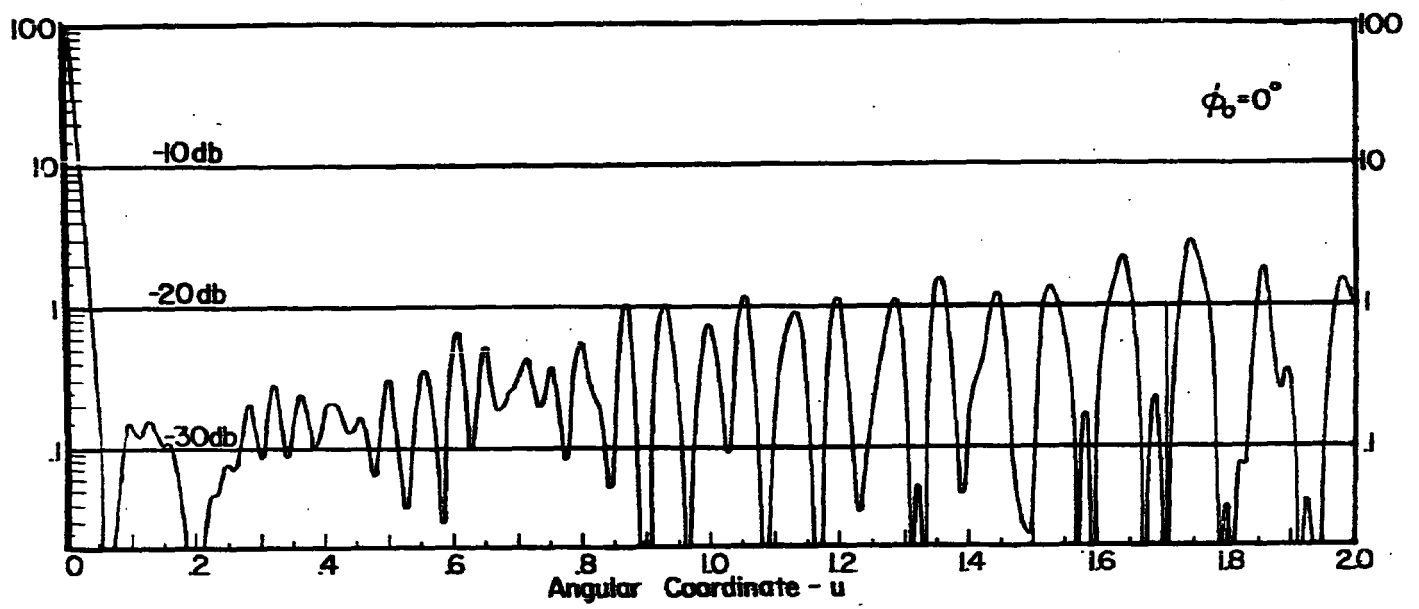

FIG.22-PATTERN WITH RINGS MATCHING AT 35 db TAYLOR DISTRIBUTION ($\lambda/2$ IMPOSED; RADIAL TAPER IGNORED). $\phi_o = 0°$

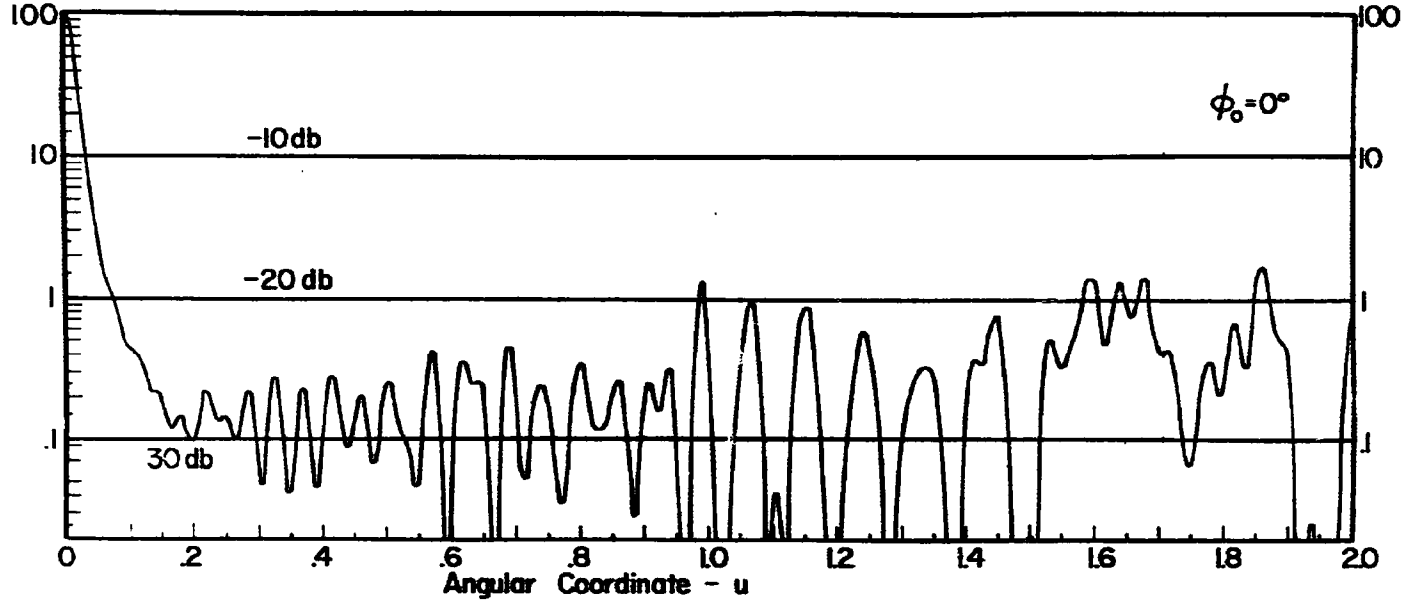

FIG.23-PATTERN WITH RINGS MATCHING AT 35 db TAYLOR DISTRIBUTION ($\lambda/2$ IGNORED). $\phi_o = 0°$

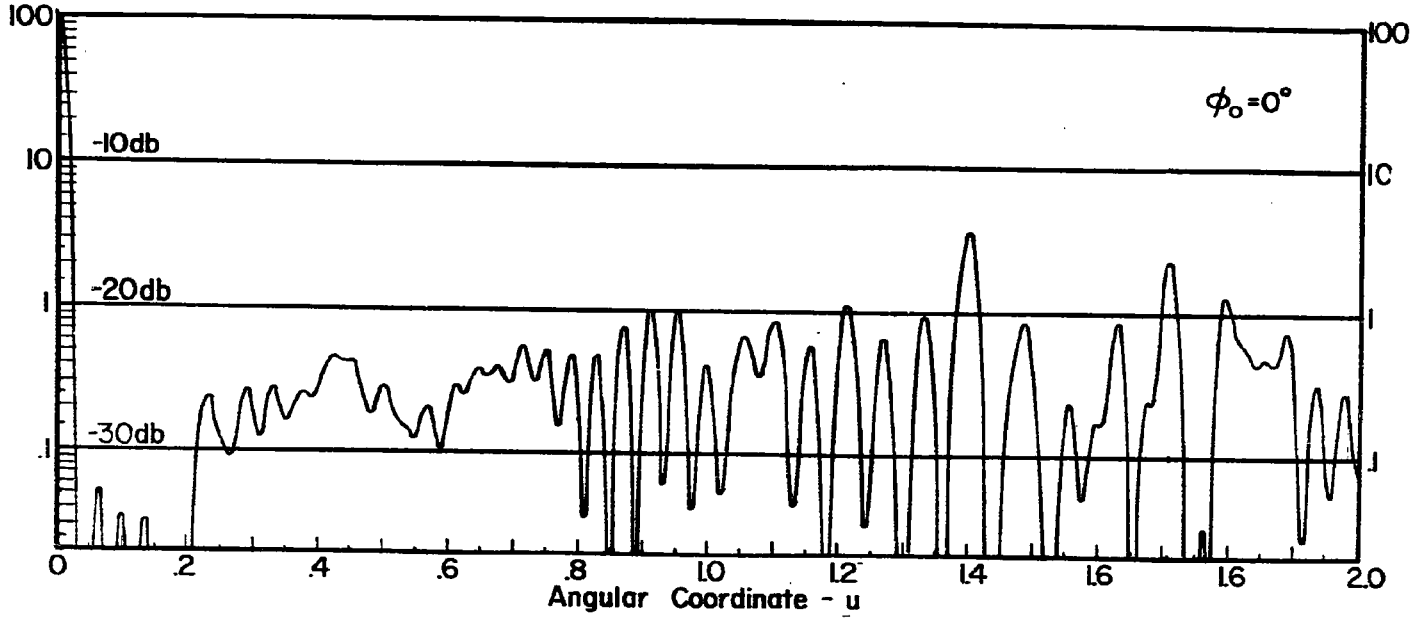

FIG.24-AS FIGURE 22, BUT COMPENSATION MADE FOR RADIAL TAPER (ϕ_o= 0°)

of the $\lambda/2$ condition is not only necessary as a practical condition but the peak sidelobe values are better. These results suggest that the $1/r$ natural taper due to the polar coordinates can be ignored in succeeding ring arrays, but the $\lambda/2$ condition is imposed.

It is readily observed that even though a space taper was made to a 35 db Taylor distribution, the peak sidelobe level is considerably higher than the design value. There appears to be very little correlation between the radiation pattern of the space taper distribution and the radiation pattern of the amplitude taper design used as a model, even for the sidelobes adjacent to the main beam. This suggests that the space taper is too severe for the number of elements being used. (Section 8 indicates that the peak sidelobe level is of the order -10 log MN/4.) A lower sidelobe level is obtained with a 30 db Taylor distribution rather than the 35 db design as indicated by the pattern in Figure 25. A very slight improvement is obtained in the visible region, but several db of improvement is obtained in the region $1 \leq u \leq 2$.

4.4 Increasing the Number of Radials

In general it is desirable to minimize the variations in the peak sidelobe levels as a function of ϕ. This variation was shown by comparing the $\phi_o = 0^o$ and $\phi_o = 5^o$ in Figures 20 and 21. If the total number of elements is kept constant, but the number of radial positions increased, then elements will not be available at every possible intersection of rings and radials, but they can be located more symmetrically in the ϕ angle. Figure 26-a is the normal position of elements and Figure 26-b shows every fourth ring using the same radial so as to generate spiral arms.

The increase in the number of available element positions by using more radials may be regarded as a rotation of each ring by a fixed amount with respect to the previous ring, and hence is described as the ring rotation technique. On any given ring the elements still remain separated by an amount $\phi_n = \frac{360^o}{N}(n-1)$. But when going from the m^{th} ring to the $m^{th}+1$ ring there occurs a rotation which depends on the additional radials being used. For the case of every fourth ring using the same radial, the rotation is 2.5^o if $N = 36$. A slight modification is required in Equation 10 to allow for the ring rotation technique, which introduces an angle ϕ_m dependent on the radial position. Equation 10 is modified so that

$$E(u, \phi_o) = \frac{2}{MN} \sum_{m=1}^{M} \sum_{n=1}^{N/2} \cos\left[kur_m \cos(\phi_n + \phi_m - \phi_o)\right] \qquad (11)$$

All quantities are defined as previously and $\phi_m = mp$ where $p = 2.5^o$ for every fourth ring using the same radial.

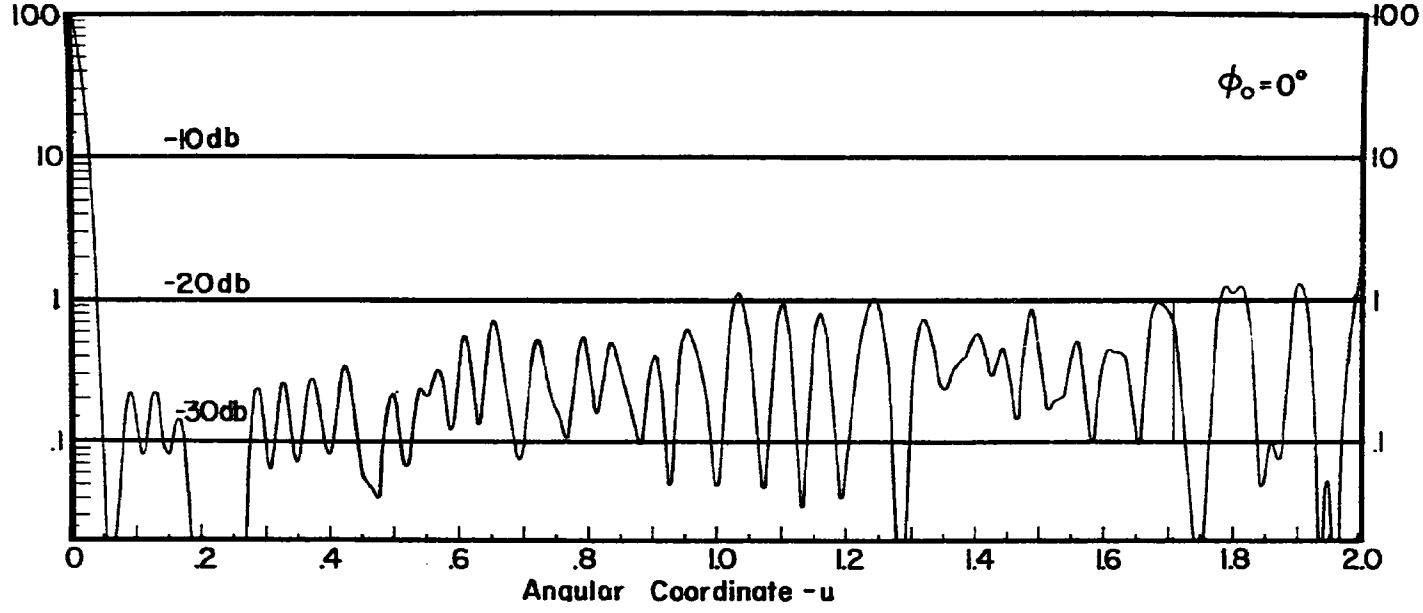

FIG.25-PATTERN WITH RINGS MATCHING AT 30 db TAYLOR DISTRIBUTION ($\phi_o = 0°$)

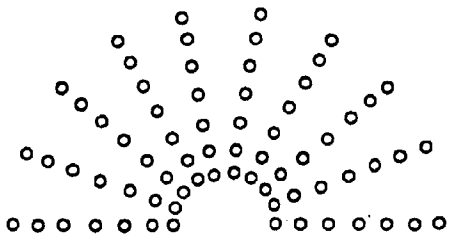

a. NORMAL GRID

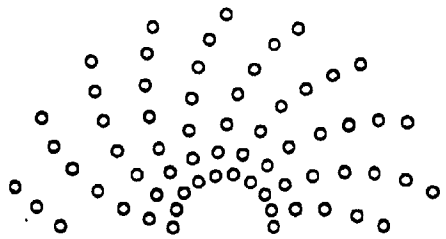

b. EVERY FOURTH RING
USING THE SAME
RADIAL.

FIG.26- ARRAY GRIDS

The 35 db Taylor distribution as used in Figure 22 also has been used to illustrate the ring rotation technique. Only two values of ϕ_o ($\phi_o = 0^\circ$ and 5°) are shown although the patterns at intermediate angles have been explored more fully. Figure 27 is a sketch of the pattern for the array of Figure 22 but with $\phi_o = 5^\circ$. Figures 28 and 29 are the patterns for $\phi_o = 0^\circ$ and 5°, respectively, of the ring rotation technique where $p = 2.5^{\circ\circ}$. The ring radii are the same as those used in Figures 22 and 27. The average sidelobe levels of these two values of ϕ are more nearly uniform and the peak sidelobes of the pattern are better than those shown in the previous figures. Figure 29, for $\phi_o = 5^\circ$, contains the highest sidelobe of the group of patterns computed for this array.

The most uniform distribution of energy as a function of ϕ should occur when every 28^{th} ring uses the same radial ($p = 0.35714^\circ$). Such a computation was made for the 35 db Taylor distribution with the $\lambda/2$ condition imposed. The radiation patterns for $\phi_o = 0^\circ$ and 5° are sketched in Figures 30 and 31, respectively. This array has a peak sidelobe of -21.7 db, although it does not occur in either of these two planes.

It is seen that the ring rotation technique reduces the peak sidelobe levels. The 35 db Taylor distribution ultimately gave the "best" pattern with respect to sidelobe peaks when used with the ring rotation method (better than the 30 db Taylor distribution even though with no rotation the overall pattern of 30 db Taylor was slightly better than the 35 db case).

4.5 Applicability of Thinned Ring Arrays

The type of antenna described here has all the advantages and disadvantages of any thinned array. Its gain is approximately equal to the number of elements. One of the advantages of a polar grid configuration of elements is the symmetry obtained in the radiation pattern. If such an array is to be steered in angle, a phase shifter must be applied to each element. However, there is no convenient relationship between the phases at each element as it is in a conventional array located on a rectangular grid. Thus there must be applied to each element a separate phase-command signal to steer the beam in angle. This is not as convenient as beam steering in a conventional array.

It is possible, however, to maintain the advantages of a ring array configuration and have the ease of steering that is characteristic of a rectangular grid by projecting the elements of the ring to the nearest intersection of a half wavelength rectangular grid.

The ring array antenna design of Figure 30 was used as the model for projecting onto the nearest half wavelength grid configuration. The patterns of this array for $\phi_o = 0^\circ$ and 5° appear in Figures 32 and 33. There is little difference in the peak sidelobes and the patterns are quite

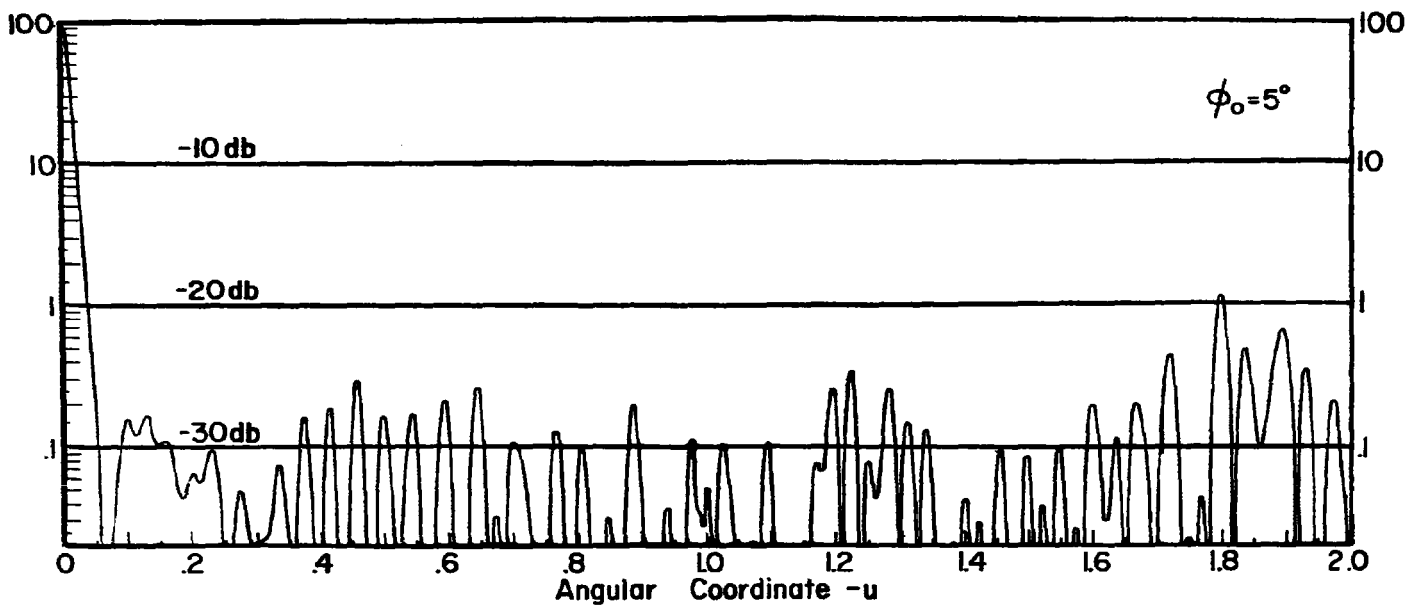

FIG. 27-AS FIGURE 22, BUT ϕ_o= 5°

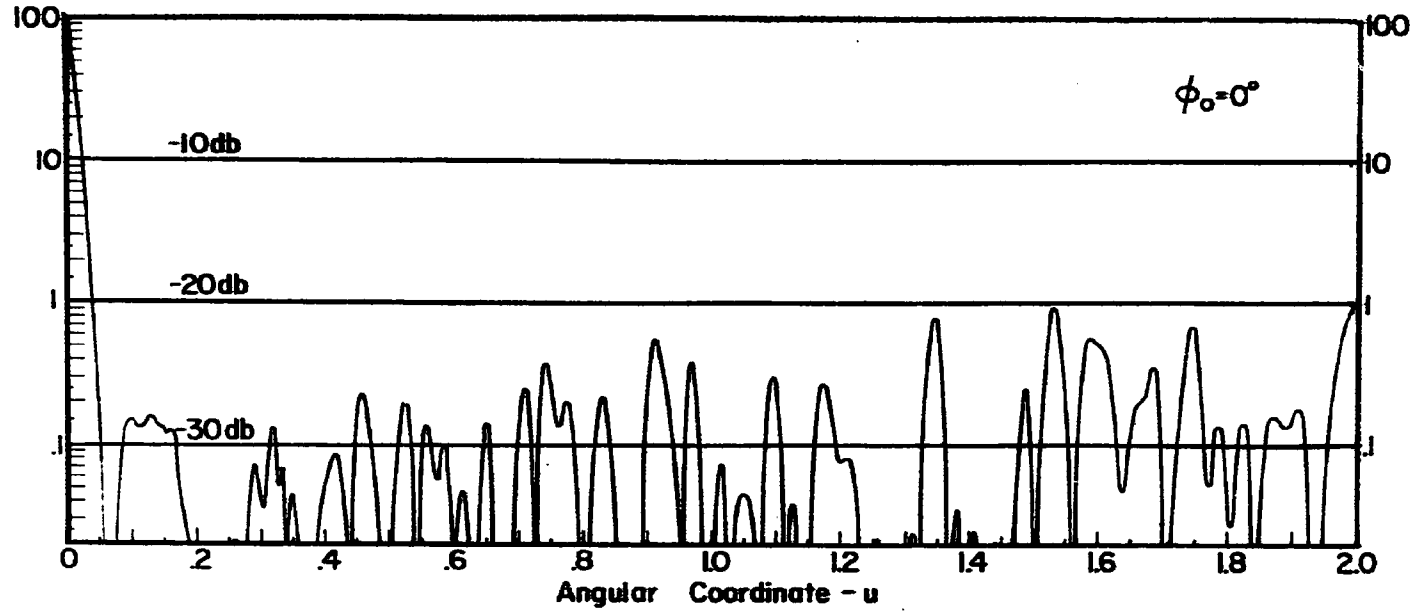

FIG.28-AS FIGURE 22, BUT EVERY FOURTH RING USING THE SAME RADIAL (ϕ_o=0°)

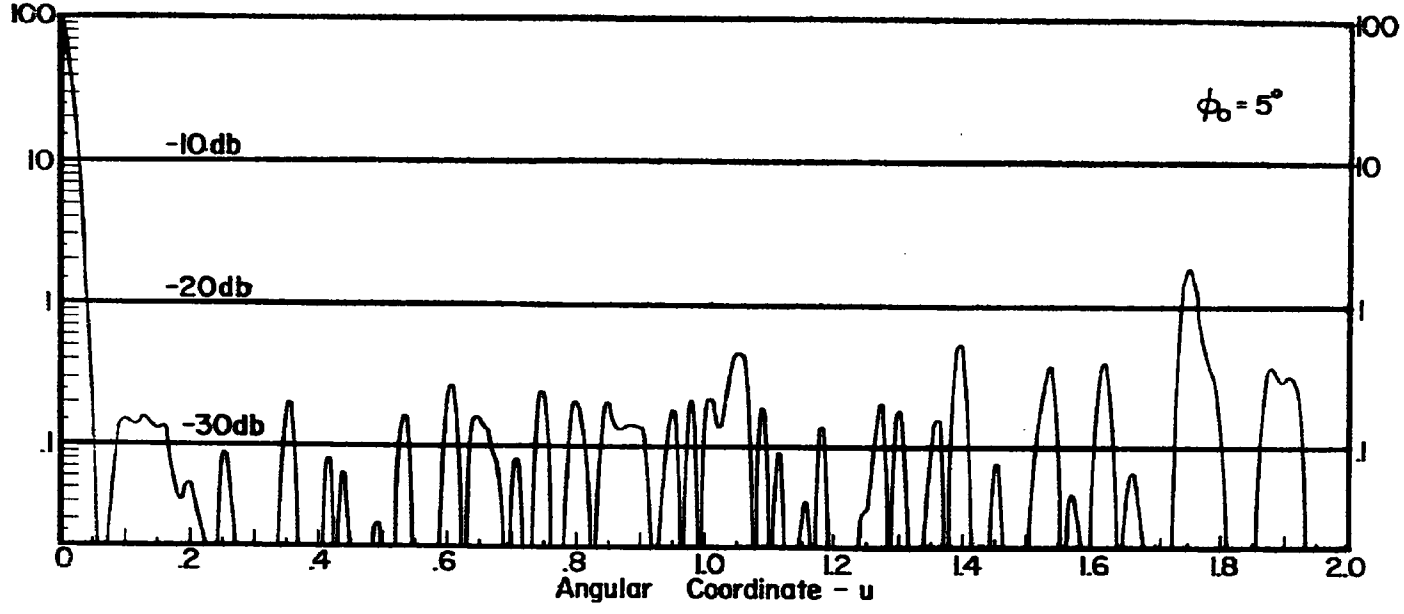

FIG.29-AS FIGURE 28, BUT $\phi_0 = 5°$

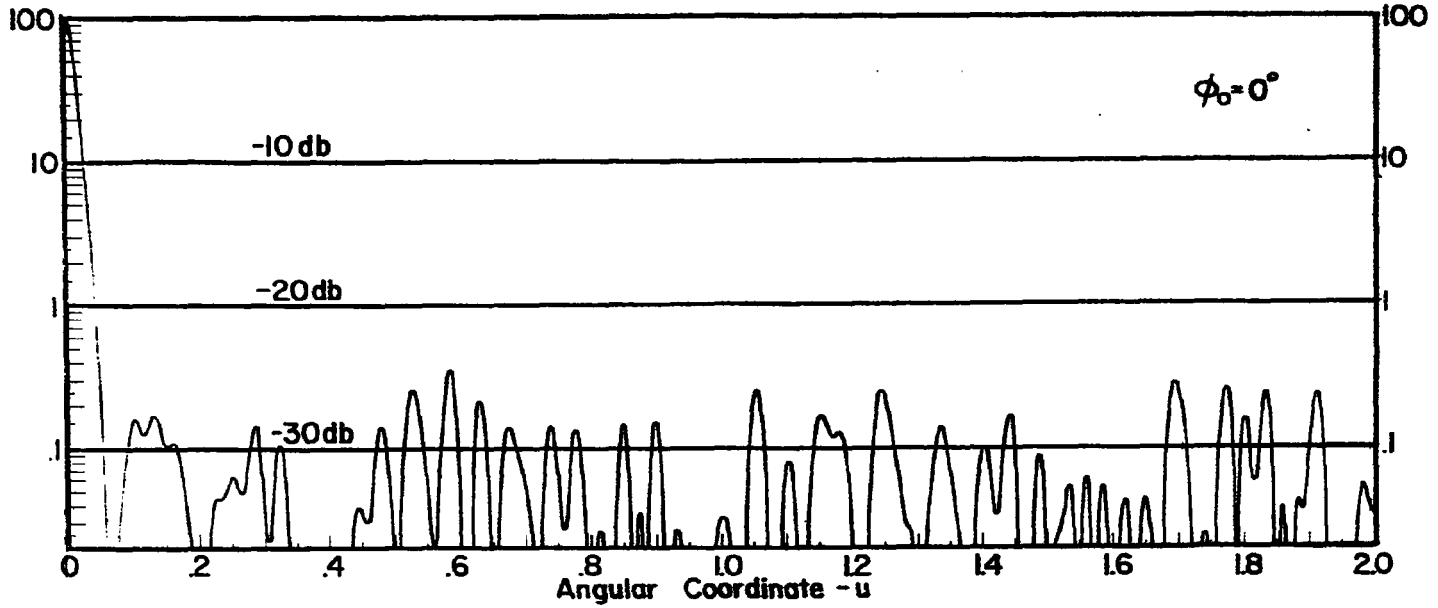

FIG.30- AS FIGURE 22, BUT EVERY 28th RING USING THE SAME RADIAL. ($\phi_o = 0°$)

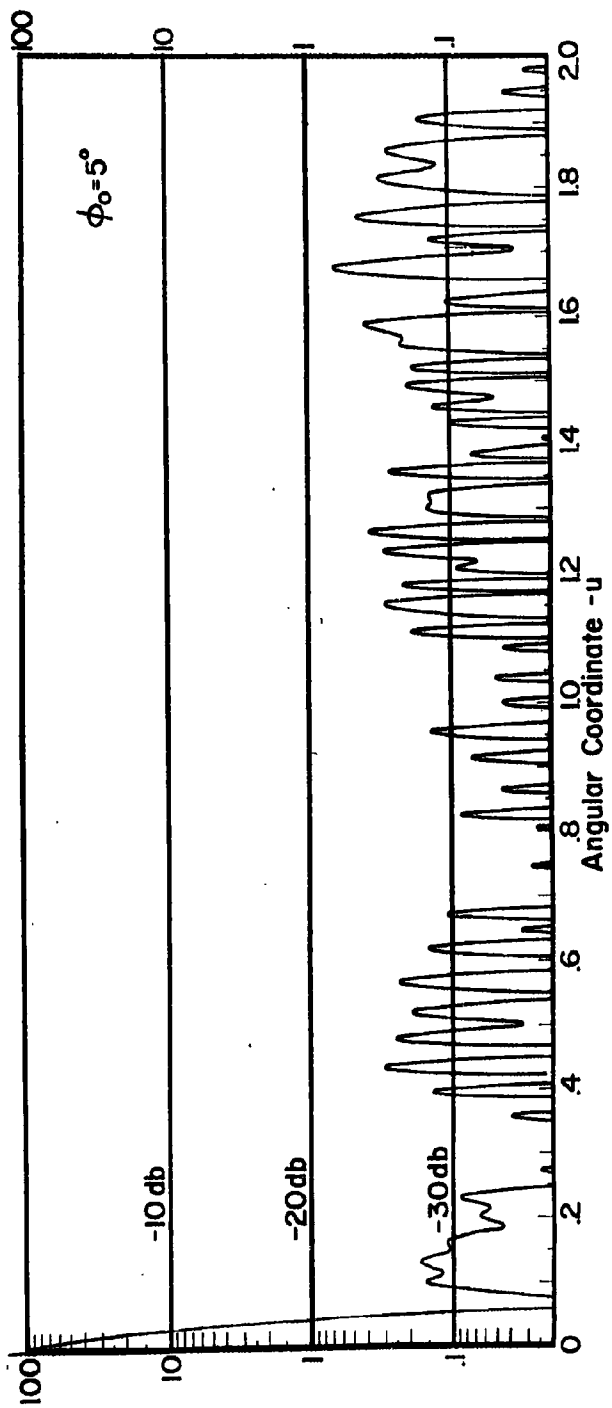

FIG. 31 – AS FIGURE 30, BUT $\phi_o = 5°$

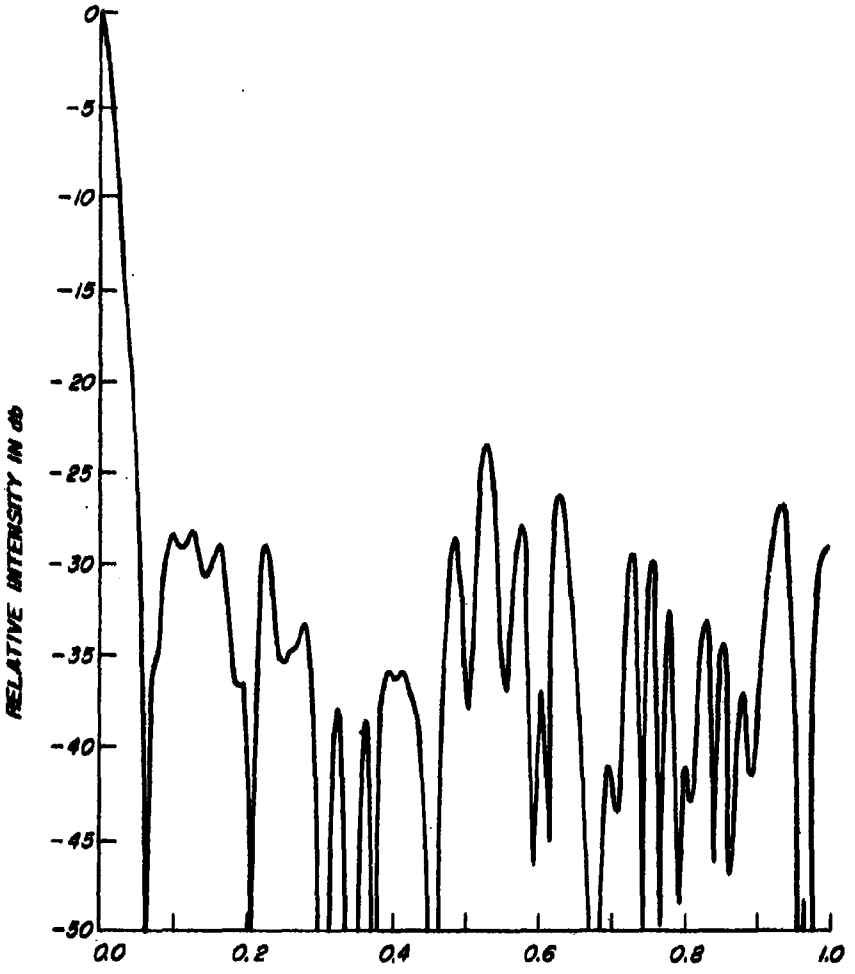

FIG.32-35 db ROTATED RING ARRAY DISPLACED TO NEAREST $\lambda/2$ POSITION ($\phi_o = 0°$)

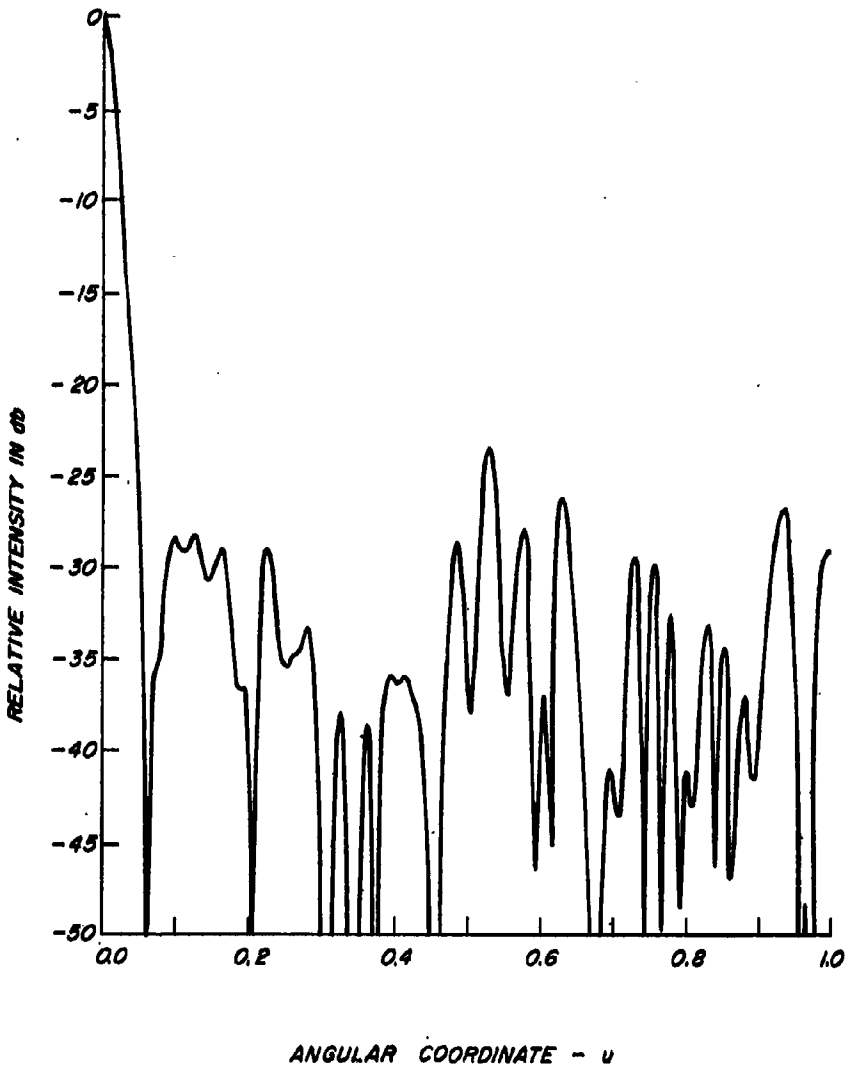

FIG.32-35 db ROTATED RING ARRAY DISPLACED TO NEAREST $\lambda/2$ POSITION ($\phi_o = 0°$)

similar in the vicinity of the main beam. In the $\phi_o = 0^\circ$ case the peak sidelobe is -24.4 db for the ring array and -23.5 db for the ring array displaced to a $\lambda/2$ grid. However, in the $\phi_o = 5^\circ$ case the situation is reversed with the ring design having a peak sidelobe of -21.8 db and the $\lambda/2$ grid is estimated to be around -24 db. It appears that the shift to the $\lambda/2$ rectangular grid can be made with no detrimental affect on the radiation pattern. Because of symmetry the pattern in the plane $\phi_o = 90^\circ$ is also that of Figure 32, and furthermore, the patterns in the $\phi_o = 10^\circ$, 20°, etc., plane are essentially the same as the sketch in Figure 32. Figure 33 is very similar to the patterns of the $\phi_o = 15^\circ$, 25°, etc., planes. Thus, the sidelobe structure should be very good even when the array is steered but obviously a grating lobe will appear when the array is steered $\pm 90^\circ$ in the principal planes. However, practical arrays are seldom steered more than $\pm 60^\circ$.

The patterns reported here were described for an aperture diameter of 56λ and with beam steering to $\pm 90^\circ$. These patterns also may be applied to an unsteered 112λ diameter array, or to any size array up to this value. For example, the patterns apply for a diameter of 74λ steered $\pm 30^\circ$, if the ring radii are multiplied by 1.33. When the patterns are used for an array having a diameter less than 56λ, some of the element spacings are less than $\lambda/2$.

4.6 Guide Lines

Section 9 discusses the array modeling technique and includes patterns of statistically designed arrays. Also included is the pattern of a ring array containing 144 elements where normally there would be 10,000 elements. The beamwidth is essentially that of a 50λ diameter planar array, so that for the number of elements in the array, it has good resolution. The -12.5 db maximum peak sidelobe is approximately that expected on the basis of Section 8. The point of emphasis is that this array was designed quickly without the use of a computer using a very simple set of guide lines which are:

1) Let the diameter and number of elements be fixed;

2) Decide in what increments of ϕ the pattern is to be symmetrical (10° appears to give satisfactory results here);

3) The number of increments of ϕ divided into the total number of elements determines the number of rings;

4) The total number of elements roughly determines the peak sidelobe level according to $-10 \log N/4$, where N is the total number of elements;

5) The innermost ring diameter is determined by investigating the effect of a hole on the pattern of a continuous, uniformly illuminated aperture of the same size as the

diameter of the ring array. Allow the diameter of this hole in the aperture to be of such size as to cause the sidelobes adjacent to the main beam to take on the value of -10 log N/4. That is

$$\frac{D_o^2}{D^2} = \frac{1}{10 \log N/4} ,$$

where D_o is the hole diameter and D the diameter of the array. The effect of the hole is discussed in Section 5.3 of Technical Note No. 2.[28] For the 144 element array $D_o \approx 12.6\lambda$. A value for $D_o = 14\lambda$ was used in this array.

6) The remaining rings are spaced equally between D_o and D at diameters of 26λ, 38λ and 50λ for the 144 element array.

If this array were a continuous, uniformly illuminated aperture then a peak sidelobe of -11.6 db would be expected. Some improvement over this was obtained, and is due to the 1/r natural taper previously discussed in this section. In addition to these guide lines, the minimum spacing between elements can change the diameter of the innermost ring. The 1008 element ring arrays were so designed that the innermost ring diameter depended solely on the minimum element spacing. It is now believed that these patterns can be improved slightly by increasing the diameter of the concentric rings nearest the array center.

4.7 Conclusions

The design of antenna arrays by using a polar coordinate configuration for element placement is a straight-forward technique for designing thinned arrays with reasonable sidelobe levels. The results achieved for a 90 percent thinned array are approximately those predicted theoretically. The peak sidelobe predicted is around -24.5 db. In the best array design the highest sidelobe found in the entire radiation pattern examined was -21.7 db, although the highest sidelobe found in the principal planes (or every 10^o from the principal planes) was -24.4 db.

Figure No.	Null Half Width	3 db Half Width	Peak Sidelobe in db Below Main Beam Over the u Region		
	Δu_o	Δu_{3db}	$0 \leq u \leq 1$	$1 \leq u \leq 1.707$	$1.707 \leq u \leq 2$
20	0.030	0.011	-22.6	-14.9	-15.4
21	0.030	0.011	-24.0	-14.3	-18.2
22	0.055	0.012	-19.8	-18.0	-15.4
23	0.124	0.015	-18.8	-18.7	-17.8
24	0.060	0.010	-20.0	-14.4	-16.4
25	0.054	0.015	-21.3	-19.6	-18.8
27	0.057	0.012	-25.2	-24.6	-19.5
28	0.061	0.011	-22.6	-20.3	-20.2
29	0.061	0.012	-25.7	-23.3	-17.3
30	0.058	0.012	-24.4	-25.3	-25.8
31	0.058	0.012	-25.0	-21.8	-23.5
32	0.059	0.012	-23.4	-23.4	Grating Lobe
33	0.059	0.012	-24.1	Not Calculated	

TABLE III

Parameters Of Array Radiation Patterns

Figure	r_1	r_2	r_3	r_4	r_5	r_6	r_7	r_8	r_9	r_{10}	r_{11}	r_{12}	r_{13}	r_{14}
22, 27, 28 29, 30, 31	3.00	3.53	4.06	4.59	5.13	5.68	6.24	6.81	7.39	7.98	8.58	9.19	9.81	10.45
23	0.63	1.26	1.89	2.52	3.15	3.78	4.41	5.04	5.67	6.30	6.93	7.56	8.23	8.93
24	3.00	4.48	5.60	6.65	7.56	8.47	9.31	10.08	10.78	11.51	12.25	12.99	13.69	14.42
25*	3.0	3.5	4.0	4.5	5.0	5.5	6.0	6.5	7.0	7.5	8.0	8.5	9.0	9.5

Figure	r_{15}	r_{16}	r_{17}	r_{18}	r_{19}	r_{20}	r_{21}	r_{22}	r_{23}	r_{24}	r_{25}	r_{26}	r_{27}	r_{28}
22, 27, 28 29, 30, 31	11.12	11.83	12.58	13.38	14.23	15.14	16.11	17.15	18.34	19.66	21.21	23.04	25.20	28.00
23	9.66	10.42	11.22	12.07	12.98	13.95	15.00	16.14	17.38	18.73	20.33	22.40	24.78	28.00
24	15.15	15.90	16.69	17.50	18.31	19.18	20.09	21.07	22.12	23.17	24.36	25.55	26.85	28.00
25*	10.0	10.5	11.1	11.7	12.3	13.0	13.8	14.6	15.5	16.5	17.7	19.2	21.2	28.0

* These spacings were not determined by the cumulative distribution technique, but were done by integration of the area under the 30 db Taylor Distribution. It is not as accurate as the cumulative method, and is considered more difficult.

TABLE IV

Ring Radii

5. DYNAMIC PROGRAMMING APPLIED TO UNEQUALLY SPACED ARRAYS

Summary

The application of the optimization technique known as dynamic programming to the design of "thinned" arrays with unequally spaced elements is described. Dynamic programming is a systematic procedure for efficiently utilizing the capabilities of modern high speed digital computing machines to find optimum solutions to problems not computationally feasible by conventional means. It is applied to the design of linear arrays of 25 elements spaced within a 50 wavelength aperture. The results obtained are compared with similar results found with other design techniques and are shown to be significantly better. The effect on the sidelobes of varying the angular region of optimization and the spacing - quantization is also explored.

5.1 Introduction

This section describes the application of the optimization technique known as dynamic programming to the design of thinned array antennas. A thinned array is one in which the number of elements is significantly less than a conventional array with elements spaced every half wavelength. The latter is sometimes referred to as a filled array. If the elements of a thinned array are equally spaced, grating lobes are produced with peak intensities equal to that of the main beam. These grating lobes are objectionable in many applications. To suppress them and to maintain low sidelobes throughout the pattern the elements must be spaced unequally. Dynamic programming is a systematic procedure for efficiently utilizing the capabilities of modern high speed digital computing machines to find optimum solutions to problems not solvable by conventional means. It is used here to determine the optimum configuration of element spacings for achieving a desired radiation pattern.

Dynamic programming is related to the trial and error conputational techniques that utilize digital computers as an important tool in obtaining the desired results economically. It differs, however, from other reported work in that it does not start with an a priori set of spacings, but builds up the design one element at a time. It is an iterative procedure which will converge to the desired spacings determined by the particular criterion programmed into the computer by the designer. This method is based on the optimization procedure first advanced by Richard Bellman[29] and widely employed in Operations Research.

A brief, qualitative description of dynamic programming and its application to unequally-spaced array antennas is given. This is followed by the results for 9-element and 25-element linear arrays. The dynamic programming results are compared with those of other

unequally-spaced-array design techniques. A more detailed description of the mathematics of dynamic programming as applied to the design of linear arrays is given in Appendix II.

It is assumed here that the purpose of an unequally spaced array is to obtain the beamwidth associated with the maximum aperture dimension without the total number of elements required in the filled array. The object in design is to control the sidelobe radiation so as not to produce objectionably high lobes.

5.2 Description

One possible method for designing an array with unequal spacings is total enumeration. In this approach all possible combinations of spacings are examined, the radiation pattern is computed for each combination, and the one which yields the best pattern is selected. Although it is possible in principle to carry out such a brute-force procedure, it is generally not practical to do so except in the simplest of cases. If each of the N elements of an array can occupy any one of m possible positions within the aperture, there are a total of m^N combinations that must be examined. For even a small number of elements and a limited number of positions for each element, the number of trials required to examine all possible configurations quickly gets out of hand because of the exponential relationship. Ten elements, each capable of occupying ten different positions, result in a total of ten billion combinations. Even with modern high speed computing devices, the brute-force approach generally is not practical.

The advantage of dynamic programming is that it drastically reduces the number of combinations that must be examined but nevertheless finds the desired spacings. This is accomplished by converting a single N-dimensional optimization problem into a sequence of N one-dimensional optimization problems. Instead of the m^N cases required for the brute-force approach, approximately $(N-1)m^2$ cases need be examined with dynamic programming. The smaller number of combinations results from the judicious programmed elimination of configurations which are determined by the computer to offer no advantage. That is, dynamic programming allows for many alternatives to be discarded before they are evaluated completely.

As applied to the design of unequally-spaced-array antennas, the application of dynamic programming determines the N values of the element spacings that achieve a desired radiation pattern. Some criterion must be established for specifying a desirable radiation pattern. There is little value in utilizing the mainbeam parameters as a design criterion since the shape of the mainbeam and the maximum gain are relatively unaffected by the precise arrangement of a given number of elements within a given size aperture. The sidelobes, however, are significantly dependent on the arrangement of elements. Thus it seems

reasonable to establish the criterion on the basis of the sidelobe properties. Analogous to the Dolph-Chebyshev[3] method of conventional antenna design it would seem desirable to make all the sidelobes of equal amplitude. This may not be possible in a thinned array of unequally spaced elements because of the lack of sufficient degrees of freedom (elements) to specify completely the radiation pattern at the required number of angular coordinates. A compromise would be to make the sidelobes as uniform as possible. This was attempted by selecting as the optimum radiation pattern the one whose highest sidelobe peak over a specified angular interval was less than the highest peak of any other pattern. This is a special case of the general criterion of minimizing maximum deviations.[30]

The radiation pattern of a linear array containing an odd number of isotropic elements symmetrically arranged about the center element is

$$E(x_1, \ldots, x_N, u) = 1 + 2 \sum_{n=1}^{N} \cos 2\pi x_n u \qquad (12)$$

where x_n is the distance of the nth pair of elements measured in wavelengths from the center of the aperture, $u = \sin\theta - \sin\theta_o$, θ = the angle measured with respect to the array normal, and θ_o is the angle to which the beam is steered. The array geometry is illustrated in Figure 34. The radiation pattern is a function of the spacings x_n and of the angular coordinate u. The elements are allowed to occupy positions whose location from the array center is an integral number of some prespecified value Δx. That is, the element locations are quantized. This not only makes the computations easier but it is consistent with actual array design. Furthermore, as described later, lower sidelobe levels result if the quantization interval is chosen properly. The spacing of the Nth pair of elements is fixed by the aperture dimension so that $2x_N = D$. Thus it remains to find the N-1 values of x_n. For example, for the 25-element array considered later, there are 11 spacings that must be chosen.

The mathematical description of dynamic programming as applied to arrays is given in Appendix II. Qualitatively, the procedure may be described as follows. The first element (or element-pair of a symmetrical array) can be placed in any one of m possible locations. Likewise, the second element can be placed in any one of m possible locations. (The number m need not be the same in each case.) The first element can occupy locations $a_1, a_2, \ldots, a_m$ while the second element can occupy locations $b_1, b_2, \ldots, b_m$. These possible locations may be overlapping. The only restriction is that adjacent elements may not be placed closer than a predetermined spacing. For each

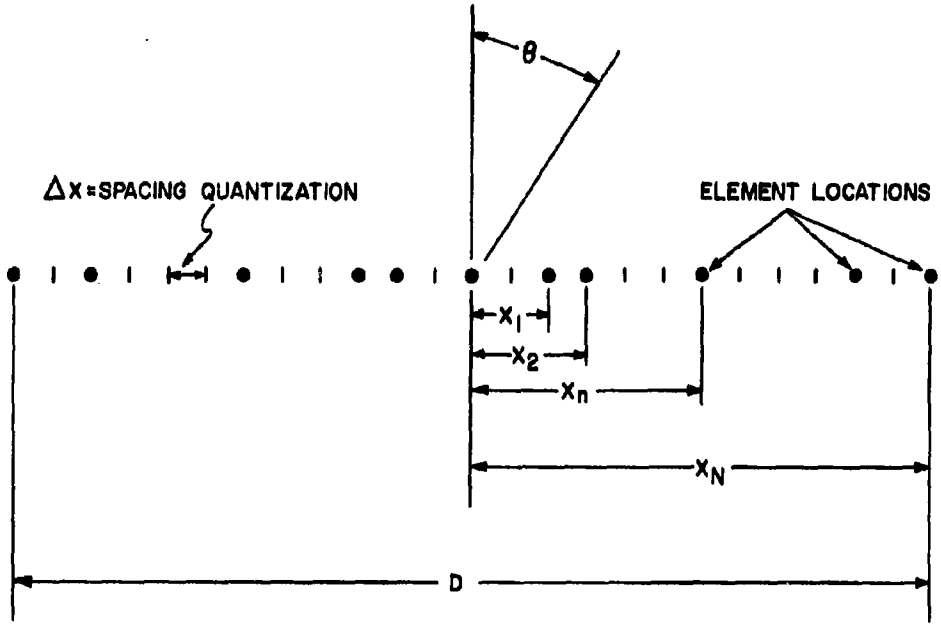

FIG.34–GEOMETRY OF THE UNEQUALLY SPACED ARRAY SYMMETRICALLY ARRANGED IN PAIRS ABOUT THE CENTER ELEMENT.

location b_j of the second element all possible locations a_1 to a_m of the first element are examined and the contribution of each to the radiation pattern is computed. For each b_j there will be a particular a_i which produces the best result. The best a_i for each particular b_j is noted and and its quantitative effect on the pattern is stored in the computer memory. All other computations performed during this stage are discarded.

The next step is to consider the third element which can be placed at any one of the locations $c_1, c_2, \ldots, c_m$. For each possible c_k of the third element it is necessary to determine the best location b_j of the second element and of the first element a_i. However, part of this problem has been solved since the optimum a_i for every b_j was determined in the previous stage. This is the saving offered by attacking a multi-stage problem by dynamic programming. Each c_k will result in an optimum b_j and hence an optimum a_i. This information, plus the contribution to the radiation pattern by the combinations of each of these three elements, is stored in the computer. Physically, the results from the three-stage calculations are a set of m combinations of spacings for the first three elements, each one of which for a particular c_k minimizes maximum sidelobe radiation of the partial array. All other possible combinations of the first three elements are discarded.

The procedure is repeated in turn for each of the remaining elements. The various possible locations of the nth element are compared with each possible location of the (n-1)th element. No further comparisons with the (n-2)nd, (n-3)rd, etc., elements are necessary since the optimums were determined in previous stages. It should be noted that each stage of the process does not determine the location of a particular element. It only determines that if a certain location is chosen for the nth element the optimum location of the (n-1)th element is determined, which determines that of the (n-2)nd element, and so on. The precise configuration is not given until the last element is examined and its optimum location found.

Thus the design of the complete array is built up from successive optimal designs of partial arrays. From a rigorous point of view this does not guarantee an optimal complete array. However, the results obtained seem to approximate optimum conditions very closely as will be illustrated by several examples.

5.3 Examples

A program was written for the IBM 7094 digital computer with the capability of determining the optimum spacings of up to 25 pairs of elements (51 elements total). The program can compute a maximum of 400 discrete u values ($u = \sin\theta - \sin\theta_o$) in determining the pattern of a particular configuration of elements. The number of

discrete u values that must be computed depends on the total aperture dimension (which determines the spatial frequency and hence the maximum possible separation between adjacent u values) and the total region of u over which the pattern is to be optimized. By analogy to the Shannon sampling theorem of information theory,[31] the radiation pattern in the u-region must be sampled at intervals of $\Delta u = \frac{\lambda}{2D}$, where D = maximum aperture dimension and λ = wavelength. Each element position x_n is chosen from among 30 possible consecutive positions specified a priori. As mentioned previously, the criterion for selecting an optimum element configuration is that the maximum sidelobe level be a minimum over the u-region of interest.

Nine-Element Array - Two different linear array configurations were examined. One was a nine-element array 19 wavelengths in extent. The other was a 25-element array occupying a 50-wavelength aperture. The nine-element design was performed as a check of the computer program since it could be hand calculated conveniently. It took one man with a desk calculator approximately one week as compared to the several seconds of time taken by the IBM 7094. The spacing of the outer pair of elements was fixed at 19λ, or 9.5λ from the center, where λ = wavelength. Thus, in this simple case there were three locations that had to be determined. If the outer pair of elements were not fixed there would be four spacings to determine. In preliminary trials, when the outer element position was made to vary between 9.5λ and 10.5λ from the array center, it was found that the optimum was always 9.5λ, the closest position allowed. Therefore, it was decided to always fix the outer element location.

Each of the three pairs of elements, other than the fixed outer pair, are located within the 19λ aperture subject to the following two constraints: (1) no two adjacent elements can be closer than a predetermined spacing, in this case a half-wavelength, and (2) the number of possible positions an element can occupy is limited by quantizing the aperture into discrete increments, in this case, half-wavelength intervals. Both of these constraints are consistent with practical array design. It is shown in Appendix III that if the locations are quantized into $\lambda/2$ intervals the radiation pattern is symmetrical about u=1 (as well as about u=0, u=1, u=±2, etc.). This fact permits a reduction in the required computations. Only the u region extending from u=0 to u=1 need be examined in order to determine the behavior of the radiation pattern in the much larger region $-2 \leq u \leq 2$. The minimum value of u must be large enough to lie outside the main lobe but cannot be so large that a high sidelobe would appear in the vicinity of the main beam. Because the exact position of the first null is not always known it may be necessary to try different values of u_{min} as was indeed the case for the first 25-element design attempted.

The spacings, measured from the array center, of each pair of elements in the nine-element array as found by both the computer and hand-calculated dynamic programming are $x_1 = 1\lambda$, $x_2 = 2.5\lambda$, $x_3 = 6.5\lambda$, and $x_4 = 9.5\lambda$. The radiation pattern corresponding to the above spacings is shown in Figure 35. The maximum sidelobe is 4.7 db below the main beam.

Twenty-five Element Array - The radiation pattern of the 25-element linear array occupying a 50 wavelength aperture is shown in Figure 36. The element spacings are given by the solid circles of Figure 37. Because the possible element positions were quantized in half-wave increments the radiation pattern is symmetrical about u=1 and the region from u=1 to u=2 need not be plotted. Over the sidelobe region in which the minimax criterion applies ($0.02 \leq |u| \leq 1.98$) the sidelobes are more or less uniform. The maximum sidelobe level is about -8.8 db below that of the main lobe and occurs for u = 0.15. This is considerably better than similar arrays designed by other techniques. For example a number of designs were attempted by selecting the spacings completely at random subject to thr restriction that no two elements could be placed closer than a half-wavelength. The best random distribution achieved a maximum sidelobe of only -6 db. The best of the empirically designed 25-element unequally-spaced arrays achieved previously by ECI had sidelobes of about -7 db. In Section 6 and in Figure 18 25-element space-tapered designs with the same average spacing (2λ) are shown to result in maximum sidelobes of 6.5 db. These comparisons show the improvement that can be achieved with dynamic programming.

In the nine-element design of Figure 35 each pair of elements could be located anywhere within the aperture subject only to the restriction that the minimum inter-element spacing be no less than half-wavelength. It was not possible to have such freedom with the present computer program applied to the 25-element design. Each element could be placed in any of 30 consecutive prespecified locations. With 0.5 wavelength quantization this corresponds to an interval 14.5 wavelengths in extent. (The maximum possible interval with a 50 wavelength symmetrical array is 25 wavelengths.) The allowed interval for each element is quite broad. It does not seem too likely that a wider region will give significantly different results when the spacing quantization is 0.5 wavelengths. An example of the intervals used for obtaining the radiation pattern of Figure 36 is shown in Figure 37. If several elements are found to lie on the boundary of the allowed intervals, the intervals can be changed and the computer can be asked to repeat the design to determine if there is a better configuration.

The computer will select those element locations which give the best pattern. The answer supplied by the computer may not be unique since several different configurations of elements might give

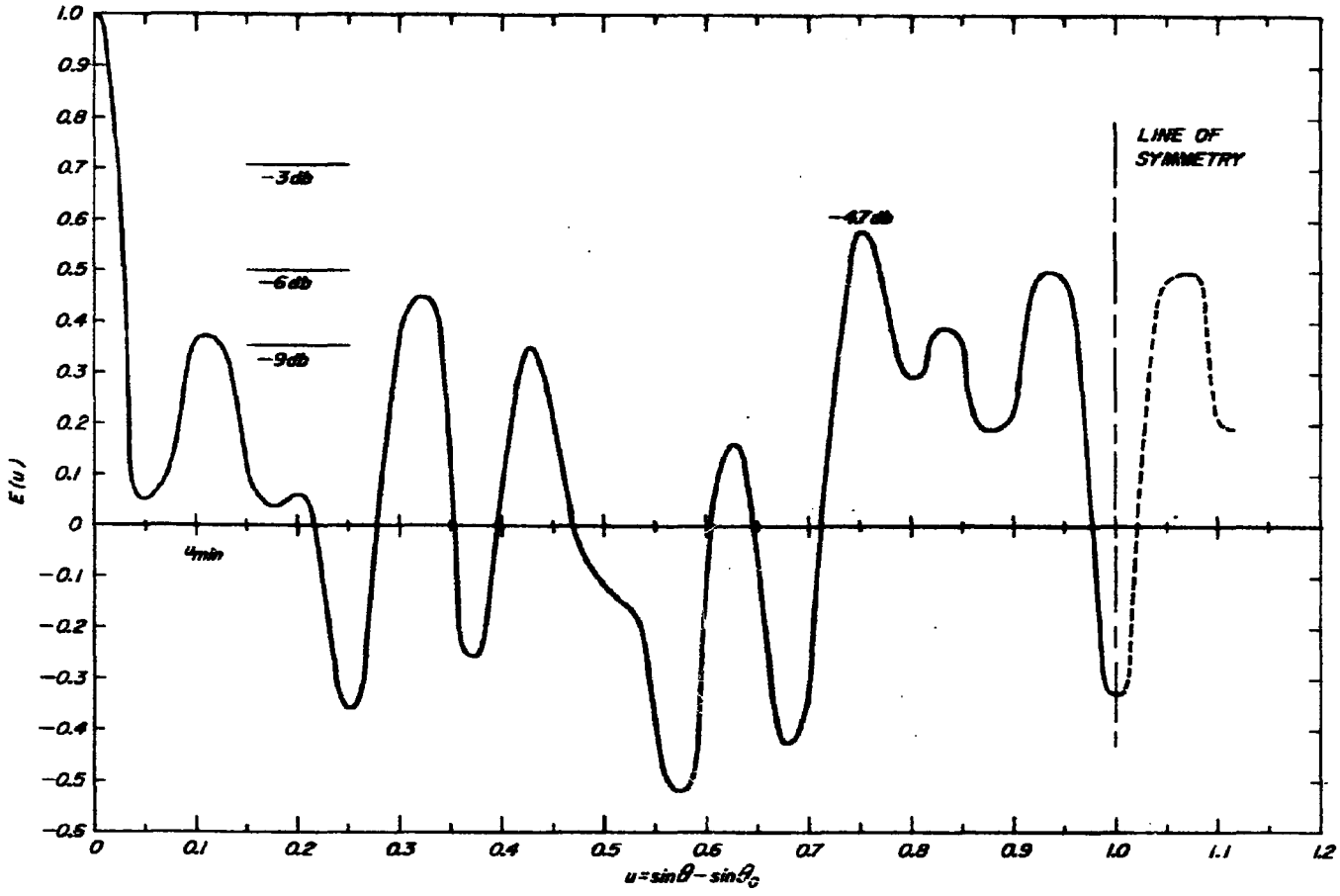

FIG. 35 – RADIATION PATTERN OF 9-ELEMENT UNEQUALLY SPACED ARRAY IN 19λ APERTURE DESIGNED ACCORDING TO DYNAMIC PROGRAMMING.

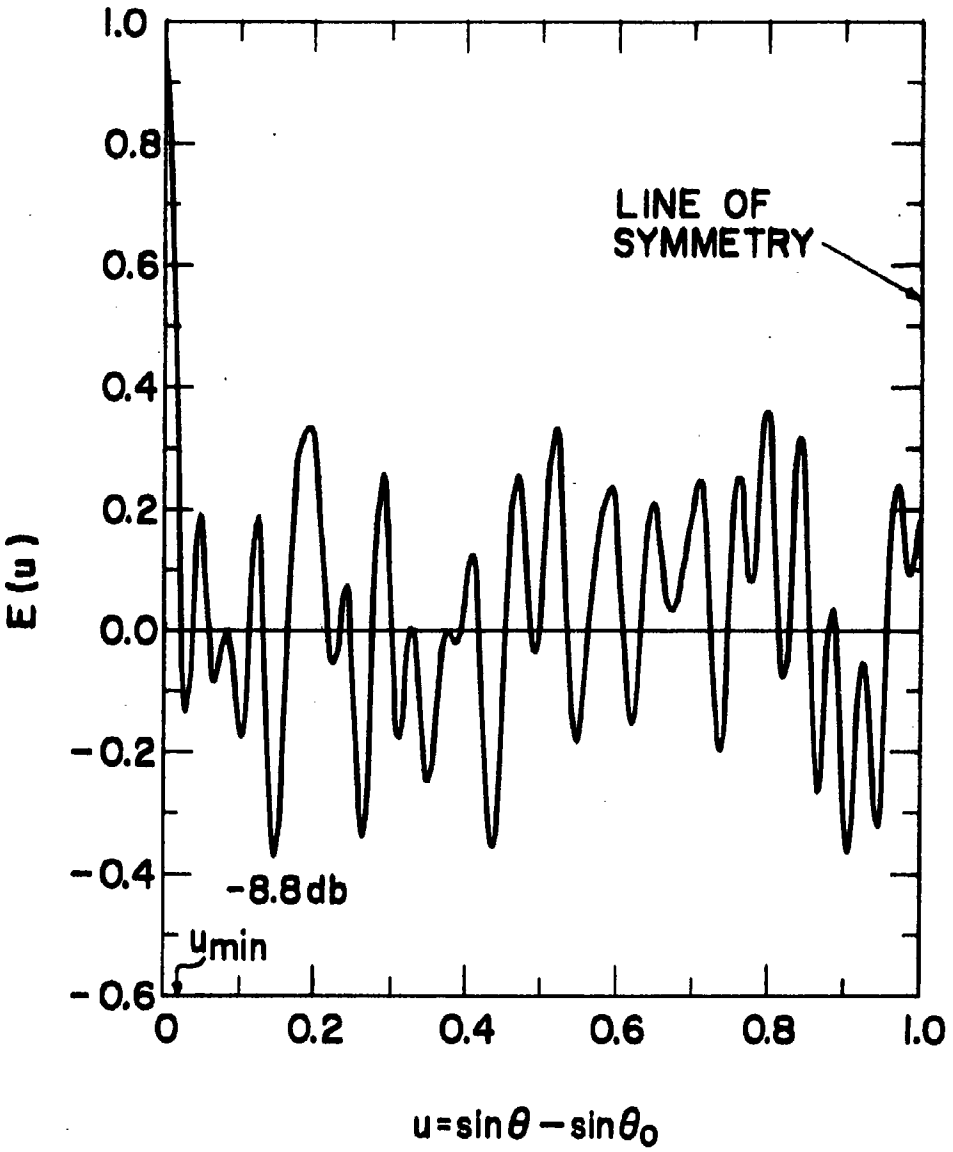

FIG. 36 - DYNAMIC PROGRAMMING ARRAY PATTERN

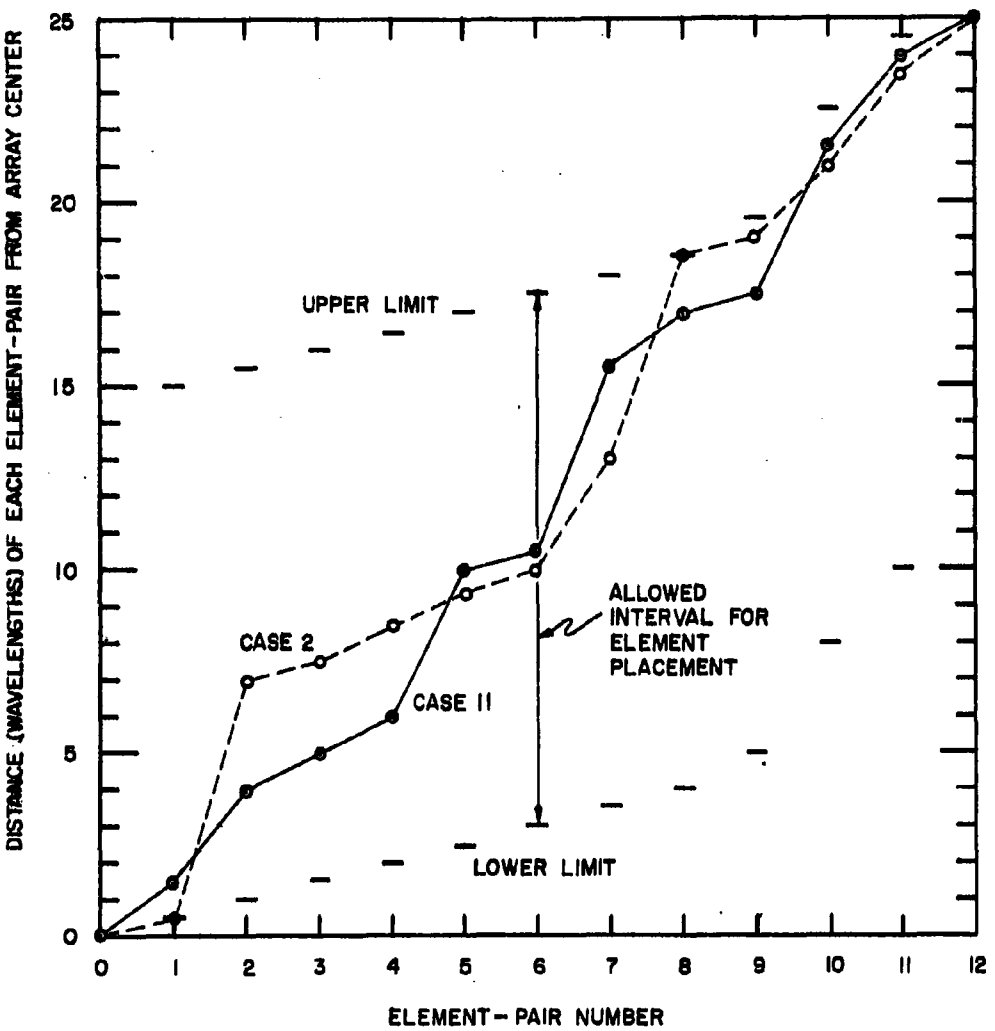

FIG.37 - PLOT OF ELEMENT LOCATIONS FOR TWO 25-ELEMENT ARRAYS. SOLID CURVE REPRESENTS THE CASE WHOSE RADIATION PATTERN IS SHOWN IN FIG. 3. BOTH CASES RESULT IN APPROXIMATELY THE SAME PEAK SIDELOBE LEVEL.

radiation patterns with approximately identical maximum sidelobes, at least to the accuracy designed into the computer program. Thus slight variations in the input conditions might result in a different set of element locations and a different radiation pattern, but with essentially identical peak sidelobe levels. For example, when the computer was programmed to calculate the radiation pattern over the sidelobe region of interest in increments of $\Delta u = 0.01$, a slightly different set of element locations were obtained. However, the peak sidelobes in the two cases were within a tenth of a db. A similar result occurred when a modification was made to the allowed element intervals for the radiation pattern of Figure 36. The spacings found by the computer for this slightly different set of allowed intervals are shown by the open circles of Figure 37. The maximum sidelobes for the two designs shown in Figure 37 were within a tenth of a db.

5.4 Variation of Design Parameters

The flexibility of dynamic programming can be employed to determine how the radiation pattern is affected by varying the input conditions. One of the parameters examined was the angular region, or u-region, over which the antenna pattern was to be optimized. This is of practical importance because in many applications increased sidelobes may be permitted over some angular sector if reduced sidelobes can be achieved within some specified sector.

u_{min} - Generally, the angular region over which the sidelobes are to be optimized should not include the main beam. If u_{min} is too small it might include a portion of the main beam and not give the optimum design. A u_{min} that is too large might cause the sidelobe region in the vicinity of the main beam to be higher than desired. A uniformly illuminated filled aperture of width D will produce a main lobe whose first null occurs at $u_o = \lambda/D$. For a 50λ aperture this corresponds to $u_o = 0.02$. Since it is not possible to predict the precise location of the first null in an unequally spaced array it is sometimes necessary to vary u_{min} to determine that value which just excludes the main beam. Figures 38 and 39 show the radiation patterns for $u_{min} = 0.04$ and $u_{min} = 0.08$, respectively, as compared to the pattern of Figure 36 in which $u_{min} = 0.02$. Over the u-region of optimization the sidelobe peaks are -8.8, -9.7, and -9.9 db for $u_{min} = 0.02$, 0.04, and 0.08 respectively. Thus lower sidelobes are obtained at the expense of an increased sidelobe adjacent to the main beam.

u_{max} - The radiation pattern of Figure 36 is designed with $u_{max} = 1.0$ and $u_{min} = 0.02$. Because of symmetry, the pattern is optimized over the region $0.02 \leq |u| \leq 1.98$. This permits the antenna beam to be scanned to within one beamwidth of endfire ($\theta_o = 90^o$) with a peak sidelobe no greater than -8.8 db. Few, if any, practical arrays are required to scan this far. If the radiation pattern is scanned

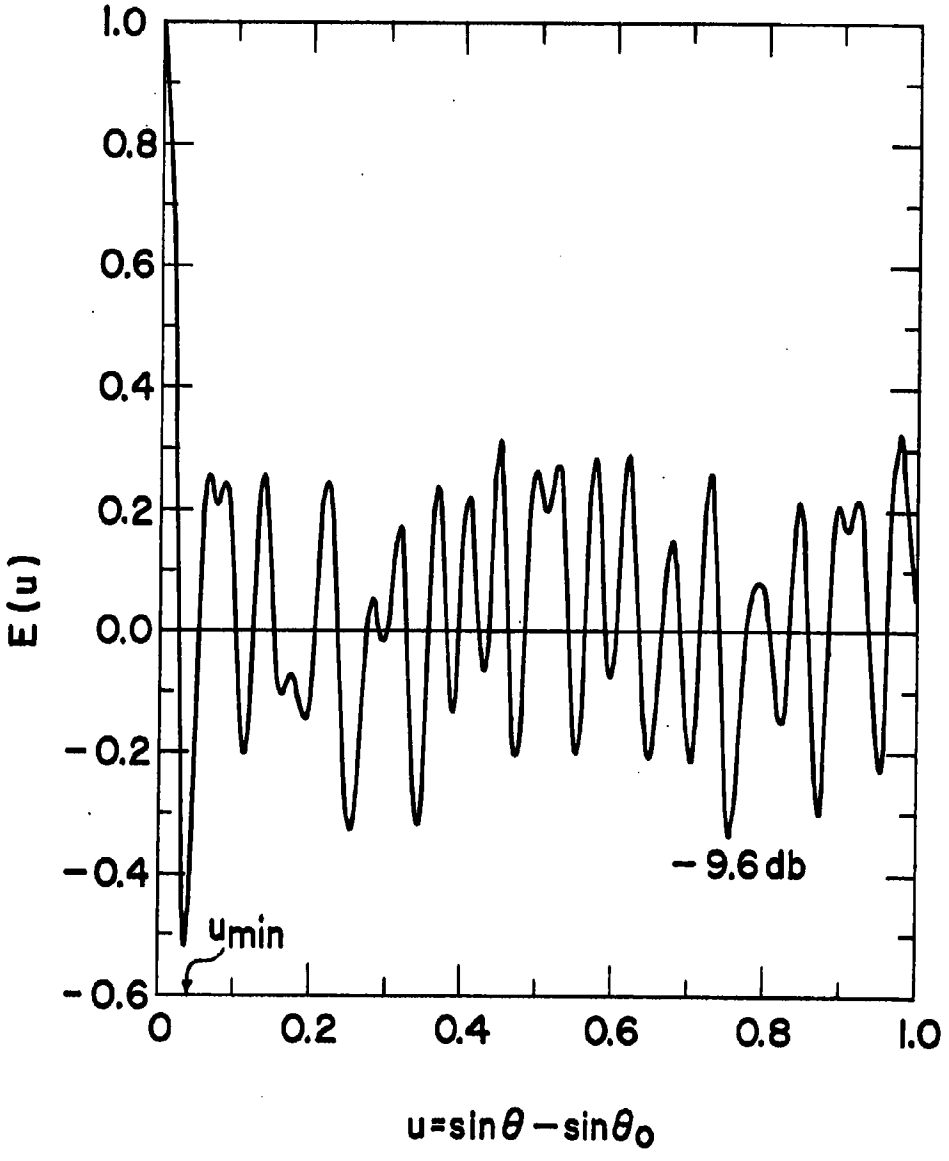

FIG. 38 – DYNAMIC PROGRAMMING ARRAY PATTERN

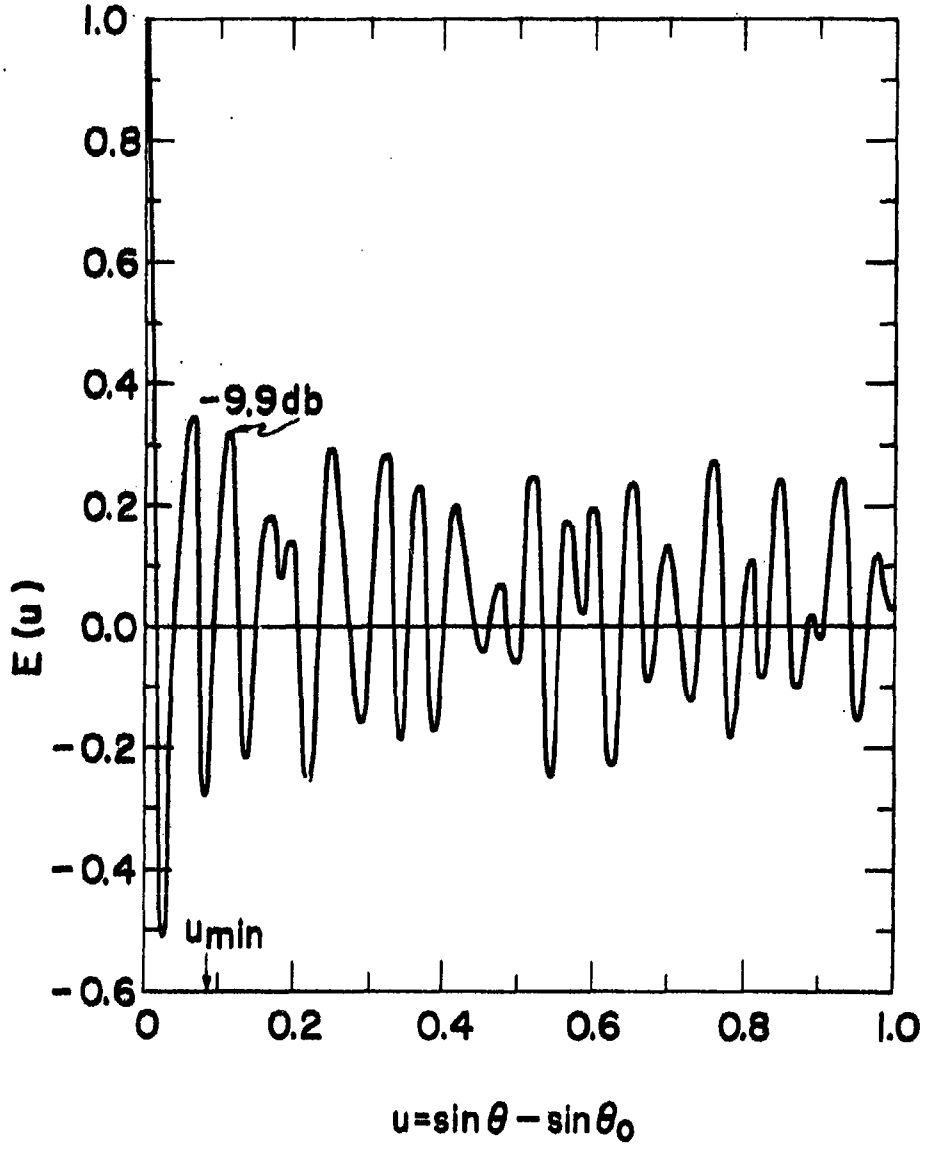

FIG. 39-DYNAMIC PROGRAMMING ARRAY PATTERN

over a smaller angle or is scanned not at all, the u region over which the pattern is to be optimized can be smaller and consequently the sidelobe level is reduced. This is illustrated by the radiation pattern of Figure 40 which was obtained for the same conditions as Figure 36 except that $u_{max} = 0.50$. This corresponds to the angular region 30^{o} to either side of the mainbeam of an unscanned array. In the region of optimization the maximum lobe is -12.6 db, a 3.8 db improvement over that obtained for the scanned array of Figure 36. In the remaining portions of the u region, however, the sidelobes increase to a value of -5.2 db.

$\underline{\Delta x}$ - The results reported above assumed that the elements could be located along the aperture of the array only at spacings quantized in half-wavelength intervals. Quarter wavelength and wavelength quantizations were also investigated.

With the present computer program only thirty possible aperture positions are available for each element from which to select the best location. With half-wavelength quantization the applicable interval in which to place elements is 14.5λ, with 0.25λ quantization the interval is 7.25λ, and with 0.125λ quantization the allowed interval is reduced to 3.625λ. The restriction on the allowed interval for the smaller quantizations might make the results subject to question if not selected with some care. However, this need not be a fundamental limitation to the dynamic programming method. It comes about in this case since only the high-speed, rapid-access storage of the computer was used. If a slower-speed storage with higher capacity is used, the restriction on the interval size in which the element spacings are allowed can be relaxed.

In spite of this possible limitation, the effect of changing the spacing quantization interval was examined and some conclusions made. Figures 41, 42, 43 are the radiation patterns for an array with 0.25λ spacing quantization and with $u_{max} = 0.5$, 1.0, and 2.0 respectively. (These patterns also show the effect on sidelobe level of changing u_{max}.) Only the angular region from u = 0 to u = 2.0 is plotted since the radiation pattern of an antenna with 0.25λ spacing quantization is symmetrical about u = 2. Thus, these patterns are indicative of behavior over the range $-4 \leq |u| \leq 4$. The radiation pattern for a design with 0.125λ spacings is shown in Figure 44 plotted out to u= 4, the point of symmetry.

The results of varying the spacing quantization Δx are summarized in Table V. No data were obtained for the two entries shown by dashes. Because of pattern symmetry the value for $u_{max} = 2.0$ and $\Delta x = 0.5\lambda$ was not examined. One might conclude from this table that the effect of decreasing the size of the spacing quantization is to lower the sidelobes. Table V also verifies the conclusion found

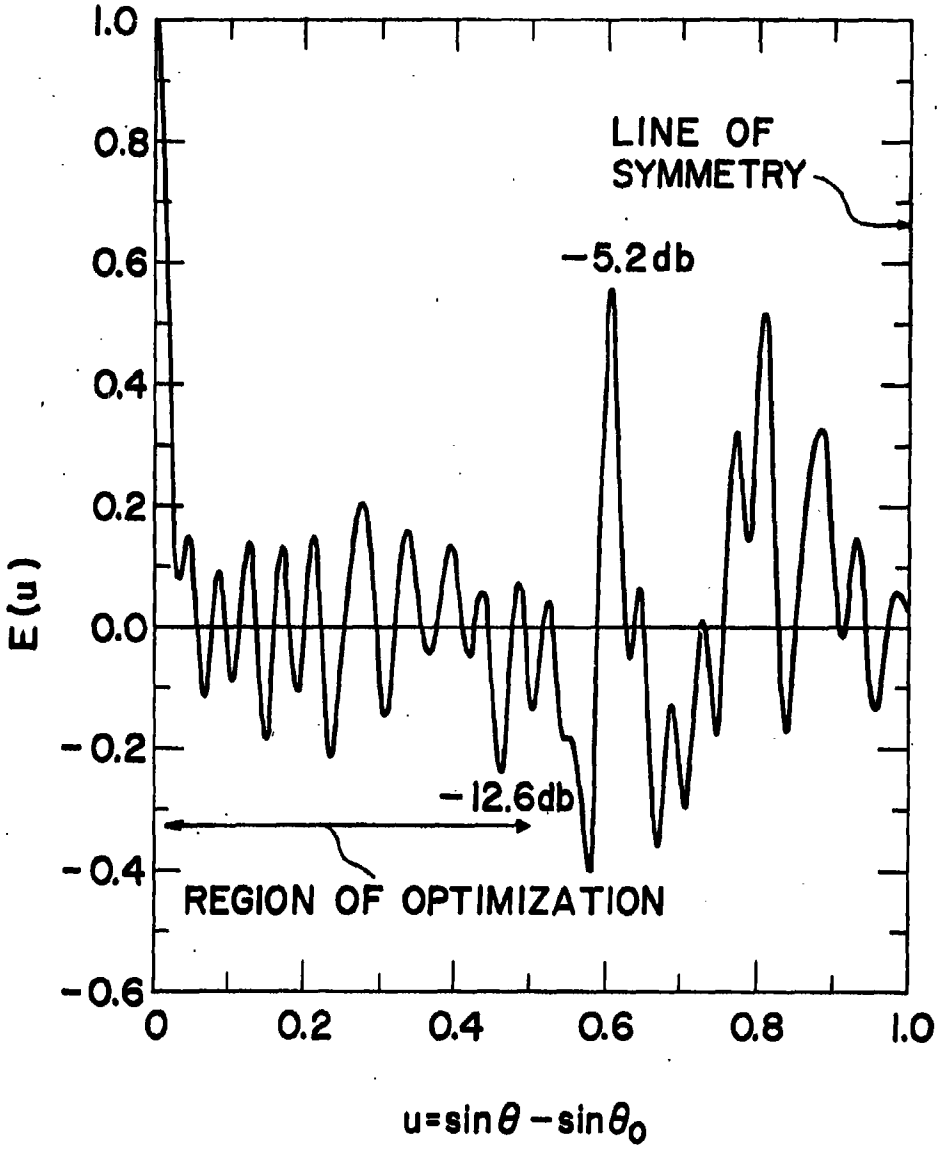

FIG. 40 - DYNAMIC PROGRAMMING ARRAY PATTERN

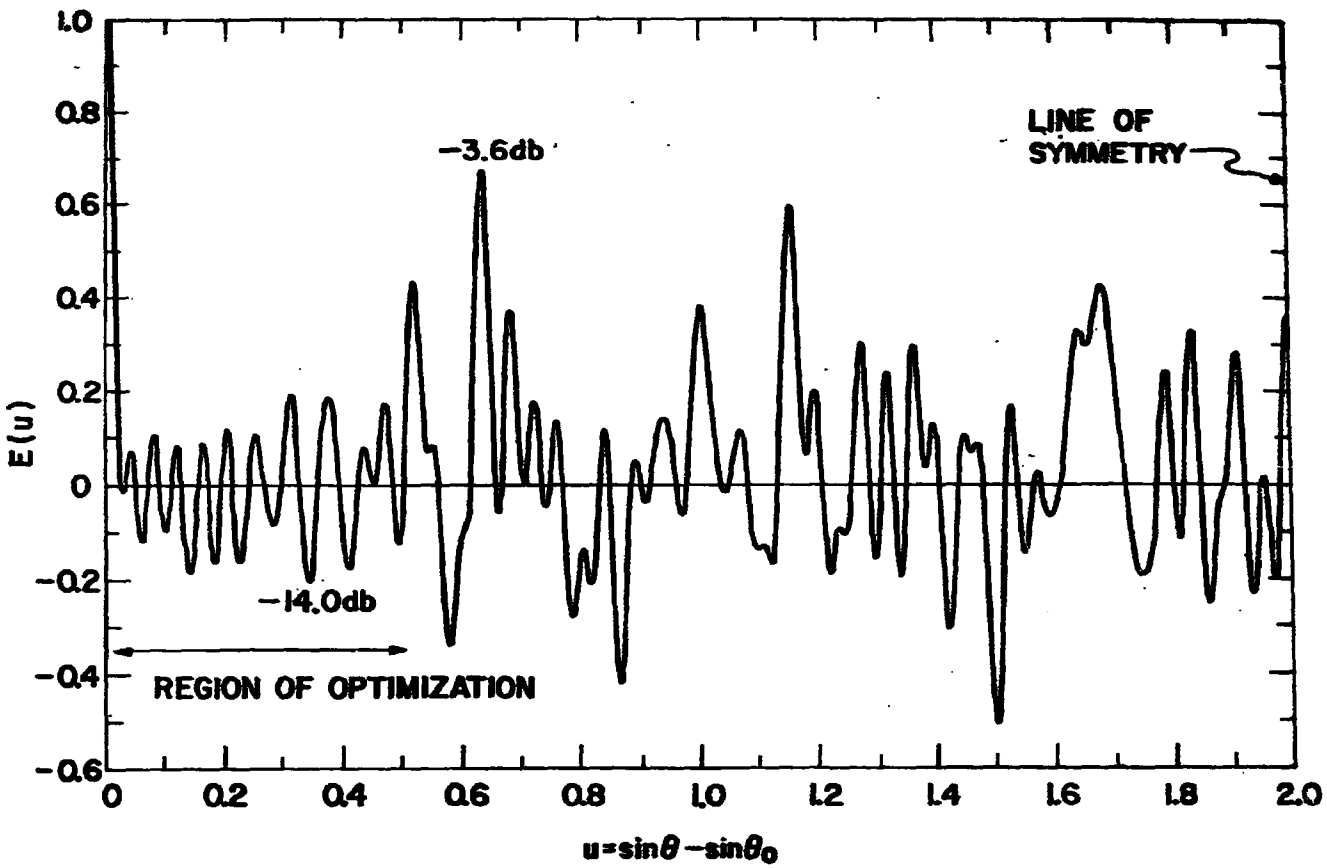

FIG. 41-DYNAMIC PROGRAMMING ARRAY PATTERN

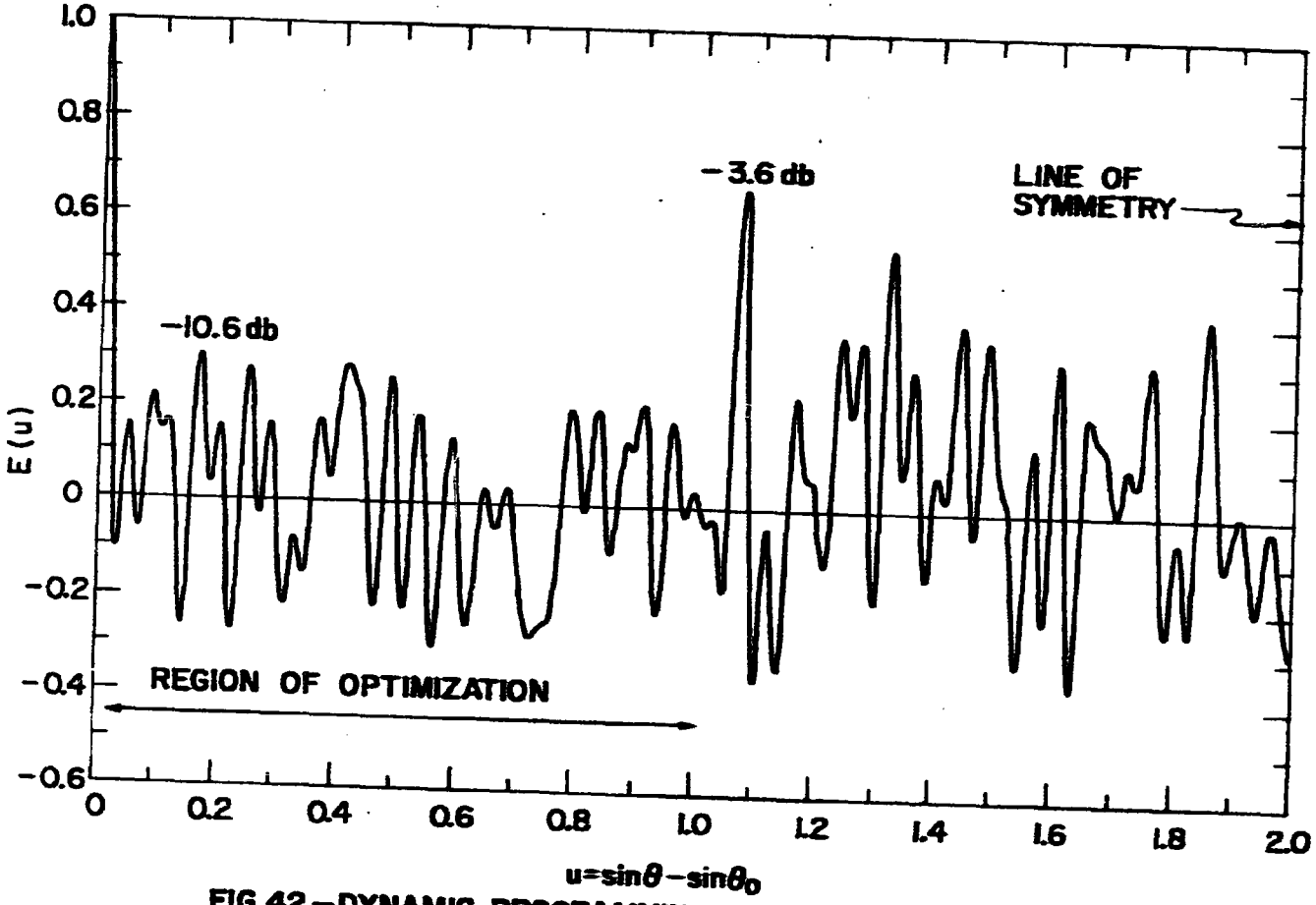

FIG. 42 – DYNAMIC PROGRAMMING ARRAY PATTERN

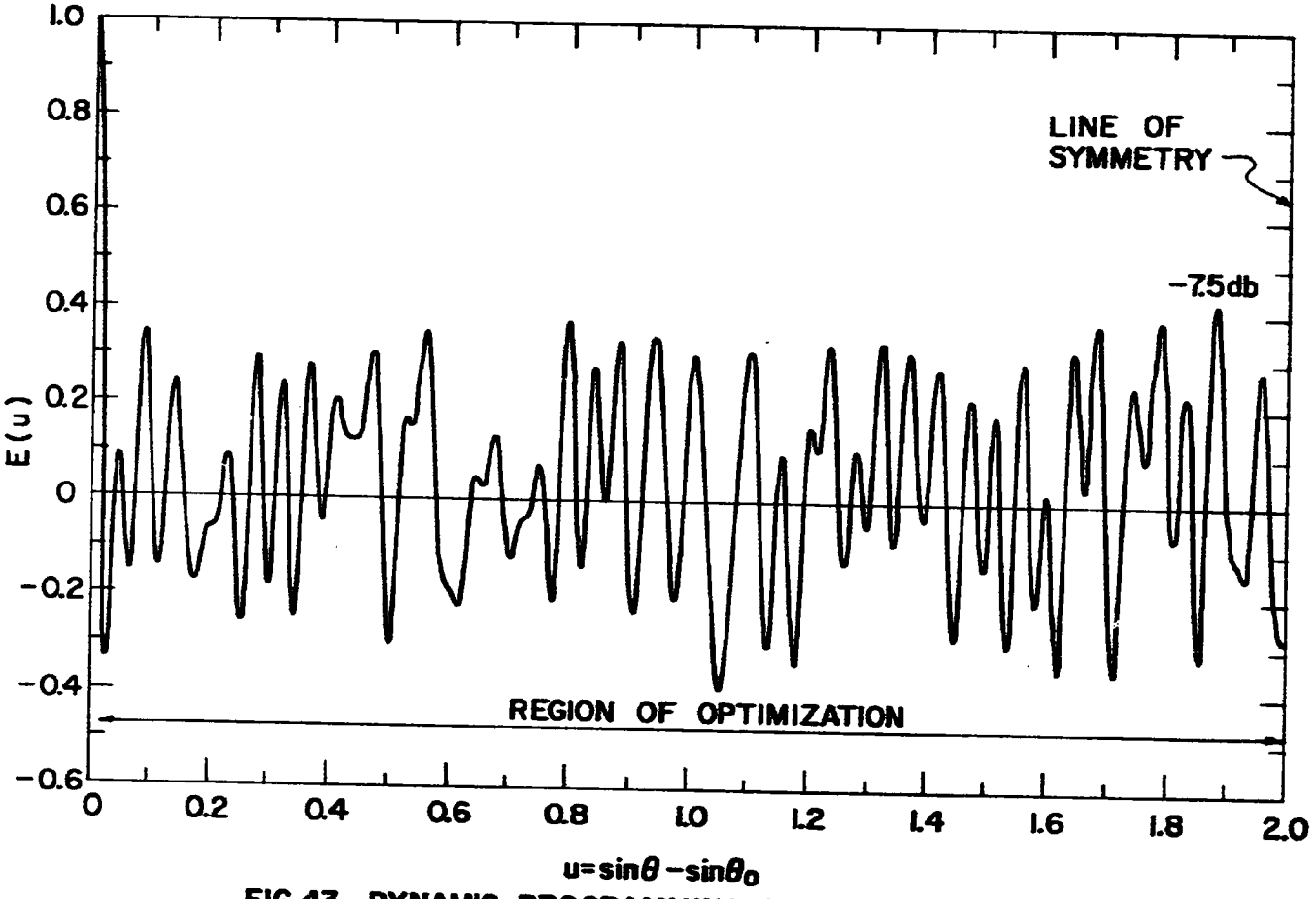

FIG. 43—DYNAMIC PROGRAMMING ARRAY PATTERN

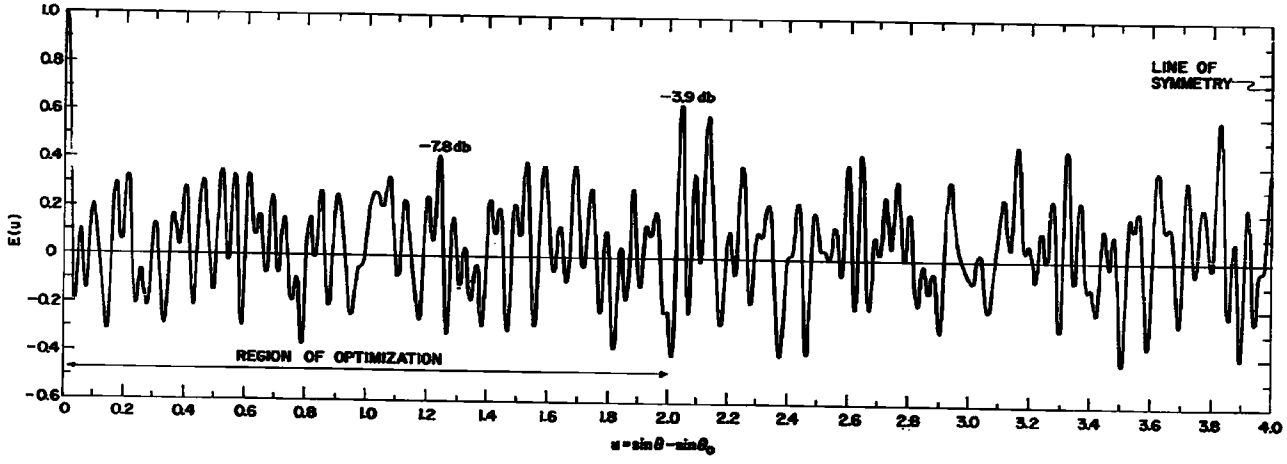

FIG. 4-4 – DYNAMIC PROGRAMMING ARRAY PATTERN

above that increasing the maximum of the u region raises the sidelobe level.

The results shown in Table V can be explained on the basis of pattern symmetry and the region over which the pattern is optimized. An antenna with 0.5λ quantization does not give the same pattern behavior as an antenna with 0.25λ quantization even though u_{min} and u_{max} may be the same. This is a consequence of the pattern symmetry giving rise to image regions in which the pattern is optimized, whether desired or not.

Consider the case, where $u_{min} = 0.02$ and $u_{max} = 0.50$. With the spacing quantization $\Delta x = 0.5\lambda$ the pattern has a peak lobe of -12.6 db over the desired interval $0.02 \leq u \leq 0.5$. But because the pattern is symmetrical about $u = 1$, the regions $1.5 \leq u \leq 1.98$, $2.02 \leq u \leq 2.5$, $3.5 \leq u \leq 3.98$ are also regions of optimization. With $\Delta x = 0.25\lambda$ the pattern is symmetrical about $u = 2$. Thus the region of optimization is the desired interval $0.02 \leq u \leq 0.05$ as well as the image region $3.5 \leq u \leq 3.98$. The total region of optimization, both desired and image regions, is twice that with 0.5λ quantization. For this reason the 0.25λ design produces lower peak lobes. In essence, the 0.25λ case has a larger "rug" under which to "sweep" the sidelobe energy. Similar behavior occurs for other values of u_{max}.

When $\Delta x = 0.5\lambda$, $u_{min} = 0.02$, and $u_{max} = 1.0$, the region $0.02 \leq u \leq 1.98$ is the region of optimization. The peak sidelobe was found to be -8.8 db. If the quantization is $\Delta x = 0.25\lambda$ and if $u_{max} = 1.98$ the symmetry arguments show that the regions of optimization are identical in the two cases and the pattern behavior should be similar. This was indeed observed, even to the point that the resultant spacings given by the program were found to have 0.5λ quantization although the computer could have selected locations with 0.25λ quantization, if it so desired.

5.5 Discussion

This initial study of dynamic programming, applied to the design of thinned unequally spaced array antennas, has shown it to be a technique capable of yielding designs significantly better than heretofore reported.

Although the principal objective was to evolve a design technique, the application of dynamic programming also uncovered some interesting properties of unequally spaced arrays. It was found that quantizing the possible element locations resulted in a pattern symmetrical in angle. This symmetry has a significant effect on the design since optimizing the pattern over a specified region of u also optimizes the pattern over the corresponding image region. The low sidelobes over the image region may not be of interest. Consequently the sidelobes in the desired region may not be as low as possible since

the region of optimization is larger than necessary. By properly selecting the spacing quantization it is possible, however, to improve the sidelobe level in the region of optimization.

The u parameter which was the abscissa for the radiation patterns was the angular coordinate $u = \sin\theta - \sin\theta_o$. It may also be interpreted as a more general parameter that includes the frequency by simply defining $u = (f_o/f)(\sin\theta - \sin\theta_o)$ where f_o is the design frequency and f is the new frequency of interest. An increase in frequency has the effect of compressing the pattern in the angular coordinate and acts as if the same number of elements were placed within an electrically larger aperture. However, the minimum spacing between elements may be greater than a half wavelength. The change in pattern with a decrease in frequency can also be observed from these plots since it effectively expands the pattern. At a lower frequency, however, the element spacings may be less than a half-wavelength, a condition not usually desired in practical arrays because of the difficulty of designing antenna elements to physically fit within the space, and more importantly because of the increased coupling between elements located in close proximity.

This first attempt in applying dynamic programming to array design has indicated its potential for determining the optimum element spacings of thinned arrays. It can be applied to larger arrays than considered here and to arrays located on planar as well as non-planar apertures. The criterion used for selecting the optimum design was that the maximum sidelobe peak should be minimized over a specified angular region. Other criteria can be considered if desired. Dynamic programming is an especially interesting technique for efficiently exploring the effects of a change in input parameters. As applied to 25-element arrays located within a 50-wavelength linear aperture, it has permitted the investigation of the effect on the sidelobes of varying the angular sector over which the pattern is to be optimized and the effect of different quantizations of the element locations.

Dynamic programming may be used to explore the properties of array antennas by varying the input parameters, examining the results, and making the proper deductions as to array behavior. It does not yield closed-form answers like some other analytical techniques (such as the calculus of variations). But it has the important advantage that it can supply useful answers where other more elegant techniques fail to provide practical solutions.

Computational difficulties may be encountered if the number of elements becomes too large. However, other techniques suffer the same limitations. The computer program that generated the results reported here can be extended and made more efficient for enlarging the scope of investigation. The upper limit of array complexity that dynamic programming can economically handle is a subject for future exploration.

Dynamic Programming has proven to be a useful tool for the design of one class of antennas and can probably be of value for other antenna design problems.

5.6 Guide Lines

It is not possible to establish rigorous and complete guide lines this early in the application of dynamic programming to antenna array design. Only an initial probe has been made and many details have not been explored. For example, it has been necessary to "home-in" on the allowed region for the ith element in the array which can occupy M possible consecutive positions. No general criterion has been developed for this parameter, but it is believed that it will depend on the array length and number of available elements.

The most interesting feature of dynamic programming has been the relatively large spacing between elements at the center of the array. Figure 37 indicates the element location for two arrays which have essentially the same peak sidelobe level, and this sidelobe peak is -8.8 db or almost 2 db better than any previously designed array of the same length and element number. Other techniques discussed in Section 6 indicate methods of reducing sidelobes adjacent to the main beam, which may also be done with dynamic programming. For example Figure 49, which is a complete sketch of Ishimaru's Figure 6 when 21 elements are placed in a 50λ array, in Section 6 may be compared to Figure 40 where the pattern was optimized from u = 0.02 to u = 0.50 and a peak sidelobe of -12.6 db obtained for this region. In the same interval Figure 49 has a peak sidelobe of -6.2 db, although it must be pointed out that there are only 21 elements used to obtain the pattern of Figure 49 and 25 used in Figure 40. It is evident that dynamic programming is superior to any previous technique in optimizing antenna array patterns with respect to peak sidelobes.

It is believed that as the number of elements increases in the array, dynamic programming might begin to place the elements more or less as the technique of density-tapering does. However, with a limited number of elements dynamic programming clearly indicates that conventional density-tapering is undesirable. Also, for limited elements this technique negates the concept of monotonic increasing element spacing as used by several authors[10, 11, 14] and as required in the number theory analysis of Section 7.

TABLE V

Summary of Peak Sidelobes Obtained by Dynamic Programming

Peak Sidelobe-Decibels

u_{max} \ Δx	0.5λ	0.25λ	0.125λ
0.50	-12.6	-14.0	- - - -
1.0	- 8.8	-10.4	- - - -
2.0	- - - -	- 7.4	-7.8

6. OTHER DESIGN TECHNIQUES

Summary

Discussed in this section are additional techniques that were explored in the study of pseudo random arrays. The manner in which the arrays may be designed using the following methods are often laborious. Some are, however, very straightforward and results are obtained which are typical to those reported in the literature for arrays of comparable size and number of elements. All studies discussed in this section are for linear arrays. The element positions for arrays discussed here are given in Table VI.

6.1 Cumulative Amplitude Distribution

The approach of using a cumulative amplitude distribution to determine a density or space taper of elements is frequently found in the literature and is the basic technique used in Section 4 on ring arrays. The technique is straight-forward and array patterns achieved in this manner typically have low sidelobes adjacent to the main beam and the sidelobes thereafter increase in peak values with increasing values of u. Figure 45 is a pattern calculated in this manner for a 15 db Taylor distribution. The magnitude of the first sidelobe is -15.9 db below the main beam and the following sidelobes diminish in magnitude until the 10^{th} sidelobe which has a magnitude of -30.4 db. From this point on the sidelobes increased with a maximum sidelobe of -2.9 db. By choosing more tapered distributions, the sidelobes may be made even lower adjacent to the main beam.

In an array where the only requirement is that the sidelobes adjacent to the main beam be low, space tapering using the cumulative amplitude distribution provides satisfactory but not too predictable results.

6.2 Amplitude-Phase Product Technique

The choosing of element positions in Section 6.1 was based solely on a space taper using an amplitude cumulative distribution. In all previous work the "spatial" phase associated with each position in the array has been ignored. The term "spatial" phase is used to denote the frequency of oscillation in the array pattern associated with each possible position in the array.

A simple means of space tapering and accounting for the "spatial" phase is to space taper according to the product of the amplitude and phase. In Figure 46 is a sketch of the Amplitude-Phase product versus displacement from the array center for a uniform distribution and for the 15, 20, 25, and 30 db linear Taylor distributions as computed by Spellmire.[26] Instead of constructing a cumulative distribution of the amplitude-phase product, the arc length of each curve was divided into equal lengths and the element position determined in this

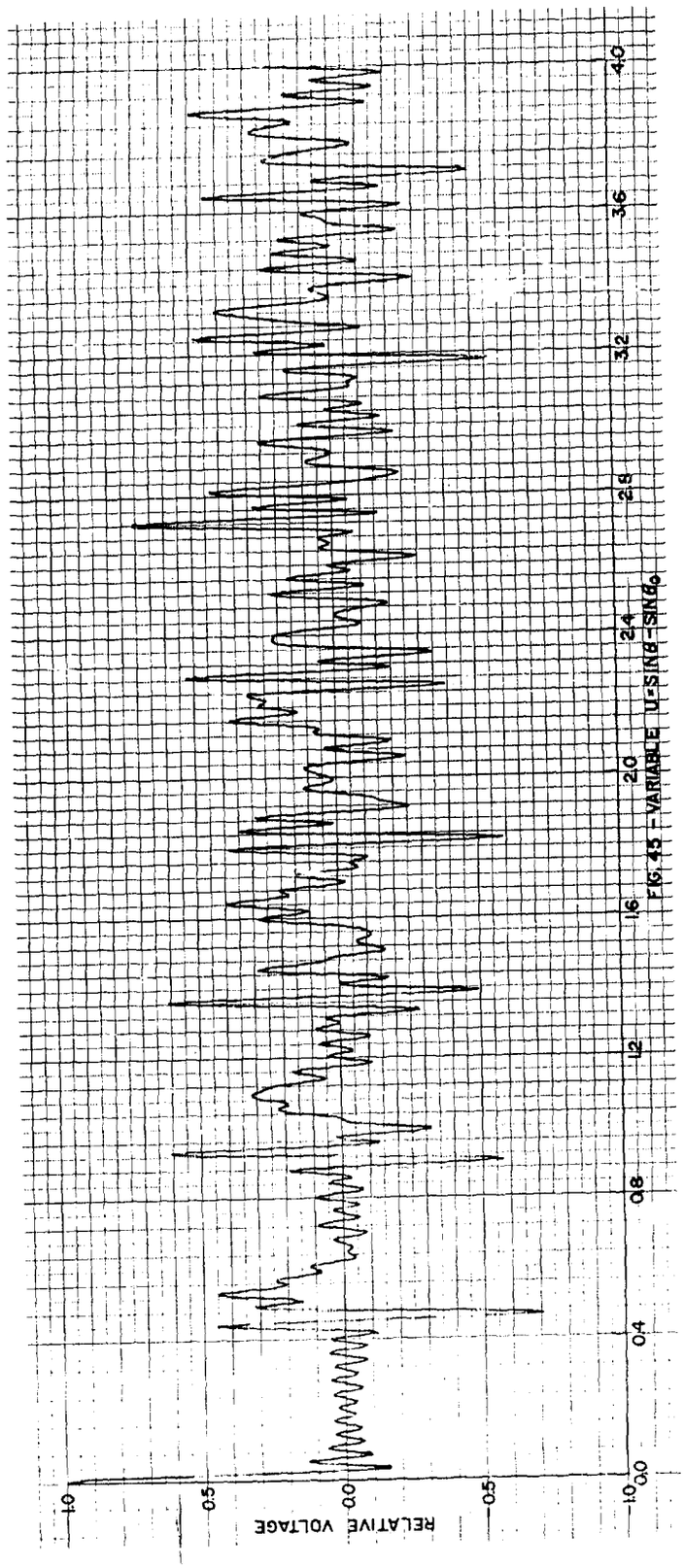

FIG. 45 - VARIABLE U-SIN θ-SIN θ

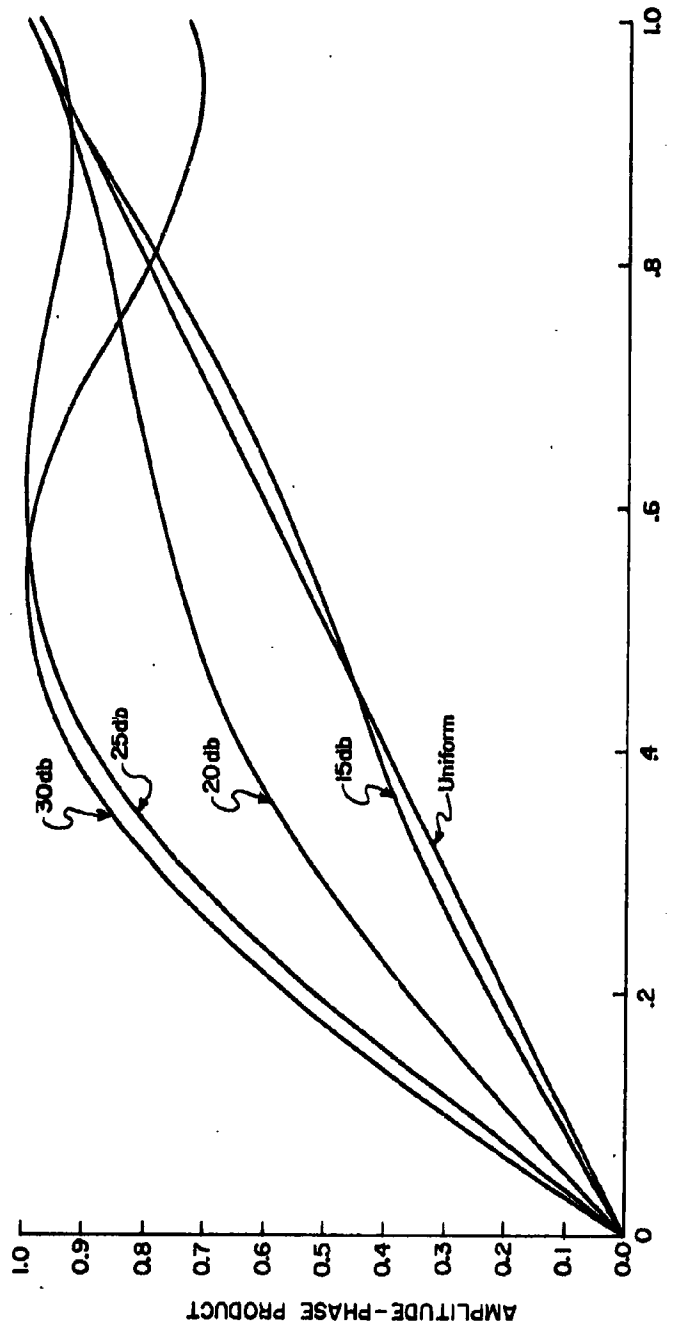

FIG. 46 – AMPLITUDE-PHASE PRODUCT CURVES

manner. This is a consistent technique in that if the amplitude distribution is uniform, then a straight line results for the Amplitude-Phase product and yields equal spacing for the element location.

An interesting feature of this curve is that element concentrations do not always appear densest at the array origin, but are dense at the origin and in some other region depending on the taper. The density of elements is greatest where the magnitude of the slope is greatest.

Figure 47 is a sketch of the pattern resulting from the 15 db space taper and Figure 48 due to the 25 db space taper. A peculiarity of these two patterns is the positive nature of the sidelobes adjacent to the main beam. No explanation is offered as to why the sidelobes are more positive. The peak sidelobes in the region from $0.05 \leq u \leq 0.4$ are 14 db and 14.4 db for the 15 and 25 db cases, respectively.

The synthesis technique developed by Ishimaru is sketched in Figure 49 where 21 elements are located in a 50 wavelength aperture.[17] (This is Figure 6 in Ishimaru's paper.) No sidelobe is higher than -12 db if the array is 13.72 wavelengths in extent. With this length the minimum spacing between elements is a half wavelength. If the arrays computed using the Amplitude-Phase product are 13.72 wavelength long then peak sidelobes of 14 and 14.4 db result for the 15 and 25 db cases, respectively, but the elements would be less than a half wavelength apart. The array in Figure 47 (15 db) can be 20 wavelengths in extent with all sidelobes below 14 db, but minimum spacing between the elements would be 0.376 wavelengths. Thus it appears from these results that the practical limitation of a half wavelength spacing between elements can be a severe one. The theory developed by Ishimaru is one to be used when the primary objective is to reduce sidelobes in the vicinity of the main beam, and not to reduce the number of elements in the array.

6.3 The Pattern-Multiplication Method

In the pattern multiplication method, the number of elements available and the length of the antenna are specified. These elements are grouped in equally-spaced subarrays to replace the isotropic elements of an array antenna. The centers of the subarrays are placed at the locations of the existing isotropic elements in the array, making it possible to express the field by the principle of pattern multiplication. A typical arrangement of elements is illustrated in Figure 50. Each subarray may have a spacing different from that of other subarrays. Only symmetrical arrays will be discussed. Suppose there exists an array of $2N_h + 1$ hypothetical isotropic elements, arranged symmetrically with respect to the center. The field from such a hypothetical array is

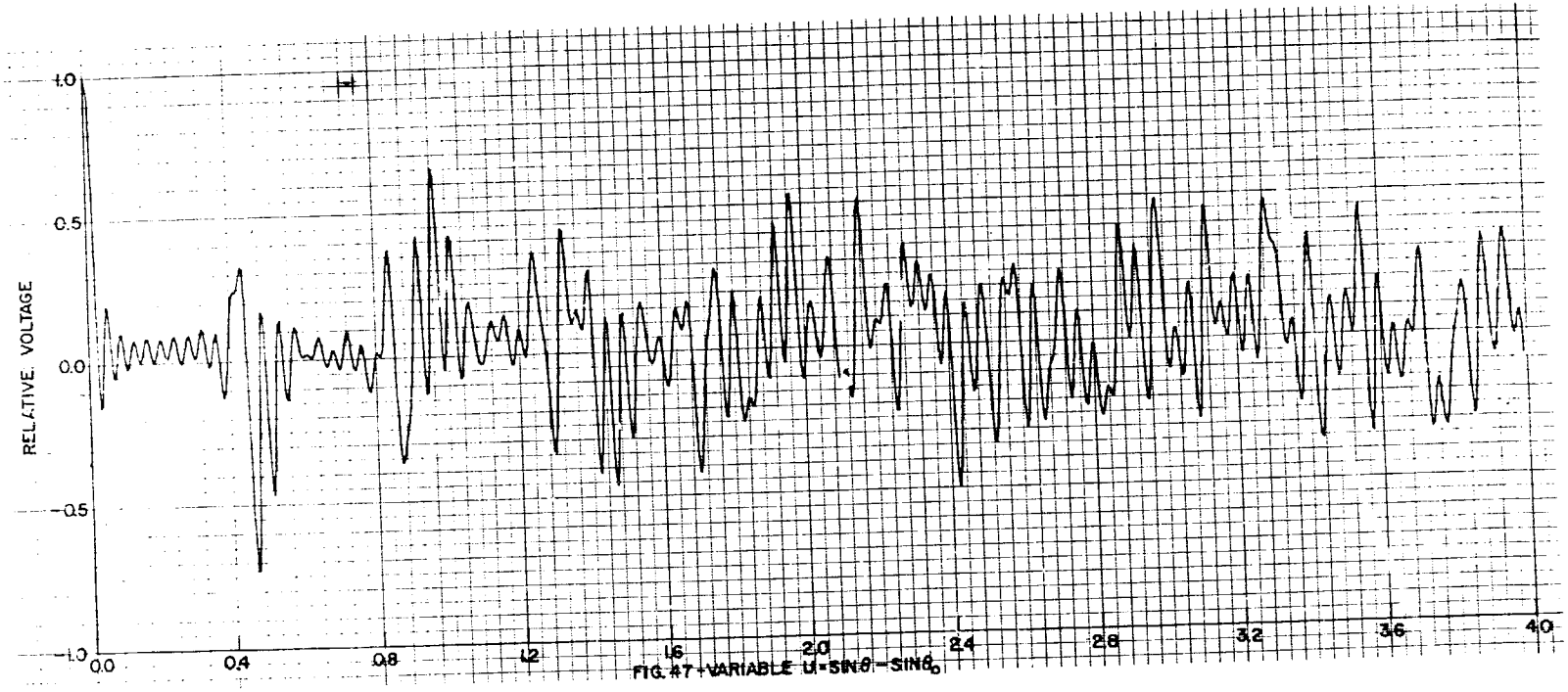

FIG. #7 + VARIABLE U = SIN θ − SIN θ$_0$

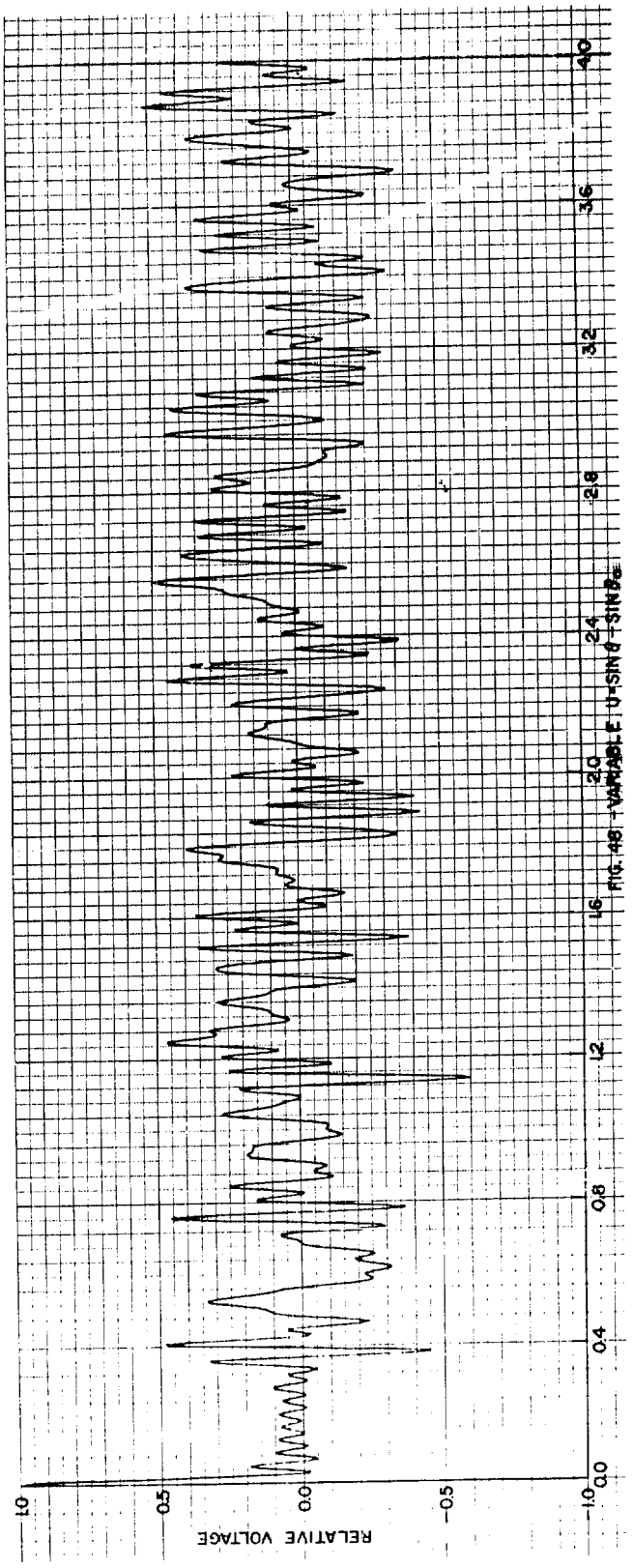
RELATIVE VOLTAGE
1.0
0.5
0.0
-0.5
-1.0
0.0
0.4
0.8
1.2
1.6
2.0
2.4
2.8
3.2
3.6
4.0
FIG. 48 - VARIABLE U-SIN θ + SIN 8θ

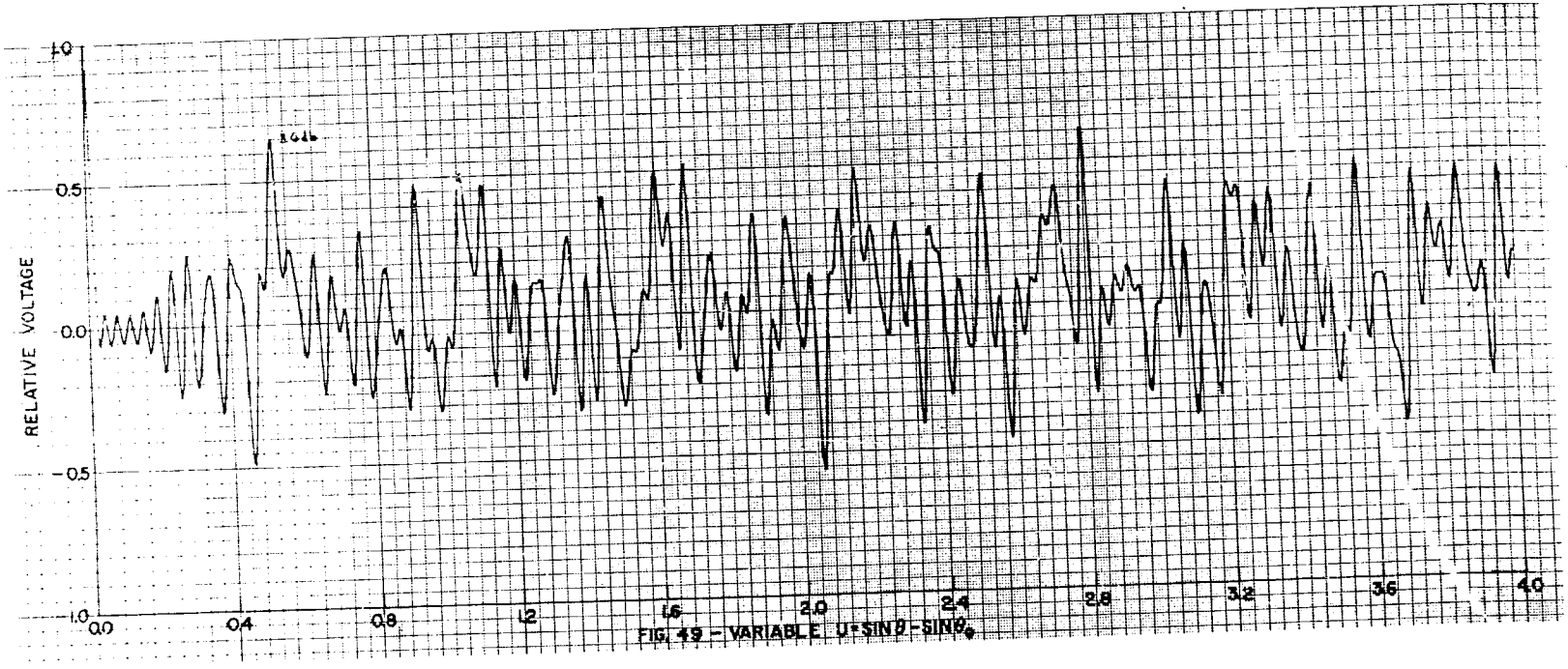

FIG. 49 – VARIABLE $U = \sin\theta - \sin\theta_0$

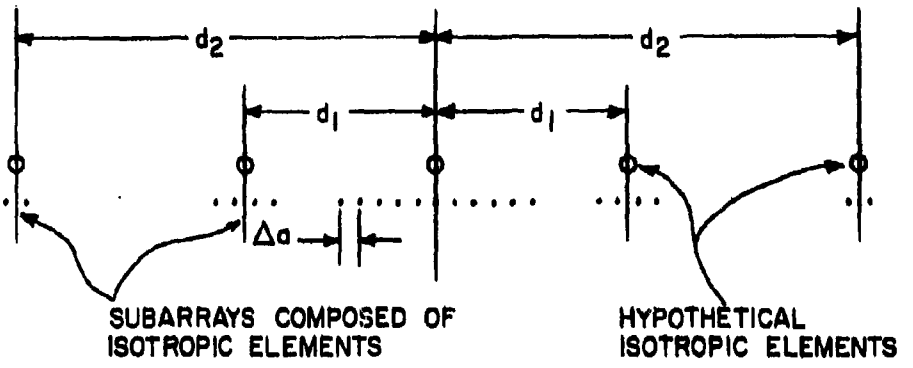

FIG. 50.– TYPICAL COORIDINATES FOR PATTERN MULTIPLICATION

$$E_h(u) = 1 + 2 \sum_{n=1}^{N_h} \cos\left(\frac{2\pi d_n u}{\lambda}\right) \tag{13}$$

By replacing the hypothetical elements with equally spaced subarrays of isotropic elements, the principle of pattern multiplication requires that the field become

$$E(u) = \left(\frac{N_{a_o}}{N_T}\right) \frac{\sin N_{a_o} \frac{\pi a_o u}{\lambda}}{\sin \frac{\pi a_o u}{\lambda}} + 2 \sum_{n=1}^{N_k} \left(\frac{N_{a_n}}{N_T}\right) \frac{\sin N_{a_n} \frac{\pi a_n u}{\lambda}}{N_{a_n} \sin \frac{\pi a_n u}{\lambda}} \cos \frac{2\pi d_n u}{\lambda} \tag{14}$$

where N_{a_n} is the number of actual isotropic elements in one of the subarrays of the n^{th} pair. The sum of the N_{a_n}'s is the total number of elements in the array, i.e.,

$$N_{a_o} + 2N_{a_1} + 2N_{a_2} + \ldots . 2N_{a_{n_k}} = N_T \tag{15}$$

where N_T is the number of actual elements available. The ratio of the N's in Equation 14 are weighting factors which specify, according to the number of elements N_{a_n} in subarray n, the influence of that subarray upon the total field. The weighting factors have been arranged so that E(u) = 1 when u=0. The element at the center cannot be neglected, if it is replaced with a subarray.

While Equation 14 appears to be awkward it is conveniently handled by a general set of curves such as those in Kraus,[32] at least when the number of elements is not large. Basically, a method of trial and error is employed. An array, consisting of several subarrays is set up, and its pattern found by use of a general set of curves. If the result is not satisfactory, then the array is altered and its pattern redone. When a good pattern is achieved, it is calculated using an equation similar to Equation 13.

Best results are obtained when the spacing between elements of all subarrays is 0.5λ (the minimum allowable element spacing). In this way the first subarray grating lobe occurs at u = 2. Since it is unlikely that the beam will need to be steered as far as u = 2, this first grating lobe will not occur on the actual field pattern. With greater subarray interelement spacing, subarray grating lobes will occur when $0 \leq |u| \leq 2$.

Twenty-five elements were arranged in 5 subarrays to form an array with 50 wavelengths between the outermost elements. One

large subarray was placed at the center. The outermost pair of subarrays had the lowest number of elements each while the center array was the largest. In all the cases discussed here, the inner pair of subarrays had 4 elements each, with different combinations of elements for the outer pair and the center subarray. The following examples summarize this work:

Case 1: 13 elements in the center subarray ($N_{a_2} = 13$) and 2 elements in each of the outer subarrays ($N_{a_2} = 2$, $d_2 = 24.75\lambda$). Two positions for the inner subarray pair ($d = 5.25\lambda$ and 5.50λ) were used with the resulting fields shown in Figures 51 and 52.

Case 2: In an attempt to eliminate the secondary peak on the main beam, the outer array pair was divided so that only one element exists in the outer array, and the other element was moved to $d = 12.5\lambda$. Field patterns were calculated for the same two values of d_1 in Case 1. Resulting field patterns are shown in Figures 53 and 54, and represent the best patterns achieved using the pattern multiplication technique. Figure 53 corresponding to $d_1 = 5.25\lambda$ has a peak sidelobe of -9.8 db and Figure 54, where $d_1 = 5.50\lambda$, has a peak of -8.8 db. The main beam is essentially unaltered due to the change in the d_1's. The grating lobe is partially suppressed in Figure 54, and the peak value of the sidelobes increased by one db. This is explained in the analysis of Section 8 dealing with the energy concept in array antennas. It appears on the surface that the results achieved here are as good as those achieved using the dynamic programming approach. This statement is true if the resolution of the arrays is ignored. Because of the broad main beam, the array determined by pattern multiplication has poor resolution. It should be noted that the input conditions to the dynamic programming problem were adjusted to allow the computer to select these patterns achieved by pattern multiplication, and the computer did not make such a selection.

In evaluating this approach the technique is useful when the number of elements is small. For a large number of elements the problem readily gets out of hand, and hence is not easily extended.

6.4 The Least Squares Criterion

The field pattern for an array of $2N + 1$ isotropic elements, all operating at unity amplitude is:

$$E(u) = 1 + 2 \sum_{n=1}^{N} \cos \frac{2\pi n d}{\lambda} u \qquad (16)$$

where λ is the wavelength at which the array is operating, d is the spacing between elements, and $u = \sin\theta - \sin\theta_o$. θ is a particular angle measured from the array normal, and θ_o (also measured from the array

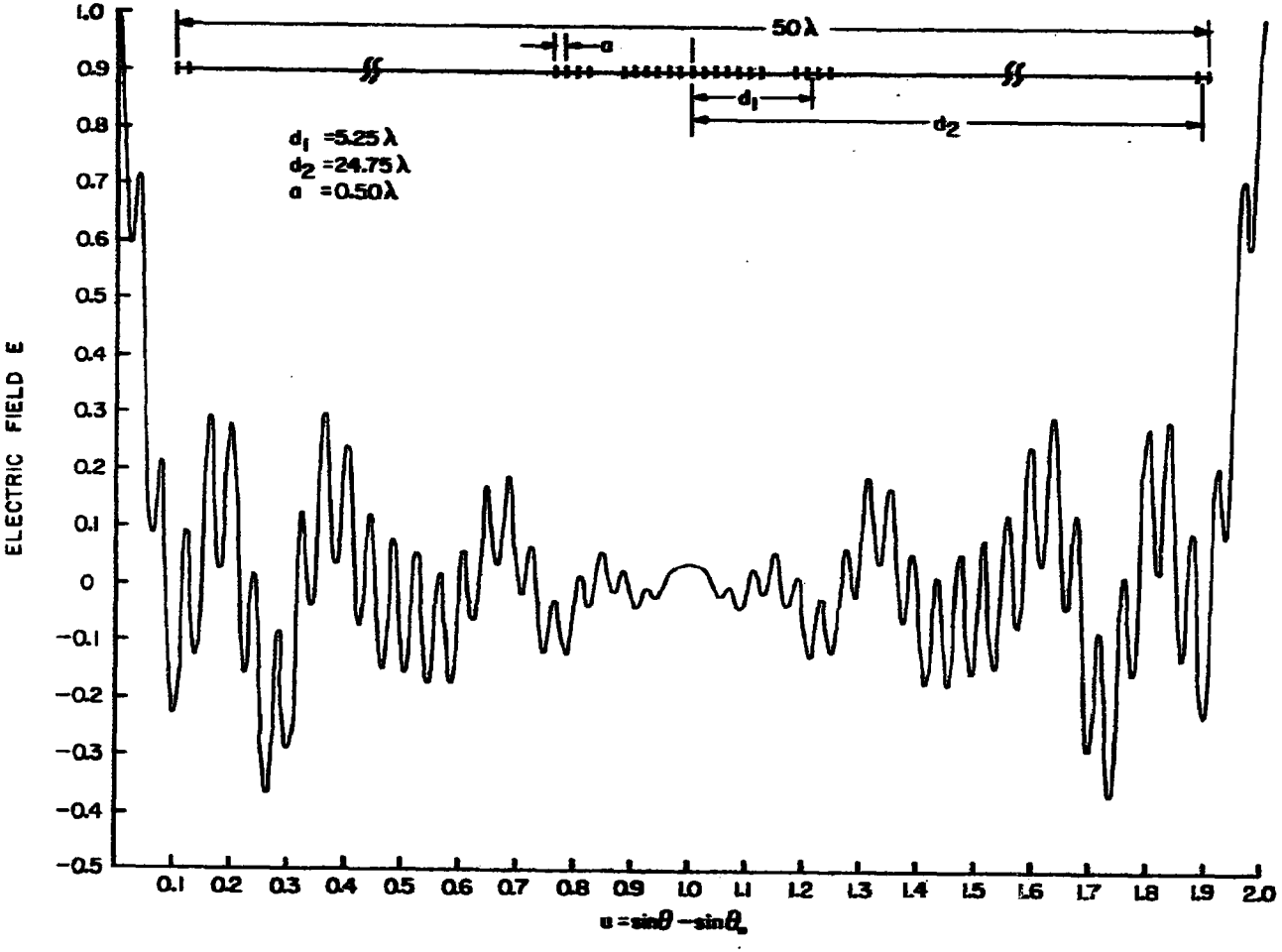

FIG. 51 —FIELD PATTERN FOR CASE 2, d_1=5.25λ

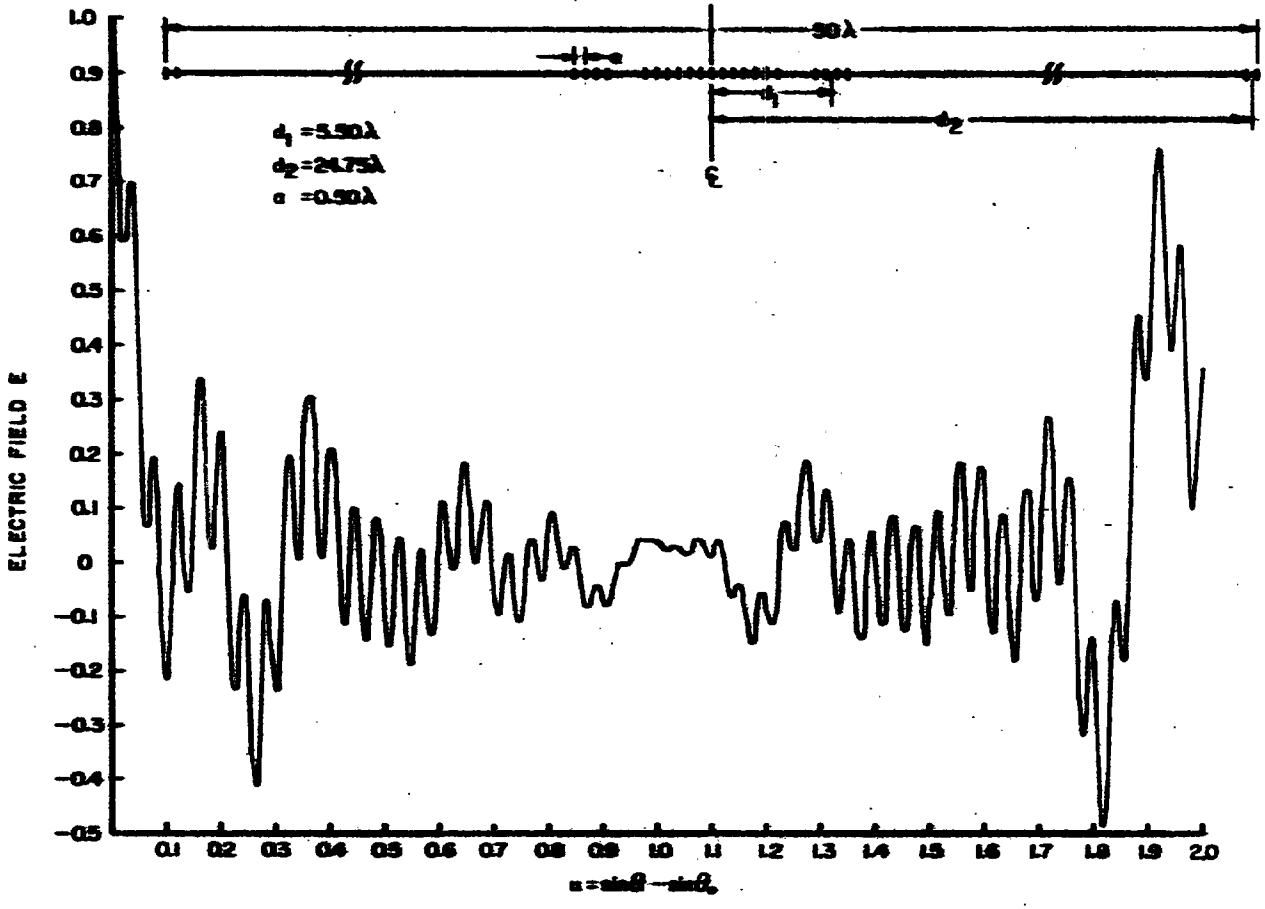

FIG. 52—FIELD PATTERN FOR CASE 2, d_1=5.50λ

FIG. 53 - VARIABLE TRANSMISSION

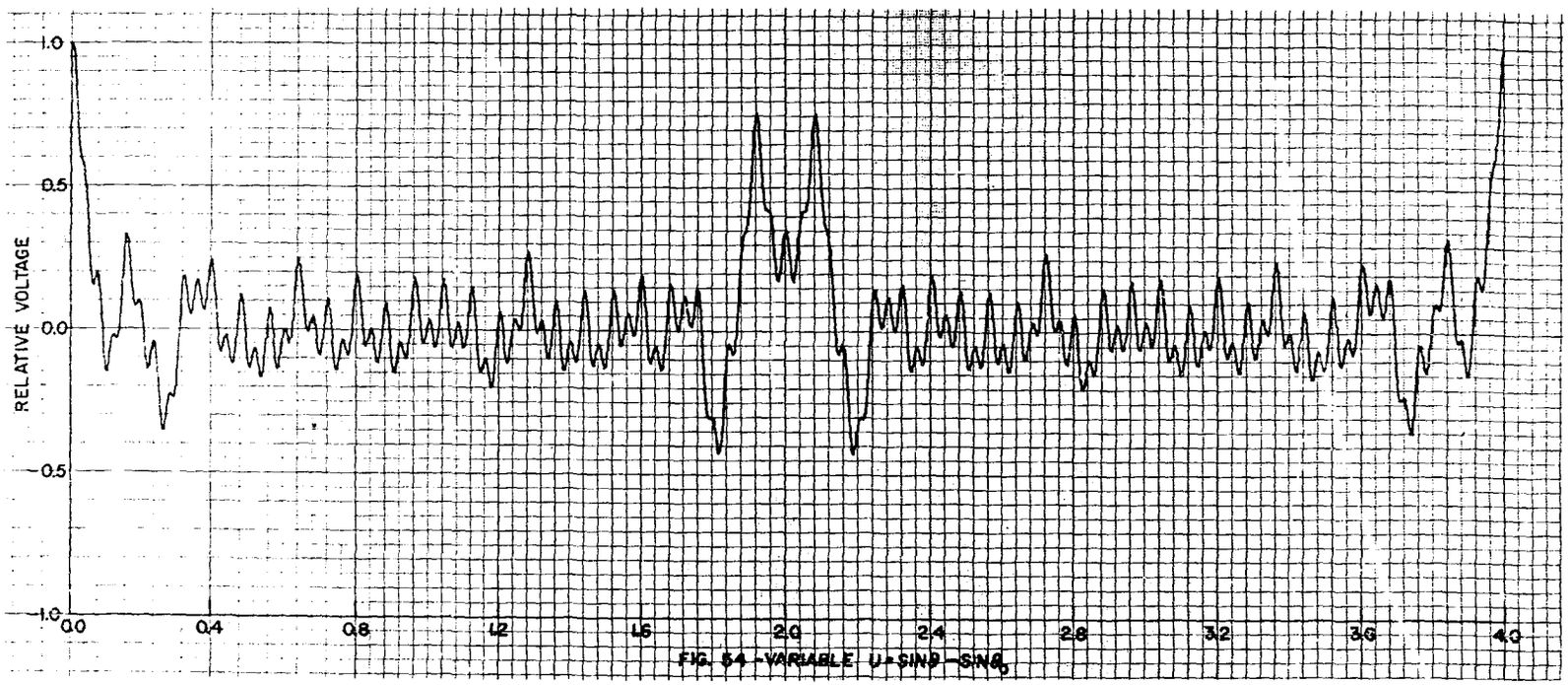

FIG. 54 - VARIABLE U = SINθ - SINθ_0

normal) is the angle to which the main beam is steered. At $u = \frac{m\lambda}{d}$, m being any integer, E(u) reaches the same peak value as at the main beam. These sidelobes at $u = \frac{m\lambda}{d}$ are known as grating lobes, and it is these grating lobes which the least squares criterion seeks to eliminate.

Figure 55-a is a plot of positions of maxima and minima along the u axis for 4 terms of $\cos \frac{2\pi nd}{\lambda} u$, or for an array of 9 equally-spaced sources. The positions of maxima are indicated by the vertical lines in the equally spaced array.

If the array is composed of 2N + 1 unequally-spaced elements distributed symmetrically about the center the voltage pattern is given by:

$$E(u) = 1 + 2 \sum_{n=1}^{N} \cos \frac{2\pi d_n u}{\lambda} \quad . \tag{17}$$

Figure 55-b is a plot of positions of maxima and minima for 4 terms of $\cos 2\pi d_n u/\lambda$, or for an array of 9 unequally spaced elements, distributed symmetrically about the center.

To eliminate the grating lobes, the distances between maxima at grating lobes for $\cos(2\pi d_n u/\lambda)$ and the first minima beyond the grating lobes for $\cos(2\pi d_{n+1} u/\lambda)$ are found in terms of d_n and d_{n+1}. These distances, some examples of which are marked by Δ in Figure 55, are squared and then added together. The resulting summation, σ_o, is minimized by differentiating with respect to the d_n's, setting the result equal to zero, and then solving for the d_n's. The resulting d_n's make σ_o a minimum, or they bring the grating lobe maxima of $\cos(2\pi d_n u/\lambda)$ as close to the next minima of $\cos(2\pi d_{n+1} u/\lambda)$ as possible.

As long as there are not many grating lobes (no more than 2 or 3) to be eliminated, this method eliminates them well. However in doing so, it creates other high sidelobes which were not present in the field pattern of the equally spaced array. To eliminate these new lobes, similar distances Δ were set up, squared, and summed. The resulting summation, σ_1, was added to σ_o, and the d_n's found so as to minimize $\sigma_o + \sigma_1$. This eliminated neither the grating lobes nor the new lobes altogether.

The least squares criterion was applied in combination with various trial-and-error methods to attempt to eliminate grating and other lobes, but no combination was found to be fully effective. No matter what lobes (grating or otherwise) were eliminated, other objectionable lobes always appeared, and the more Δ terms that were used in the summation, the less effective the method became.

6.5 Simultaneous Solution Method

The field pattern of an array of 2N + 1 unequally spaced, isotropic elements, each with unity amplitude is:

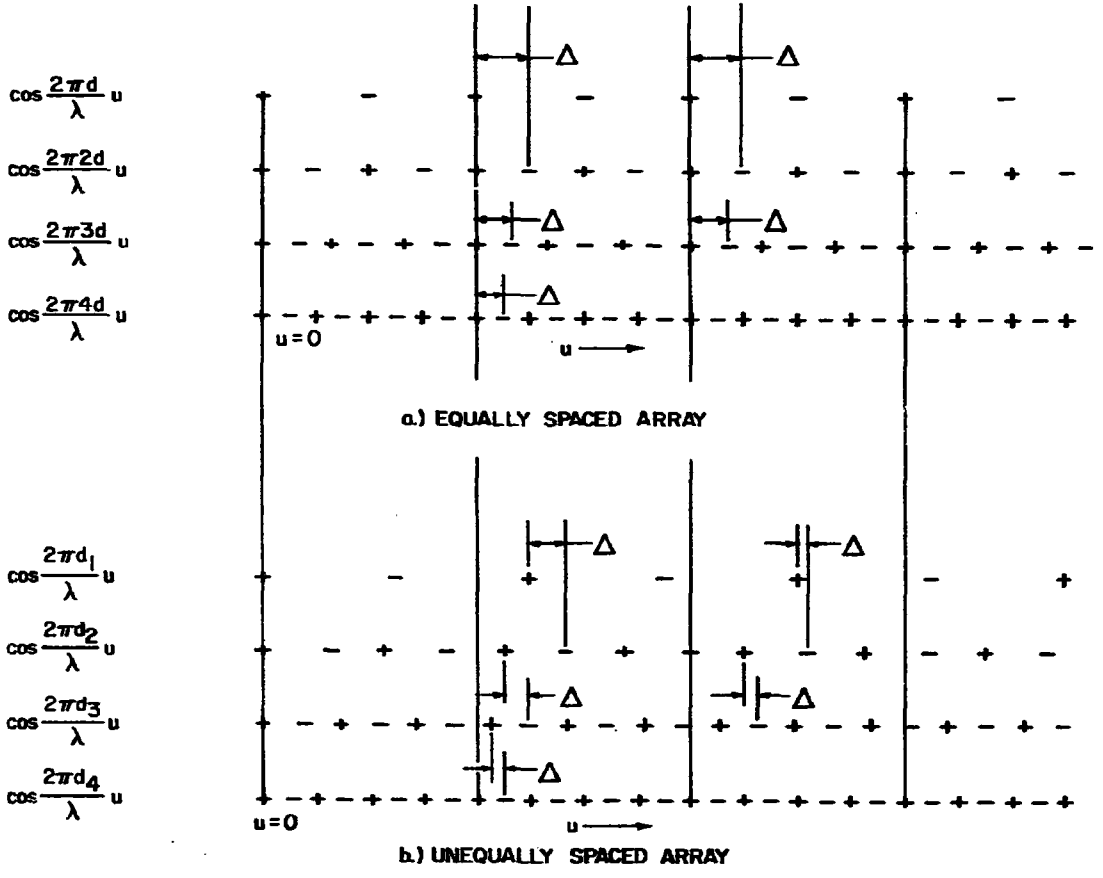

FIG. 55 – U-AXIS "MAXIMA-MINIMA" DIAGRAMS EIGHT ELEMENTS (ADDITIONAL ELEMENT AT CENTER)

\+ DENOTES A MAXIMUM
– DENOTES A MINIMUM

$$E(u) = 1 + 2 \sum_{n=1}^{N} \cos \frac{2\pi d_n}{\lambda} u \tag{18}$$

where λ is the wavelength, d_n is the distance of the n^{th} pair of elements from the center, and $u = \sin\theta - \sin\theta_o$. θ is an angle measured from the array normal, and θ_o (also measured from the array normal) is the angle to which the main beam is steered.

N values of E(u) are specified at N different values of u. This gives a set of N simultaneous equations which are transcendental and not easy to solve. They can be solved by computer, but for large N, this becomes impractical because of the large amount of computations involved. To simplify the calculations, make N even, and specify E(u) at equal increments of u as -K, +K, -K, ..., etc. Then the system of simultaneous equations becomes:

$$\begin{aligned}
E(u_1) &= 1 + 2 \sum_{n=1}^{N} \cos \frac{2\pi d_n}{\lambda} u_1 = -K \\
E(u_2) &= 1 + 2 \sum_{n=1}^{N} \cos \frac{2\pi d_n}{\lambda} 2u_1 = +K \\
E(u_3) &= 1 + 2 \sum_{n=1}^{N} \cos \frac{2\pi d_n}{\lambda} 3u_1 = -K \\
E(u_n) &= 1 + 2 \sum_{n=1}^{N} \cos \frac{2\pi d_n}{\lambda} Nu_1 = +K
\end{aligned} \tag{19}$$

where $u_m = mu_1$.

Adding these equations

$$2 \sum_{n=1}^{N} (1/2 + \cos \frac{2\pi d_n}{\lambda} u_1 + \cos \frac{2\pi d_n}{\lambda} 2u_1 + \cdots + \cos \frac{2\pi d_n}{\lambda} Nu_1) = 0 \tag{20}$$

By Lagrange's identity,[33] the left hand side can be written as

$$\sum_{n=1}^{N} \frac{\sin(2n+1)\frac{\pi d_n u_1}{\lambda}}{\sin\frac{\pi d_n u_1}{\lambda}} = 0 \qquad (21)$$

The proper values of d_n can be found by choosing the values of $\frac{\pi d_n}{\lambda} u_1$ which satisfy Equation 21. Actually, by proper arrangement of the values of the K's, Equation 21 can be made equal to anything, but arranging the K's to make Equation 21 equal to zero is the most convenient way.

To assure that the slope of E(u) is zero at $u_1, u_2, \ldots, u_N$, differentiate each of the equations of Equation 19, and set the result equal to zero. This gives:

$$\begin{aligned}
E'(u_1) &= -\frac{4\pi}{\lambda}\sum_{n=1}^{N} d_n \sin\frac{2\pi d_n}{\lambda} u_1 = 0 \\
E'(u_2) &= -\frac{4\pi}{\lambda}\sum_{n=1}^{N} d_n \sin\frac{2\pi d_n}{\lambda} 2u_1 = 0 \\
E'(u_3) &= -\frac{4\pi}{\lambda}\sum_{n=1}^{N} d_n \sin\frac{2\pi d_n}{\lambda} 3u_1 = 0 \\
&\vdots \\
E'(u_N) &= -\frac{4\pi}{\lambda}\sum_{n=1}^{N} d_n \sin\frac{2\pi d_n}{\lambda} Nu_1 = 0 \,.
\end{aligned} \qquad (22)$$

Taking the sum of these equations and dropping the factor of $-\frac{4\pi}{\lambda}$

$$\sum_{n=1}^{N} d_n \left(\sin\frac{2\pi d_n u_1}{\lambda} + \sin\frac{2\pi d_n 2u_1}{\lambda} + \ldots + \sin\frac{2\pi d_n Nu_1}{\lambda}\right) = 0 \qquad (23)$$

The left hand side can be rewritten as

$$\sum_{n=1}^{N} d_n \frac{\sin N \frac{\pi d_n u_1}{\lambda} \sin (N+1) \frac{\pi d_n u_1}{\lambda}}{\sin \frac{\pi d_n}{\lambda} u_1} = 0 \qquad (24)$$

Then values of d_n can be found by selecting values of $\frac{\pi d_n u_1}{\lambda}$ which satisfy Equation 24.

The simultaneous solution method can be used to specify values of E(u) or the slope at these fixed values of u only. It has no direct control over E(u) or its slope between these fixed points, and therefore no way (except trial and error) to hold down sidelobes in between the fixed points. This method has not proven effective.

Figure No.	Displacement From Array Center (One element present at center)											
	d_1	d_2	d_3	d_4	d_5	d_6	d_7	d_8	d_9	d_{10}	d_{11}	d_{12}
45	2.43	4.92	7.22	9.54	11.76	13.80	15.81	17.71	19.59	21.45	23.27	25.00
47	0.94	3.06	5.12	7.31	9.68	12.10	14.38	16.69	18.81	20.81	22.81	25.00
48	0.75	2.31	3.94	5.63	7.43	9.50	11.80	14.50	17.20	19.88	22.44	25.00
49	1.82	3.67	5.56	7.53	9.60	11.83	14.30	17.18	20.73	25.00		
51	0.50	1.00	1.50	2.00	2.50	3.00	4.50	5.00	5.50	6.00	24.50	25.00
52	0.50	1.00	1.50	2.00	2.50	3.00	4.75	5.25	5.75	6.25	24.50	25.00
53	0.50	1.00	1.50	2.00	2.50	3.00	4.50	5.00	5.50	6.00	12.50	25.00
54	0.50	1.00	1.50	2.00	2.50	3.00	4.75	5.25	5.75	6.25	12.50	25.00

TABLE VI

Element Locations For Arrays Of Section 6

7. AN UPPER BOUND FOR THE SIDELOBES OF AN UNEQUALLY SPACED ARRAY

7.1 Introduction

The theory of unequally spaced arrays does not seem to be on as firm a footing as that of equally spaced arrays. Most of the successful designs of unequally spaced arrays have been made without recourse to a precise theory. In an attempt to provide further analysis of this type of array, a result from number theory was applied to derive an upper bound to the radiation pattern.[34] The result does not apply to all classes of unequally spaced arrays and the derived upper bound is not low enough to be of general use for making a sharp prediction of the peak sidelobe level of practical arrays. Nevertheless it is of interest since, as far as is known, it is the only attempt yet made to predict an upper bound and it provides verification that the sidelobes are a function of the number of elements contained in the array.

The major result of this application of number theory is that the field intensity

$$E(u) = 1 + 2 \sum_{n=1}^{N} \cos 2\pi d_n u \tag{25}$$

$$|E(u)| < 1 + 2 \left[2 + |f'(N) - f'(1)|\right] \left[1 + \frac{3}{\pi} + \frac{4}{\sqrt{\pi\gamma}}\right] \tag{26}$$

where $f(x)$ is the function describing the element spacings, $f'(N)$ and $f'(1)$ are the derivatives of $f(x)$ at the endpoints $x = N$ and $x = 1$ of the interval defining the allowable values of the element spacings, and γ is defined such that $f''(x) \geq \gamma > 0$. The array consists of a center element plus N pairs of symmetrically located elements. Equation 26 is derived in Appendix IV. The assumption made in the derivation of the upper bound restrict the class of element spacings for which this expression is applicable. One of the most important restrictions is that the spacings between elements be monotonic increasing (or monotonic decreasing). This eliminates almost all of the optimum configurations found by the dynamic programming technique described in Section 5.

7.2 Applications

A convenient form for application of the theorem to an array is to assume a quadratic spacing of the elements. Let the spacing of the n^{th} element from the array origin be given by

$$d_n = An + \frac{B}{N} n^2 . \tag{27}$$

The constant A determines the spacing in the equally spaced array and the constant B perturbs the equal spacing and increases the array length. If ℓ is the length of the array then $\ell/2 = N(A+B)$. With the spacing of Equation 27, f(x) = f(n) becomes

$$f_n = u\left(An + \frac{B}{N} n^2\right), \tag{28}$$

which with proper substitution, Equation 26 predicts that

$$|E(u)| < 1 + 4\,[Bu + 1]\,\left[1 + 3/\pi + 4/\sqrt{\frac{2\pi Bu}{N}}\right],$$

or

$$|E(u)| < 1 + 4\,[Bu + 1]\,\left[1.9549 + 1.5964\sqrt{\frac{N}{Bu}}\right] \tag{29}$$

There are several general observations that can be made about this expression. First, the sidelobe pattern is independent of A, i.e., the perturbed equally spaced array. Second, for large N, the sidelobe region is determined primarily by the $\sqrt{N}$. For example, if

$$\sqrt{\frac{N}{Bu}} \gg 1, \quad \text{then}$$

$$|E(u)| < 6.4\,(Bu + 1)\sqrt{\frac{N}{Bu}} \quad .$$

This result is considered significant since other independent analyses predict the same $\sqrt{N}$ dependency. It is shown in Section 3 that the predicted statistical average sidelobe level approaches $\sqrt{N}$ when the degree of thinning is large. Section 8 discusses arrays from an energy viewpoint and there again the average sidelobe level is shown to be $\sqrt{N}$ for severe thinning. Third, the sidelobe level will be higher as u is increased.

The upper bound estimate of Equation 26 was applied to several examples of unequally spaced arrays of 25 elements (N = 12) designed by various techniques. In all cases, the upper bound was larger than the maximum of the main lobe. For a 201 element (N = 100) quadratically spaced array the estimates were high but less than the main lobe.

Improvement is obtained as the number of elements increases, but even then the results are quite conservative. If the array as described by Lo[36] is arranged in a quadratic fashion so that 19,000 elements remain in each arm which is $7 \times 10^3 \lambda$ in extent and 80λ wide, then, in Equation 27

$$A = 3.18 \times 10^{-3},$$

$$B = 3.68 \times 10^{-1},$$

$$N = 9.5 \times 10^3 .$$

Using these values Equation 29 predicts that the sidelobes will lie below 22.7 db in the vicinity of u = 1. Lo's data predicts that 84% of the sidelobes in this array will be below 30 db.[36]

7.3 Conclusions

The upper bound of the sidelobes obtained from number theory requires that the function for the element spacing be monotonic. Unless the number of elements is large, the predicted sidelobe levels are too gross.

Further study was made of eliminating the monotonic condition on the spacings. Success was achieved in this area and reasonable sidelobe levels are predicted although they are still conservative.[35] The difficulty with the elimination of the monotonic condition is that the expression for the upper bound becomes as difficult to calculate as the original expression. The purpose of applying number theory was to achieve simple expressions to predict sidelobe behavior.

While number theory predicts results too gross to be of real benefit, the predicted behavior supports results achieved both statistically and deterministically. For example, the sidelobe behavior in voltage is determined by the square root of the number of elements. Also, the sidelobe level is expected to rise when the array is steered (i.e., increasing u) if the spacings are monotonic.

Further details may be found in Technical Notes 2 and 3 prepared for this contract.[28, 35]

8. DISCUSSION OF ANTENNA ARRAYS FROM AN ENERGY VIEWPOINT

Some insight may be gained into the behavior of thinned arrays by investigating equally-spaced antenna arrays from an energy viewpoint. The total energy radiated by an array is found by integrating the field intensity over all space. Since the integration is simpler for a linear array, it will be used in this discussion. The results, however, are applicable in a qualitative sense to planar arrays because (1) the continuous line source pattern (in regard to energy) is similar to that of a continuous rectangular aperture, and (2) the principal plane patterns of a planar array of equally spaced elements is identical to the pattern of a linear array of the same total length and spacing between the elements.

The energy in the main beam of a continuous line source is 81.5% of the total energy radiated, and this is also the precentage of energy in the main beam of a continuous rectangular aperture. Thus, it is believed that the following results are applicable to the planar array with minor modifications although the linear array will be the basis for the analysis.

8.1 Energy Radiated by a Linear Array

There are several sources[37, 38] which discuss the total energy radiated by an array of N elements. This total energy may be shown to be

$$\text{Energy}_{\text{Total}} = W_T = 4\pi \left[N + 2 \sum_{n=1}^{N-1} (N-n) \frac{\sin nkd}{nkd} \right] \tag{30}$$

If this work is further generalized for electronically steered arrays composed of equally-spaced, isotropic elements, Equation 30 becomes

$$W_T = 4\pi \left[N + 2 \sum_{n=1}^{N-1} (N-n) \cos(nkd \cos \theta_o) \frac{\sin nkd}{nkd} \right] \tag{31}$$

where N = total number of elements

$k = 2\pi/\lambda$

λ = wavelength

d = spacing between elements

θ_o = angle to which the beam is electronically steered as measured from the plane of the array

If the array is not electronically steered, so that the phase is a constant across the array, then $\theta_o = \pi/2$, and Equation 31 reduces to Equation 30.

It is recognized that the total energy radiated by an array is not a constant if the spacing is varied, which results in the "gain" of the array varying as sketched in Figure 56 taken from Milazzo and D'Angelo.[38] One reason for this phenomenon is the variation in the mutual coupling between the elements.[12]

An important quantity is the fractional part of the energy found in the main beam. It can be shown that the intensity, $|E(u)|^2$, of an equally spaced array of N isotropic elements is

$$|E(u)|^2 = N + 2 \sum_{n=1}^{N-1} (N-n) \cos nkdu \,, \tag{32}$$

where

$$u = (\cos\theta - \cos\theta_o) \,.$$

The main beam half-null width is given by λ/Nd (This can be shown by considering that $\frac{\sin N\, kdu/2}{N \sin kdu/2} = 0$, when $u = \pm\lambda/Nd$). To find the energy in the main beam, W_{mb}, it is necessary to integrate the intensity over the region of the main beam, i.e., from $u = \pm\lambda/Nd$.

$$W_{mb} = 2\pi \int_{-\lambda/Nd}^{\lambda/Nd} |E(u)|^2 \, du \,,$$

or

$$W_{mb} = \frac{4\pi\lambda}{d} \left[1 + 2 \sum_{n=1}^{N-1} \left(\frac{N-n}{N}\right) \frac{\sin 2\pi u}{2\pi u} \right] \tag{33}$$

There are several interesting features about Equation 33 that need mentioning. First, the energy in the main beam is inversely proportional to the distance (d) between elements. This does not however, mean that the fractional part of the energy in the main beam is inversely proportional to d, because the total energy radiated W_T, also varies with d. A sketch has been made of the ratio of W_{mb}/W_T and is given in Figure 57. Here the number of elements was fixed at N = 10 and the spacing varied. This curve points out quite clearly the effect of increasing the spacing in an array. The percent of energy in the main beam can be reduced considerably by only slightly increasing

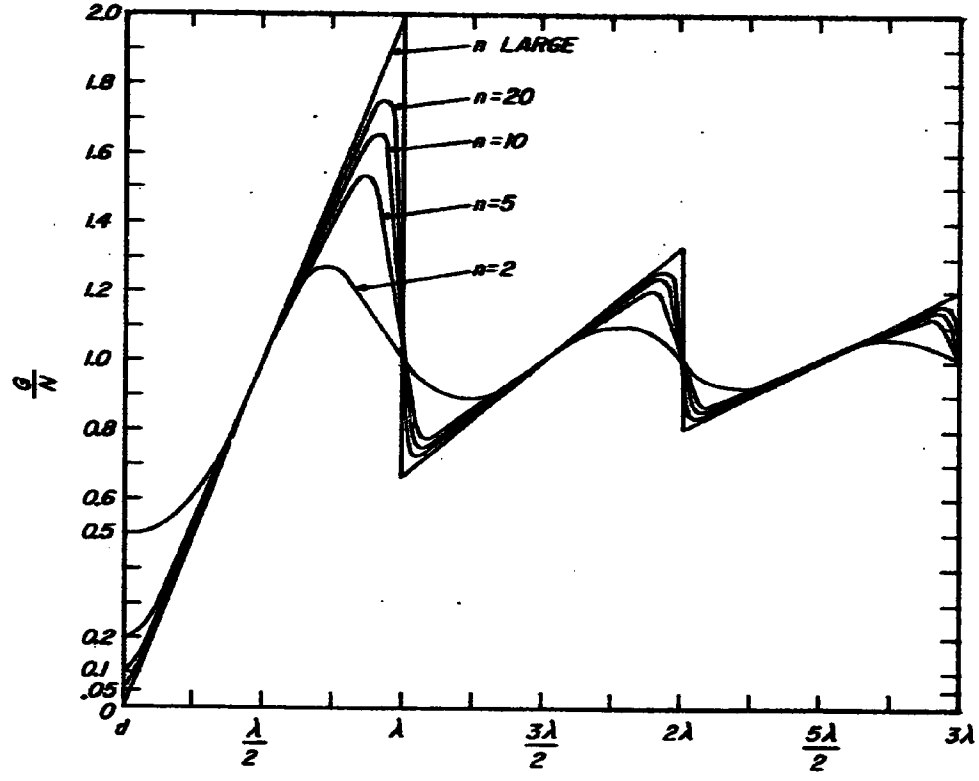

FIG.56 — GAIN vs SPACING FOR MULTI-ELEMENT LINEAR ARRAYS

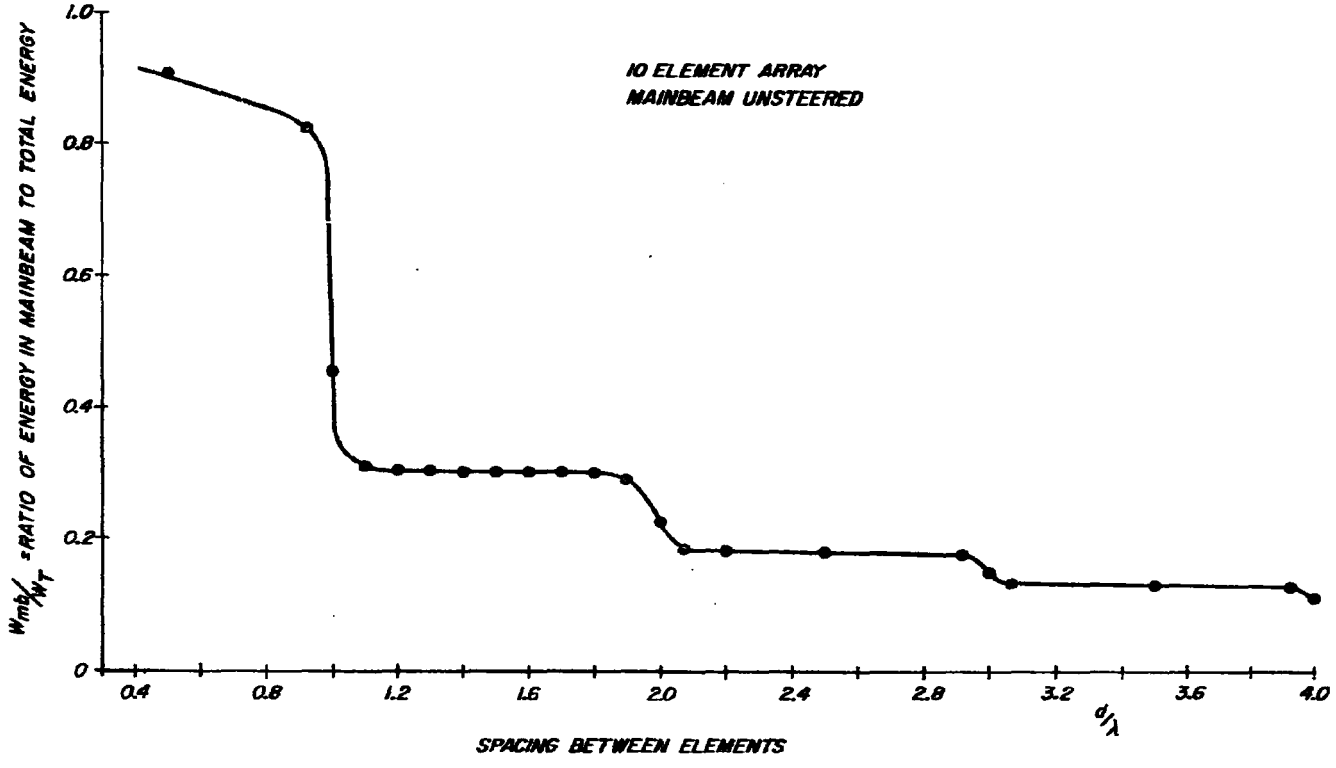

FIG. 57 — RATIO OF ENERGY IN MAINBEAM vs ELEMENT SPACING

the spacing, i.e., going from $d = 0.9\lambda$ to $d = 1.1\lambda$. By using curve-fitting techniques it is possible to show that the ratio W_{mb}/W_T can be approximated by

$$\frac{W_{mb}}{W_T} = \frac{1}{1.11\,(M+1)} \tag{34}$$

where M is the number of grating lobes in the visible region i.e., M=2 for $\lambda \leq d \leq 2\lambda$, M = 4 for $2\lambda \leq d \leq 3\lambda$, etc. Table VII shows the values of W_{mb}/W_T calculated by Equation 34 and this can be compared to Figure 57.

d	M	W_{mb}/W_T
$\lambda/2 \leq d < \lambda$	0	.910
$\lambda \leq d < 2\lambda$	2	.300
$2\lambda \leq d < 3\lambda$	4	.180
$3\lambda \leq d < 4\lambda$	6	.129

TABLE VII

Second, the energy in the main beam is independent of the scan angle. This is not inconsistent with the fact that the gain of an array is reduced as the array is electronically scanned. The quantity u is linear, but $u = \cos\theta - \cos\theta_o$ so that θ represents a larger angle when $\theta_o \neq 90^\circ$ than when $\theta_o = 90^\circ$ (broadside). Hence, the gain decreases not because the energy in the main beam decreases, but because the solid angle into which this energy is radiated is increased, and also the total power radiated depends upon the steering angle. The fact that the total power radiated depends upon the steering angle is a direct consequence that the total power radiated depends upon the spacing, and steering an array electronically changes the electrical distance between the elements. Examine Equation 31 for $\theta_o = 0^\circ$ (end fire) and $\theta_o = 90^\circ$ (broadside).

$$\theta_o = 0^\circ: \; W_T = 4\pi \left[N + 2 \sum_{n=1}^{N-1} (N-n) \, \frac{\sin 2nkd}{2nkd} \right] \tag{35}$$

$$\theta_o = 90^\circ: \; W_T = 4\pi \left[N + 2 \sum_{n=1}^{N-1} (N-n) \, \frac{\sin nkd}{nkd} \right] \tag{30}$$

When Equations 30 and 35 are normalized with respect to N, then they

are identical in form, but have a different frequency in the argument of the sine function. Equation 35 has twice the frequency. This means that Figure 56 may be used for the gain of an array steered to the end-fire condition by doubling the frequency of the abscissa (i.e., multiply the values of the spacing by 2). Again observe that this statement can only be made for isotropic elements.

8.2 Element Reduction in An Equally Spaced Array

The effect of reducing the elements in an array can be investigated from an energy standpoint by maintaining a constant number of elements, increasing the spacing between the elements, and keeping this spacing equal. Increasing the spacing means that the array is being thinned if compared to a full array, i.e., an array of half-wavelength spacing. Thus an array of one wavelength spacing is said to be thinned approximately 50 percent. If N = 10, and the fraction of energy outside the main beam is compared to the fraction of elements removed, the curve shown in Figure 58 results. Shown dotted is the curve "Fraction of Energy Outside the Main Beam" equal to the "Fraction of Elements Removed". Thus, it is shown that when the elements are spaced equally at large spacings, the fraction of energy outside the main beam is approximately equal to the fraction of elements removed (i.e., removed from an array with elements at half wavelength spacing). Observe the spacing is equal so that many grating lobes exist, and hence the designation "energy outside the main beam".

Define the following quantities:

N = number of elements in the full array

N_R = number of elements removed from the array

$N_E = N - N_R$ = number of elements remaining in the array

W_{mb} = energy in the main beam

W_{SL} = energy outside the main beam

and W_T = total energy radiated by the array

With these definitions it can be seen that

$$W_T = W_{mb} + W_{SL} \tag{36}$$

and from Figure 58 it is recognized that

$$\frac{W_{SL}}{W_T} = \frac{N_R}{N} \tag{37}$$

since for large spacing between elements the fraction of energy outside the main beam $(\frac{W_{SL}}{W_T})$ is equal to the fraction of elements removed $(\frac{N_R}{N})$.

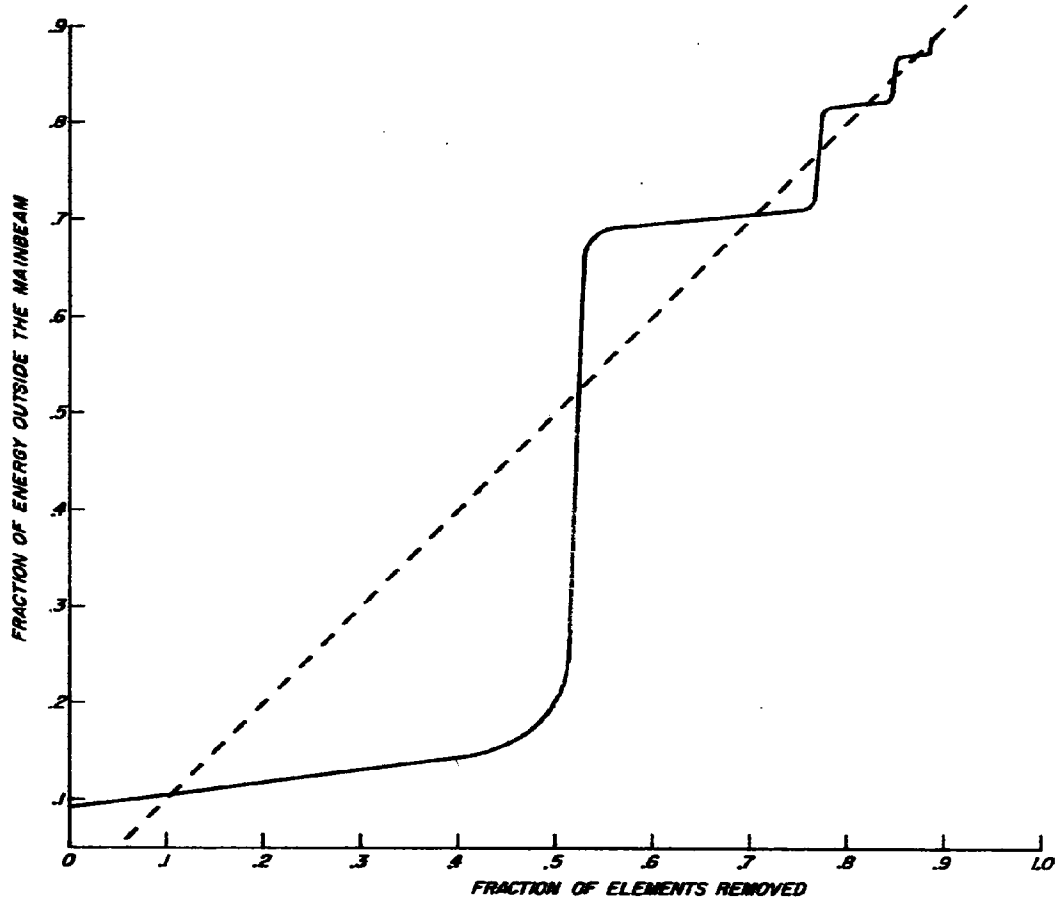

FIG. 58 -RELATION BETWEEN ENERGY AND ELEMENTS REMOVED

From Equations 36 and 37 a most important relationship can be established for a "thinned" array.

$$\frac{W_{mb}}{W_{SL}} = \frac{N_E}{N_R} \tag{38}$$

Equation 38 is an expression which relates the ratio of energy found in the main beam to that outside the main beam to the ratio of the number of elements in the array to the number of elements removed. Knowing the ratios given in Equations 37 and 38 another feature of the energy distribution can be found.

$$\frac{W_{mb}}{W_T} = 1 - \frac{W_{SL}}{W_T} = 1 - \frac{N_R}{N} = \frac{N_E}{N} \tag{39}$$

It can be shown that the gain of an array with N_E elements is N_E, i.e., $G = N_E$. Therefore from Equation 39

$$\frac{G}{N} = \frac{W_{mb}}{W_T} = 1 - \frac{N_R}{N} \tag{40}$$

Equation 40 is really an identity and not an equation. However, what is important is G/N represents the gain reduction of a full array, and a similar expression is derived by statistical means in Appendix I. Using the convention of this section the gain reduction is shown to be

$$1 - \frac{N_R}{N} = \frac{N_E}{N}$$

for $\rho a = 1$.

Equation 37 has been obtained deterministically from the data available in Figure 58. Hence agreement exists between the deterministic approach using an equally spaced array as a model and the purely statistical method.

The similarity of results between the two approaches is emphasized because of the work presented in the following section (Section 8.3). The work performed was done using an array of equal, but large, spacing between the elements, and the comparable results achieved agree with those obtained by statistical means. The agreement exists when large spacings are considered. Thus, it appears that for large spacings between the elements (i.e., $d \geq 2\lambda$) the division of energy between the main beam and the non-main beam region does not depend significantly on the element position. This implies that while grating lobes are formed in the equally spaced case with low sidelobes in the non-main beam region, approximately the same amount

of energy is radiated into the non-main beam region (i.e., the usual sidelobe region) for unequally spaced elements. The result of spacing in a non-periodic fashion is to destroy the grating lobes of the equally spaced array and redistribute the energy contained in these grating lobes throughout the sidelobe region.

The distinction has been made between the sidelobe region of an equally spaced array, and the sidelobe region of an unequally spaced array. This was done because grating lobes, which are not the usual type of sidelobes, exist in the non-main beam region of an equally spaced array. However, the distinction will no longer be made since the energy outside the main beam is assumed to be independent of element position for widely spaced elements. Thus, the non-main beam region will be the sidelobe region, and the energy outside the main beam will be the energy is the sidelobe region.

8.3 Prediction of Average Sidelobe Levels

Knowing the ratio of energy in the main beam to energy in the sidelobes, i.e., Equation 38, it is possible to make a determination of the average sidelobe level of a linear array. To do this a model for the array pattern must be chosen. The main beam shape is taken to be $\sin u/u = 1 - u^2/3!$, which is a good approximation for small values of u ($u = \pi a \sin\theta/\lambda$). The average sidelobe is a constant level. Hence, the model takes the form sketched in Figure 59 where

$$E(u) = N_E - (N_E - E_o)\frac{a^2}{\lambda^2}u^2 \qquad 0 \le u \le \lambda/a \tag{41}$$

$$E(u) = E_o \qquad \lambda/a \le u \le 1$$

It was shown in Section 8.1 that the energy radiated into some portion of the u region was

$$W \alpha \int_{u_1}^{u_2} |E(u)|^2 \, du$$

So that the energy radiated into the main beam according to the assumed model is

$$W_{mb} \alpha \int_0^{\lambda/2} |E(u)|^2 \, du = \frac{\lambda}{a} \cdot \frac{1}{15} \cdot [8N_E^2 + 4N_E E_o + 3E_o^2] \tag{42}$$

and into the sidelobes

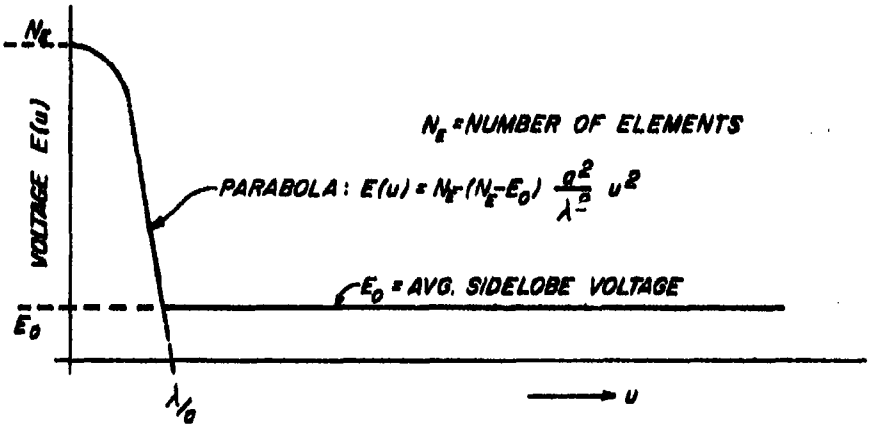

$$E(u) = N_E - (N_E - E_0)\frac{a^2}{\lambda^2} u^2 \qquad 0 \le u \le \lambda/a$$

$$= E_0 \qquad \lambda/a \le u \le 1$$

FIG. 59 – MODEL FOR APPROXIMATING THE AVG. SIDELOBE VOLTAGE.

$$W_{SL} \propto \int_{\lambda/a}^{1} |E(u)|^2 \, du = E_o^2 \, (1 - \lambda/a) \tag{43}$$

But the term λ/a is approximately

$$\lambda/a = 2/N \, . \tag{44}$$

so that Equations 42 and 43 become

$$W_{mb} \propto \frac{2}{15N} \left[8N_E^2 + 4N_E E_o + 3E_o^2 \right] \tag{45}$$

and

$$W_{SL} \propto E_o^2 \left[1 - 2/N \right] \tag{46}$$

Using Equation 38 with Equations 45 and 46 the following relation is found.

$$\frac{\frac{2}{15N} \left[8N_E^2 + 4N_E^2 + 3E_o^2 \right]}{E_o^2 \left[1 - 2/N \right]} = \frac{N_E}{N_R}$$

Performing some algebra

$$E_o = \frac{1}{2} \left[\frac{(8/15) N_R N_E}{(2/5) N_R - N N_E + 2 N_E} + \sqrt{\left(\frac{(8/15) N_R N_E}{(2/5) N_R - N N_E + 2N} \right)^2 - 4 \frac{(16/15) N_R N_E^2}{(2/5) N_R - N N_E + 2 N_E}} \right] \tag{47}$$

This expression predicts the average sidelobe level (in voltage) in terms of N, N_E and N_R, where $N_E = N - N_R$. For severe thinning the relationship between NN_E, N_R and N_E may be written as

$$NN_E >> N_R > N_E \tag{48}$$

so that Equation 47 becomes

$$E_o \approx 4 \left[\frac{N_R}{15N} + \sqrt{\frac{N_R}{15N} \left(\frac{1}{15} \frac{N_R}{N} + N_E \right)} \right]$$

Dividing the inequality in Equation 48 by N so that $N_E >> N_R/N$

$$E_o \approx 4 \left[\frac{1}{15} \frac{N_R}{N} + \sqrt{\frac{1}{15} \frac{N_R}{N} \cdot N_E} \right] \tag{49}$$

The ratio R of the main beam peak to the average sidelobe level is

$$R = \frac{N_E}{4\left[\frac{1}{15}\frac{N_R}{N} + \sqrt{\frac{1}{15}\frac{N_R}{N}\cdot N_E}\right]} \tag{50}$$

Since $N - N_E = N_R$ it is seen that

$$\frac{N_R}{N} = 1 - \frac{N_E}{N}$$

so that

$$R = \frac{N_E}{4\left[\frac{1}{15}\left(1 - \frac{N_E}{N}\right) + \sqrt{\frac{1}{15}\left(1 - \frac{N_E}{N}\right)N_E}\right]}$$

If

$$1 \ll N_E \ll N$$

then,

$$R \cong \frac{1}{4}\sqrt{15 N_E} \approx \sqrt{N_E} \tag{51}$$

Equation 51 is a very powerful result in that it predicts the voltage ratio of the main beam peak to the average sidelobe level in terms of the number of elements in the array. While such relationships are not new[11, 14, 18], this is the first non-probabilistic, non-intuitive, derivation.

To generalize the work of other authors, the ratio R in terms of voltage is a constant times the square root of N_E, i.e., $K_1\sqrt{N_E}$.

The average sidelobe level, which has been estimated here is in reality not possible to achieve. This is best explained by Gibbs phenomena in Fourier analysis. It would take an infinite number of elements to yield a constant value over an interval of u when sine terms are summed. Because sine terms are being summed, it is reasonable to assume that the best pattern that could be achieved in the sidelobe region would be a sine function which has an average value equal to $\sqrt{N_E}$ and a peak value $\sqrt{2}$ times the average value. In terms of the ratio R, this means that

$$R = \sqrt{\frac{N_E}{2}} \tag{52}$$

which is the same value achieved by Andreasen[11] for large average spacings in an array.

It has been shown in this section that essentially the same average value results for the sidelobe region, when an equally spaced array is analyzed, as when some other model is assumed. This is important, because it implies that the energy in the sidelobe region is independent of element position and depends primarily on the number of elements in the structure. The analysis performed here does require that the average spacing, d_{av}, be large in terms of wavelength. That is,

$$d_{av} \geq 2\lambda$$

The derivation was performed for a linear array, but it can be extended to planar arrays since planar arrays are separable in rectangular coordinates. The average sidelobe level for a planar array is equal to $\sqrt{N_E}$. If the sidelobe region is considered to be a two dimensional sine wave with an average value of $\sqrt{N_E}$, then the ratio of the main beam peak to the peak sidelobe level is

$$R = \sqrt{\frac{N_E}{4}} \tag{53}$$

This is also the result achieved by Willey when the thinning is large.[16]

With the prediction of sidelobes in terms of the number of elements that has been outlined here for planar arrays, it is theoretically possible to achieve -24 db sidelobes from a 10,000 element planar array thinned 90%. For convenience Figure 60 has been prepared which relates the fraction of elements removed to the "best" possible achievable peak sidelobes for a 10,000 element planar array subject to various amounts of thinning.

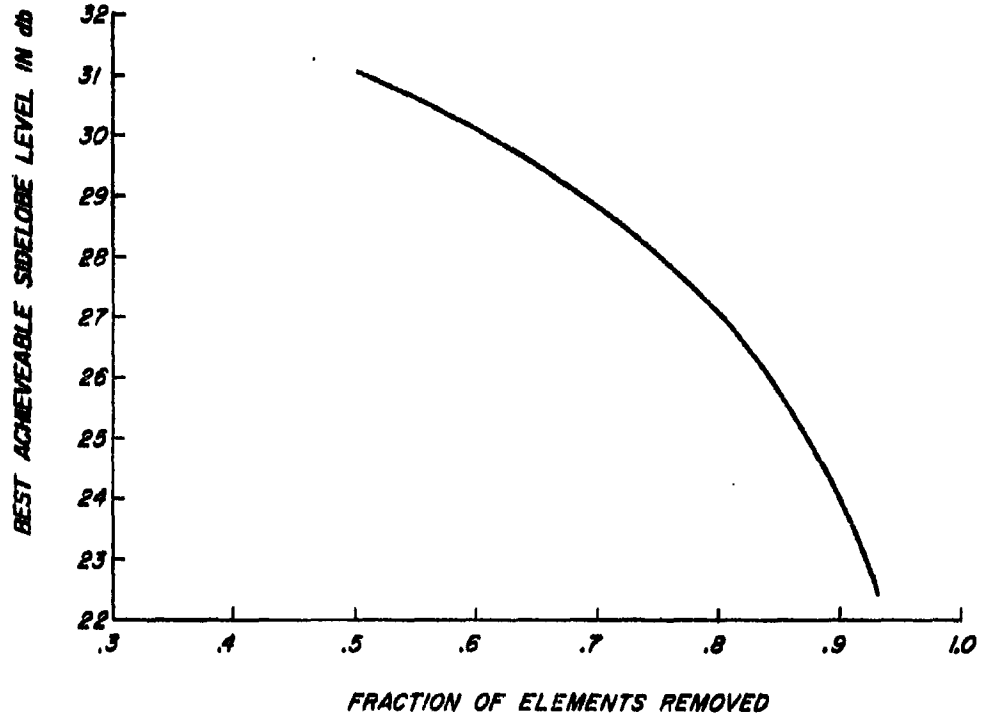

FIG. 60 – RELATIONSHIP BETWEEN BEST SIDELOBE vs THINNING IN A 10,000 ELEMENT ARRAY.

9. MODEL ARRAY PATTERN MEASUREMENTS

9.1 The Pattern Measuring System

Pattern measurements of multi-element array antennas can be greatly simplified by frequency scaling the array and making the measurements at millimeter wavelengths. In this investigation the problems involved in supplying signal to each element separately have been avoided by use of an array modeling technique called the "holey-plate."[24] This process involves the cutting or, as in this case, photo etching of an array of holes in a ground plane. These holes or slots are of a size, shape and configuration so as to be a scale model of the full size antenna. Patterns of the array can then be made by placing the model aperture across a plane electromagnetic wavefront. A description of the system used in this investigation follows.

Previous experience gained during the development of this model pattern measurement technique had shown that a crystal video detection system would not have enough sensitivity for pattern measurements of the multi-element array antennas to be investigated.[39] It was therefore necessary to instrument the antenna pattern range for operation as a 70 Gc superheterodyne system. See Figure 61.

9.1.1 Transmitting

The complete transmitter consists of an RF signal source, horn antenna, phase-correcting lens, and the model array under test. The RF source is an Amperex DX 151 reflex klystron operating at 70 Gc and modulated with a 1000 cps square wave from a fork-tuned modulator. The output of the klystron is then fed, through RG-98/U waveguide, to a 15 db gain horn antenna located at the focus of the lens. A phase-correcting lens, 19" in diameter, is mounted 36" in front of the horn. The purpose of this lens is to create a plane wave over the test array aperture. The model array, etched in a copper-clad dielectric disk 12-3/4" in diameter, is mounted in a ground plane 2' x 3' x 1/8" thick. The mounting arrangement insures a smooth and electrically good joint on both sides of the ground plane.

To prevent the possibility of stray radiation interfering with the desired measurements, the transmitter is housed in a large aluminum tunnel lined with B.F. Goodrich VHP-2 absorber. This absorber has a surface of many pyramids which gives it a high absorption, low reflection characteristic at all incidence angles. The tunnel containing the transmitting equipment is then mounted on a rotating table connected to the pattern recording equipment.

9.1.2 Receiver

The receiver is essentially made up of a collector horn, diode mixer, local oscillator, and IF amplifier. Several other

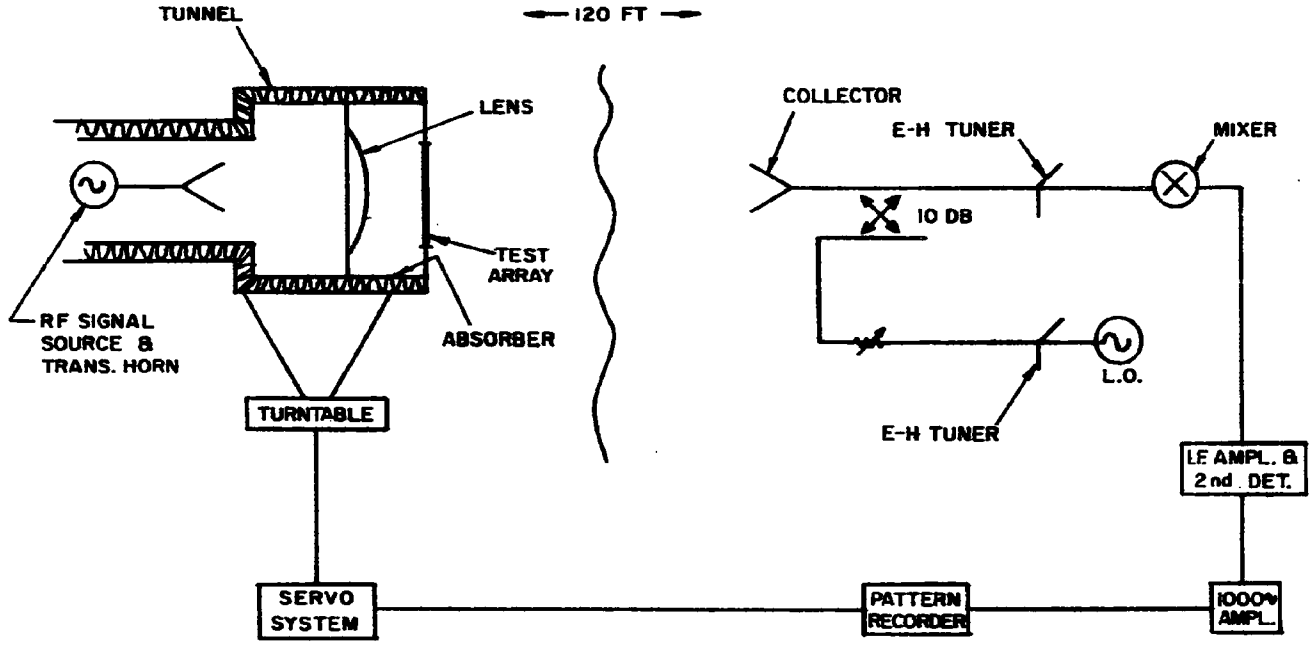

FIG. 61 - MODEL ARRAY PATTERN MEASUREMENT SYSTEM

waveguide components, such as, E-H tuners, variable attenuators and directional couplers are used in the system but since they are standard items a description will be omitted. The collector horn and the local oscillator are identical to those used in the transmitter. The diode mixer is one which was designed and fabricated by ECI personnel. It employs a tungsten catwhisker mounted in a section of RG-99/U waveguide and a silicon die mounted on a differential drive mechanism which is inserted opposite the whisker. With this assembly repeated contacts can be made until a good, stable output is observed. The L.O. signal is applied to the mixer through a waveguide directional coupler. The IF amplifier has a bandpass of 90 to 200 Mc with a gain of 60 db, but, a low pass filter, f_c = 130 Mc, is inserted between the output of the mixer and the amplifier to reduce the noise. The output of the IF amplifier is then applied to the Selective Filter Amplifier of the pattern recorder.

Although a 240 foot antenna range is part of the ECI test range facilities, this distance was not required for far field pattern measurements. Because of the heavy LO and IF amplifier power supplies which would have to be mounted on a 30' tower a shorter antenna range (120 feet) was used with all of the receiver equipment placed on a prefabricated scaffold on the roof of the ECI laboratory at the same level as the transmitter. The receiving equipment was enclosed in a heated box to protect the equipment from freezing and dampness. When tests were run a sliding door facing the transmitter was opened exposing the collector horn.

Two photographs of the range illustrate the system. In Figure 62 the tunnel, transmitting klystron and pattern recorder are visible in the foreground, and through the window the location of the receiver may be seen. Figure 63 shows the tunnel with the 45° steering adaptor in place and the manner of locating the holey plate in the ground plane. The tunnel is reversed from its normal position with respect to the receiver that is visible in the background.

9.1.3 Operation

Before the system became operative it was feared that one of the greatest problems would be to hold the two klystrons at a difference frequency within the IF passband. An AFC system could be employed but would entail much more equipment. In actual operation these fears proved to be unfounded. Little difficulty was encountered except on days with strong gusty winds. It was found that after approximately 1/2 hour warm-up the two klystrons were relatively stable and required only occasional reflector voltage adjustments.

Before testing of the multi-element arrays was begun, radiation patterns of a 17λ square aperture were measured.

FIG. 62 – VIEW OF TUNNEL, TRANSMITTER AND RECORDING EQUIPMENT. RECEIVER IN BACKGROUND.

FIG. 63—VIEW OF HOLEY PLATE IN GROUND PLANE USING 45° STEERING ADAPTOR, RECEIVER IN BACKGROUND.

Since theoretical patterns of a square aperture are readily available, a comparison of measured and calculated results could be made to check-out the system for such things as transmitter-receiver alignment, phase and amplitude distribution across the aperture, and amplifier linearity. After correcting several minor difficulties, patterns were obtained which closely followed the theoretical pattern of such an aperture although minor variations were consistently present. After much experimental investigation, it was decided that these variations were caused by a slight deviation from the ideal plane-wave illumination of the aperture but were of such small proportions that the effect would be negligible.

The dynamic range of linear signal available for recording patterns was normally on the order of 40 db above noise. At certain times a range of only 30 db was available and, although much time was spent trying to track down the cause, the efforts met with little success. The term "linear signal" should be clarified. By inserting a preamplifier between the mixer and IF amplifier, it was possible to investigate sidelobes on the order of -50 db below the main beam. But, under these conditions, the IF amplifier would saturate when on the main beam and give false indication of relative amplitudes of the main beam with respect to the side lobes. Several detailed patterns of side-lobes were recorded in this manner.

9.2 Patterns of Test Arrays

9.2.1 Evaluation of the Measuring System

The ECI Holey Plate pattern measuring equipment provides a simple means of determining the radiation patterns of antenna arrays. The purpose of such measurements in this study is to verify the pattern calculations for several types of arrays examined. It is unnecessary to test each of the different arrays considered so two arrays were modeled – a 30 db, naturally thinned, statistically designed array, and a 25 db, ninety percent thinned statistically designed array. These arrays are shown in Figure 13 and 14 of Section 3. The patterns are measured for the E-plane in all cases. The verification of the computed results by these two arrays should indicate any effects in the radiation pattern that were ignored in the calculations. Of primary concern is the effect of mutual coupling between elements, a factor not expressed in the computed results. The elements used in the test array are of low gain (0.46λ diameter circular holes). If mutual coupling effects deteriorate the patterns with these elements, then higher gain elements that might be used in an actual array would cause further deterioration of the calculated pattern.

The pattern measuring equipment has a dynamic range of 35 to 40 db for which the system components are linear. The arrays being measured have all sidelobes below 29.5 db for the 30 db naturally thinned array, and 22 db for the ninety percent thinned

25 db array. Therefore most of the sidelobes being measured are at the lower limit of the dynamic range of the system. In order to make a real comparison of predicted versus measured sidelobes, the magnitude of the radiated energy in the main beam was allowed to run into the non-linear region of detection. Figure 64 is the measured pattern from 0° to 90° for the 30 db naturally thinned array. Superimposed on this measured pattern is the calculated pattern. The relative level of the main beam with respect to the sidelobes is determined from Figure 65, where the entire pattern was measured in the linear range of the system. The second sidelobe at approximately 4.5° which is 29.5 db below the main beam of Figure 65 was used to establish the relative intensity of that sidelobe in Figure 64. The calculated pattern is that of Figure 3 in Section 3, and it has a peak sidelobe of -29.5 db which was superimposed at this relative level on the measured pattern.

Before evaluating the differences in the two patterns it is necessary to establish some reasonable estimate of experimental error in the measuring system. The expansion of the angular coordinate in Figure 64 gives a measure of the noise component of the pattern because the period of the noise is much less than the sidelobe width. The noise component is as much as ±1.5 db in the -35 to -40 db region. The noise component period is of the same order of magnitude as the sidelobe width on a normal pattern (i.e., the angular scale of Figure 65), and thus deviations of as much as 3 db may be anticipated due to noise. Other errors in the system, aside from systematic errors, can be determined by the repeatability of pattern measurements. Successive runs of the enlarged angular coordinate as in Figure 64 indicate the patterns to agree within ±3 db, at power levels between -35 and -40 db. The deviations are due in part to the variation of temperature and air flow to the klystrons in the system. Hence, it is possible that the total deviation due to noise and random errors might cause discrepancies of as much as 9 db between calculated and measured patterns on the normal angular scale, and 6 db on the enlarged angular scale. An unmeasurable error is the effect of removing and inserting the test array in the ground plane. This is due to the test array structure which is not as rigid as sheet metal of the same thickness. A slight buckling was noted in the holey plates, and there existed no systematic way to evaluate this error. Hence when the model array was removed and inserted, there was no guarantee the array was in its former position.

Two known systematic errors should be pointed out. One is in the lens discussed in Section 9.1, and its effect is considered to be a minor one causing a slight deviation in the patterns of square test apertures. The reason is the lens does not create a perfectly plane phase front across the array. The second systematic error is independent of the pattern measuring system. It causes sidelobes in the negative region of θ to consistently be higher than the identical sidelobe in the positive region of θ within the previously

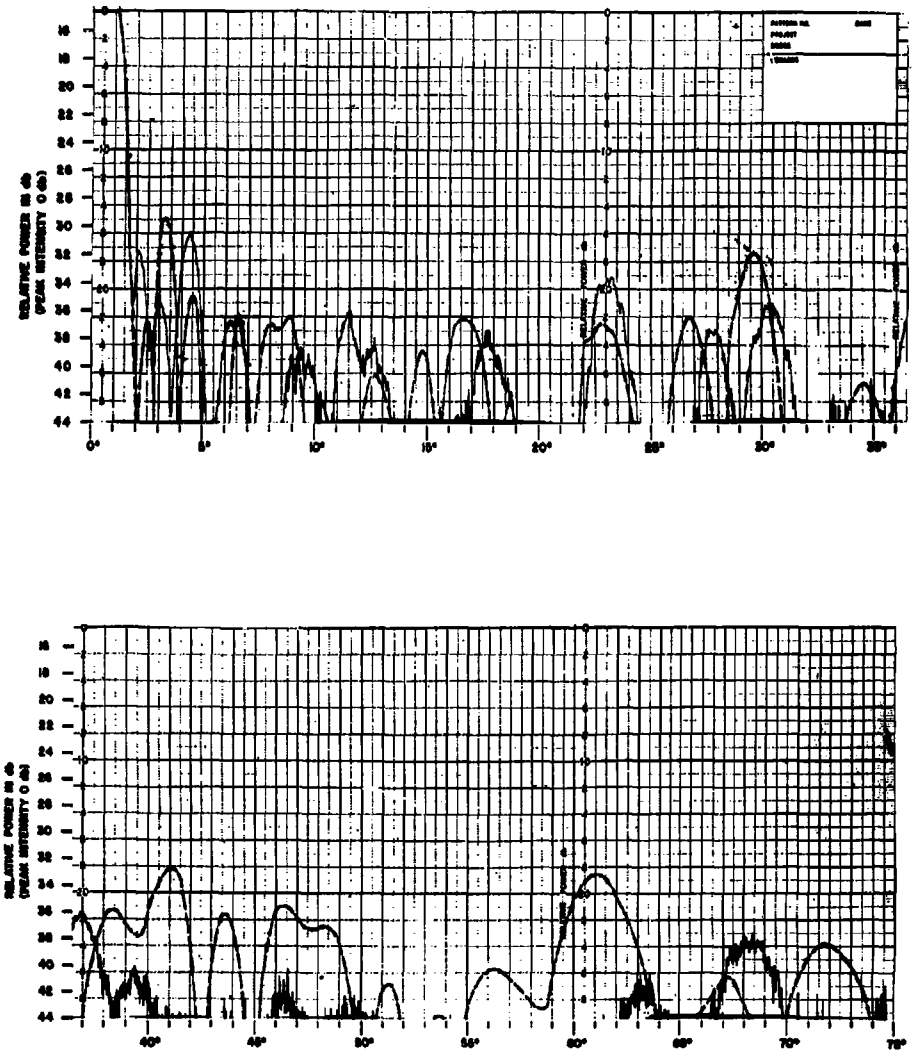

FIG. 64 —COMPARISON OF EXPERIMENTAL (SOLID LINE) AND CALCULATED (BROKEN LINE) PATTERNS OF THE 3775 ELEMENT ARRAY FOR $\phi_0 = 0°$

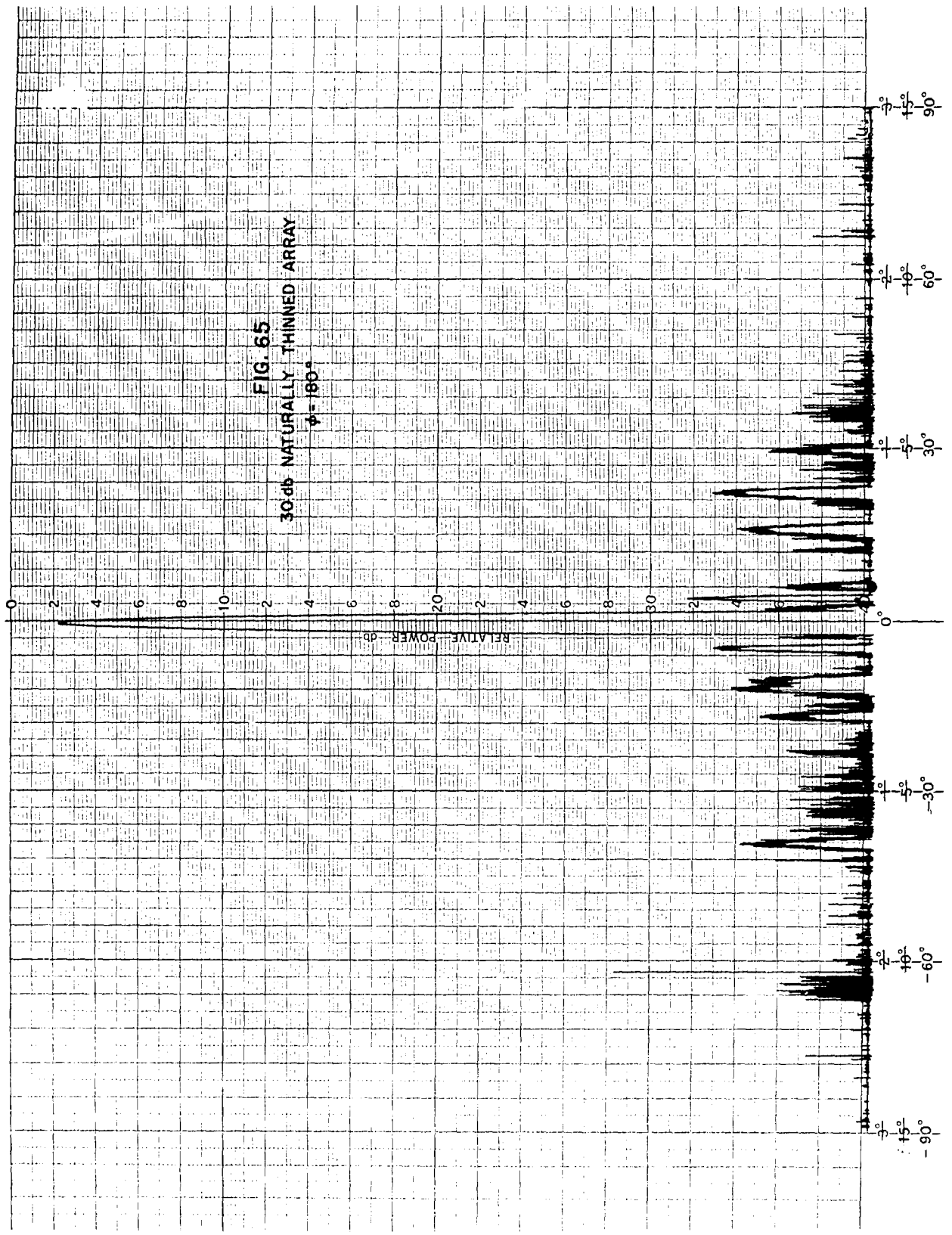
FIG. 65
30 db NATURALLY THINNED ARRAY
ϕ = 180°
RELATIVE POWER - db
0
2
4
6
8
10
20
30
0°
1°
2°
3°
5°
10°
15°
30°
60°
90°
-30°
-60°
-90°

discussed errors. The deviation is especially true of the angles $\theta = -12^{\circ}$, -17°, and -42°, approximately, although this effect is not pronounced in Figure 65. There was no parameter in the system that would eliminate the non-symmetry of the pattern if the parameter was varied. It is concluded that there existed some multiple reflection path at these angles, although nothing could be observed visually.

In comparing the calculated and measured patterns of Figure 64 it is observed that the sidelobes adjacent to the main beam differ by as much as 5.5 db. Three db variations can be expected to exist between any calculated and measured pattern (6 db between any measured patterns) plus variation due to noise. This still means that there exists a discrepancy of approximately 2.5 db. This could be due to the unmeasurable systematic and random errors. In part it could be effects of mutual coupling. This is further discussed in Section 9.3.

The point of significance in the experimental patterns is no measured peak sidelobe exceeded the predicted peak sidelobe. While there are deviations between expected and achieved sidelobes of 5.5 db in the vicinity of the main beam in Figure 64, the highest peak in each case is the same as predicted, i.e., -29.5 db. The deviation adjacent to the main beam is emphasized since larger deviations are anticipated as the magnitude of the angle increases. This is due to the element factor of the array.

Another error that is unexplained is the slight variation between the angular position of the sidelobes in the predicted and measured patterns. Adjacent to the main beam it appears that the frequency is higher than the design frequency of 70 Gc since the measured sidelobes are more compressed than the calculated sidelobes, and for θ greater than 15 degrees the situation is reversed. Hence, an error in the frequency is not the explanation.

The errors of the system have been evaluated – at least to make evident any drastic effects due to the ignored quantities in making the calculations – so that it is possible to explore in detail the patterns of the two test arrays.

9.2.2 Test Arrays

The radiation patterns of the two test arrays were sampled throughout all space. The measurements were made with respect to θ for various values of ϕ as indicated in the coordinate system of Figure 1.

Typical patterns as sketched in Figures 66 to 70 represent the field in the region from $\phi = 135^{\circ}$ to 170° (Figure 65 is the 180° pattern of this 45° sector) for the naturally thinned, 30 db density-tapered array. The highest measured sidelobe is -26 db below

FIG. 66
30 db NATURALLY THINNED ARRAY
$\phi = 135°$
RELATIVE POWER db
0
2
4
6
8
10
20
30
0°
1°
2°
3°
5°
10°
30°
60°
90°
-30°
-60°
-90°

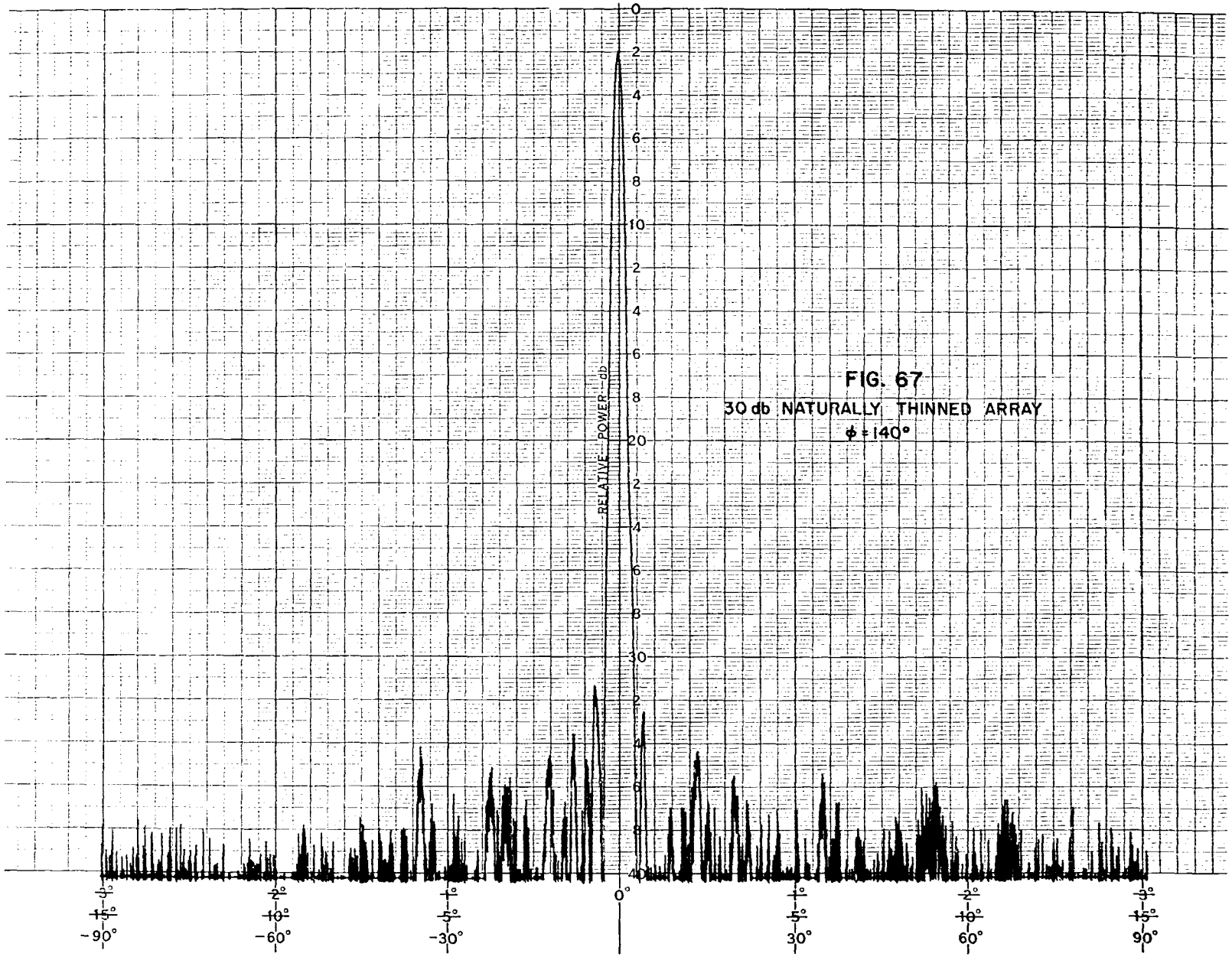

FIG. 67
30 db NATURALLY THINNED ARRAY
$\phi = 140°$

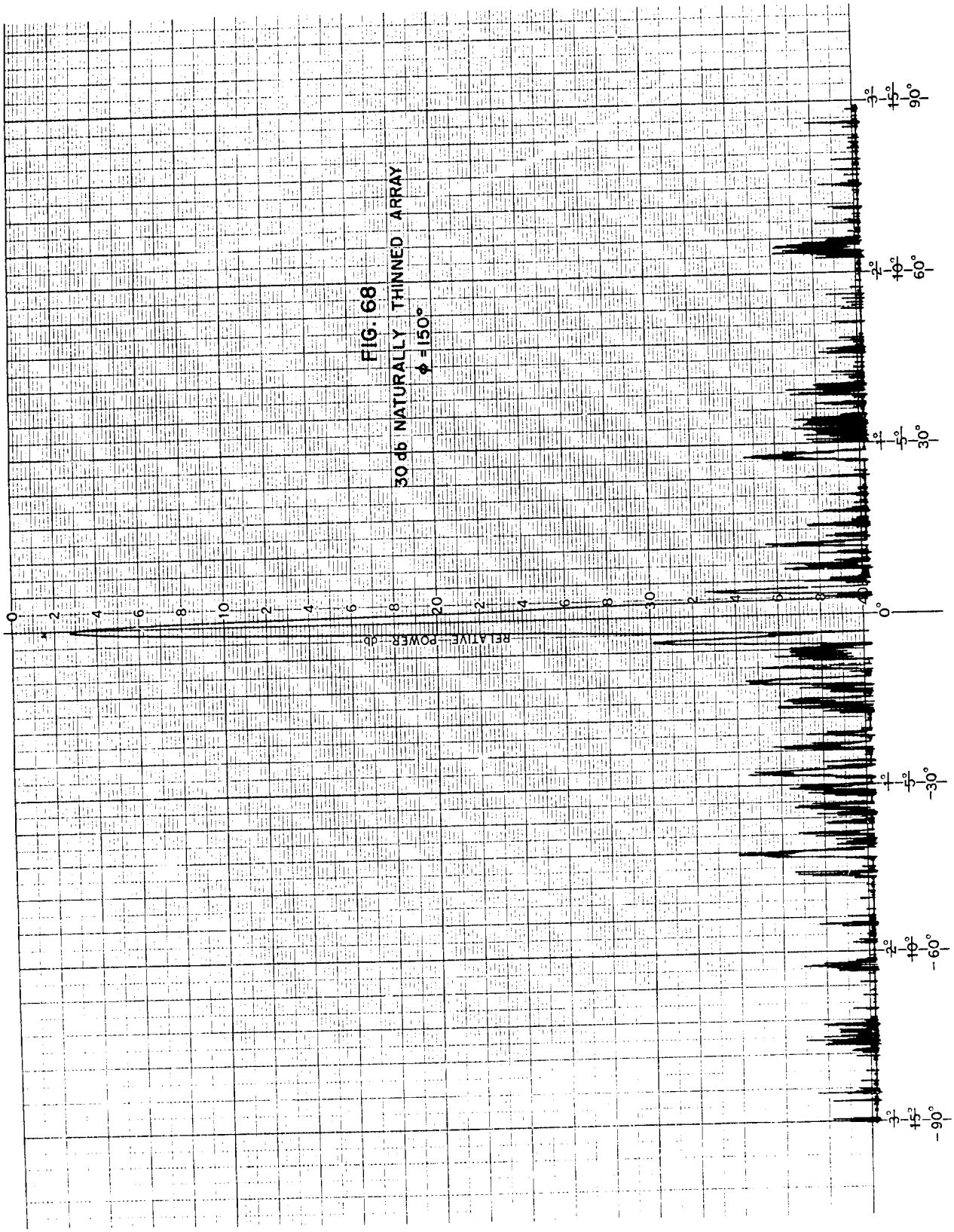
FIG. 68
30 db NATURALLY THINNED ARRAY
φ = 150°
RELATIVE POWER - db
0
2
4
6
8
10
20
30
3°
1.5°
90°
2°
1.0°
60°
1°
.5°
30°
0°
1°
.5°
-30°
2°
1.0°
-60°
3°
1.5°
-90°

FIG. 69
30db NATURALLY THINNED ARRAY
ϕ=160°
RELATIVE POWER—db
0
2
4
6
8
10
20
30
0°
90°
60°
30°
-30°
-60°
-90°

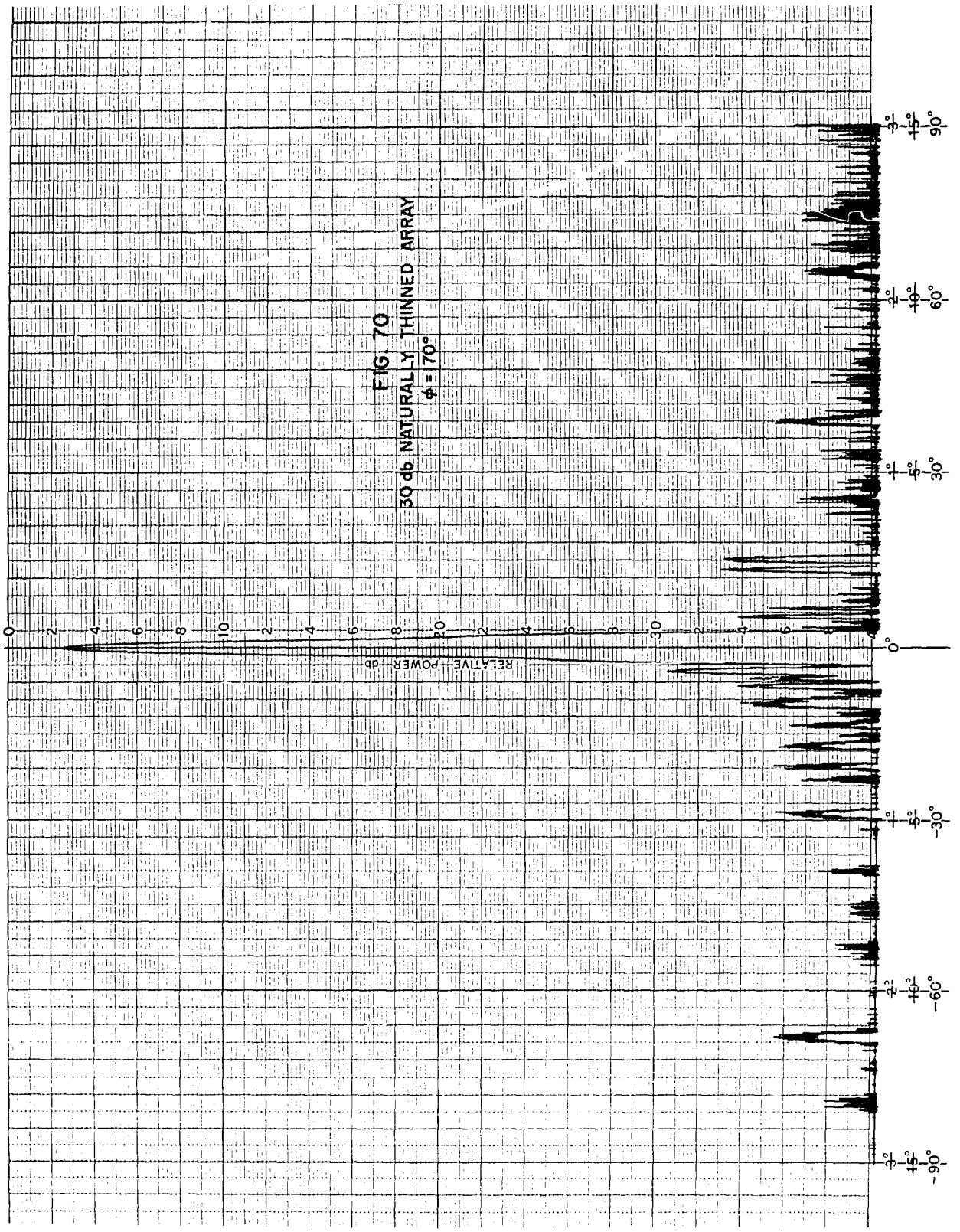
FIG. 70
30 db NATURALLY THINNED ARRAY
$\phi = 170°$
RELATIVE POWER—db
0
2
4
6
8
10
20
30
0°
1°
5°
30°
2°
10°
60°
3°
15°
90°
-30°
-60°
-90°

the main beam and occurs in the $\phi = 160^{\circ}$ plane (Figure 69). These cuts are typical of the radiation pattern found in any sector. A finer subdivision for a 10° sector of ϕ was measured for $\Delta\phi = 2^{\circ}$. Within this sector no sidelobe was found greater than -29 db. Thus the sidelobes throughout the entire pattern of the 30 db naturally thinned, density-tapered array do not exceed -26 db.

Similar measurements have been made for the 90% thinned 25 db density-tapered array. The principal plane patterns of this array are sketched in Figures 71 and 72 for $\phi = 0^{\circ}$ and $\phi = 90^{\circ}$, respectively. No sidelobes exceed a peak value of -22 db in either plane. Further exploration of the radiation pattern indicated that there are no sidelobes greater than -22 db for any value of ϕ. Figure 10 in Section 3 is the calculated pattern of this array for $\phi = 0^{\circ}$. The calculated peak sidelobes are also -22 db, so good agreement exists between experiment and theory for this array.

These arrays were also steered to $\theta_o = 45^{\circ}$ and the patterns measured. While the calculated patterns indicate that the values of the peak sidelobes remain the same as the unsteered arrays, actual measurement at these angles would indicate if mutual coupling would have an adverse effect on beam steering. In Figures 73, 74, and 75 for the 30 db naturally thinned, density-tapered array, the effect of steering the main beam to $\theta_o = -45^{\circ}$ in the $\phi = 0$, 45° and 90° planes, respectively, may be examined. The effect of steering this array appears to have no detrimental effect on the pattern. The main beam is slightly broadened, but this is to be expected. Peak sidelobes are essentially unchanged. In Figure 73 the first sidelobe is bled into the main beam and has a peak value of -27.5 db, whereas it was -29.5 db in the unsteered pattern.

Two patterns for the 25 db 90% thinned, density-tapered array steered to $\theta_o = -45^{\circ}$ are shown in Figures 76 and 77 ($\phi = 45^{\circ}$ and 90°, respectively). The patterns of this array are considered even more satisfactory than the steered patterns of the naturally thinned array. The peak values of sidelobes remain the same as they were in the unsteered case, i.e., -22 db. The effect of the element factor must therefore be small.

9.2.3 Extremely Thinned Arrays

An extremely thinned antenna array of the ring array design was constructed for another antenna study.[40] It is included in this report because of its interest and is an example of a severely thinned array. A ring array composed of 144 elements located on 4 rings with 36 elements per ring was constructed with radii of 7λ, 13λ, 19λ and 25λ with radials located every 10°. The pattern at $\phi = 0^{\circ}$ (and hence every 10°) is shown in Figure 78. Peak sidelobes are 12.6 db below the main beam. This array has the same beamwidth as the two previously

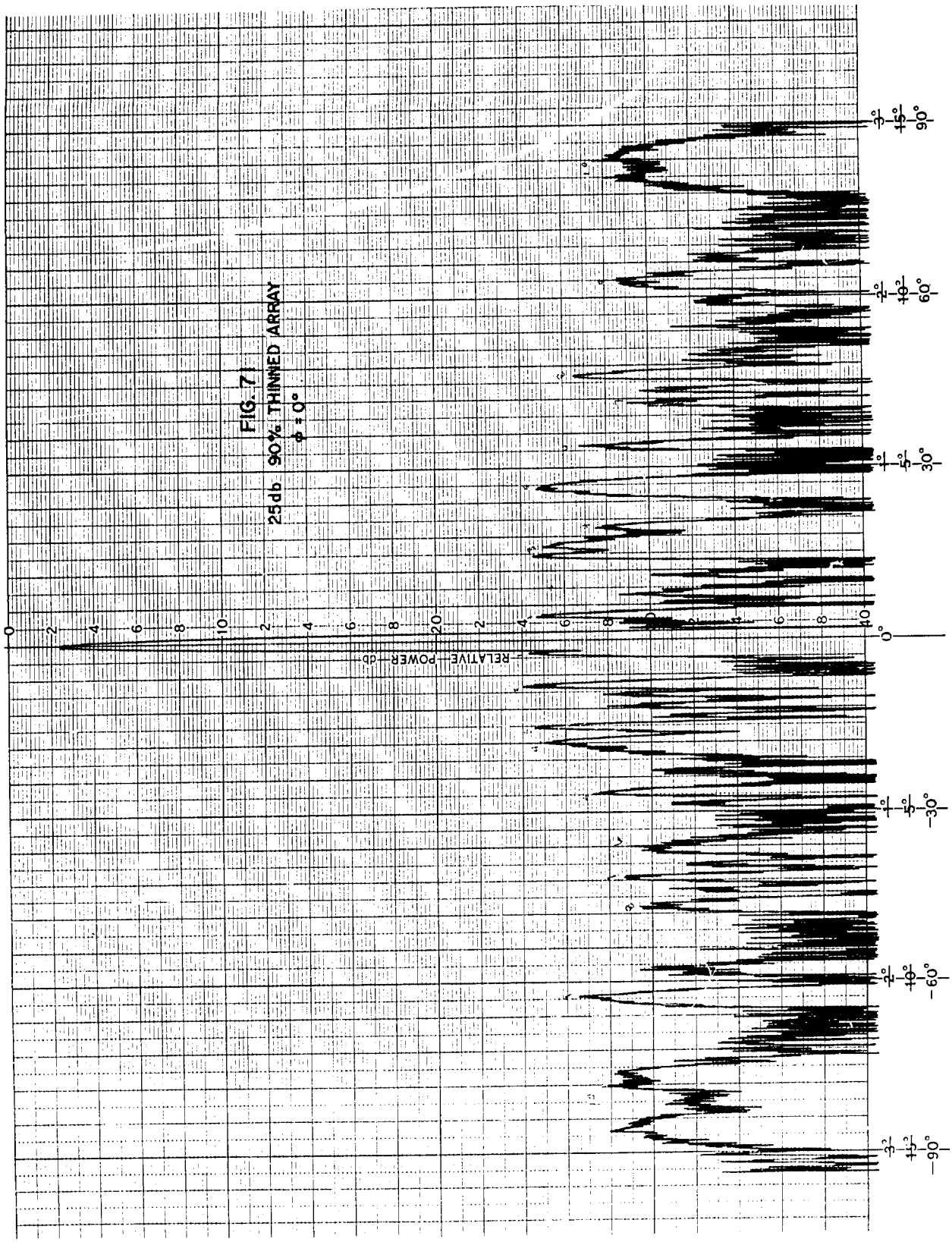
FIG. 7
25 db 90% THINNED ARRAY
φ = 0°
RELATIVE POWER — db
0
2
4
6
8
10
20
0°
90°
60°
30°
-30°
-60°
-90°

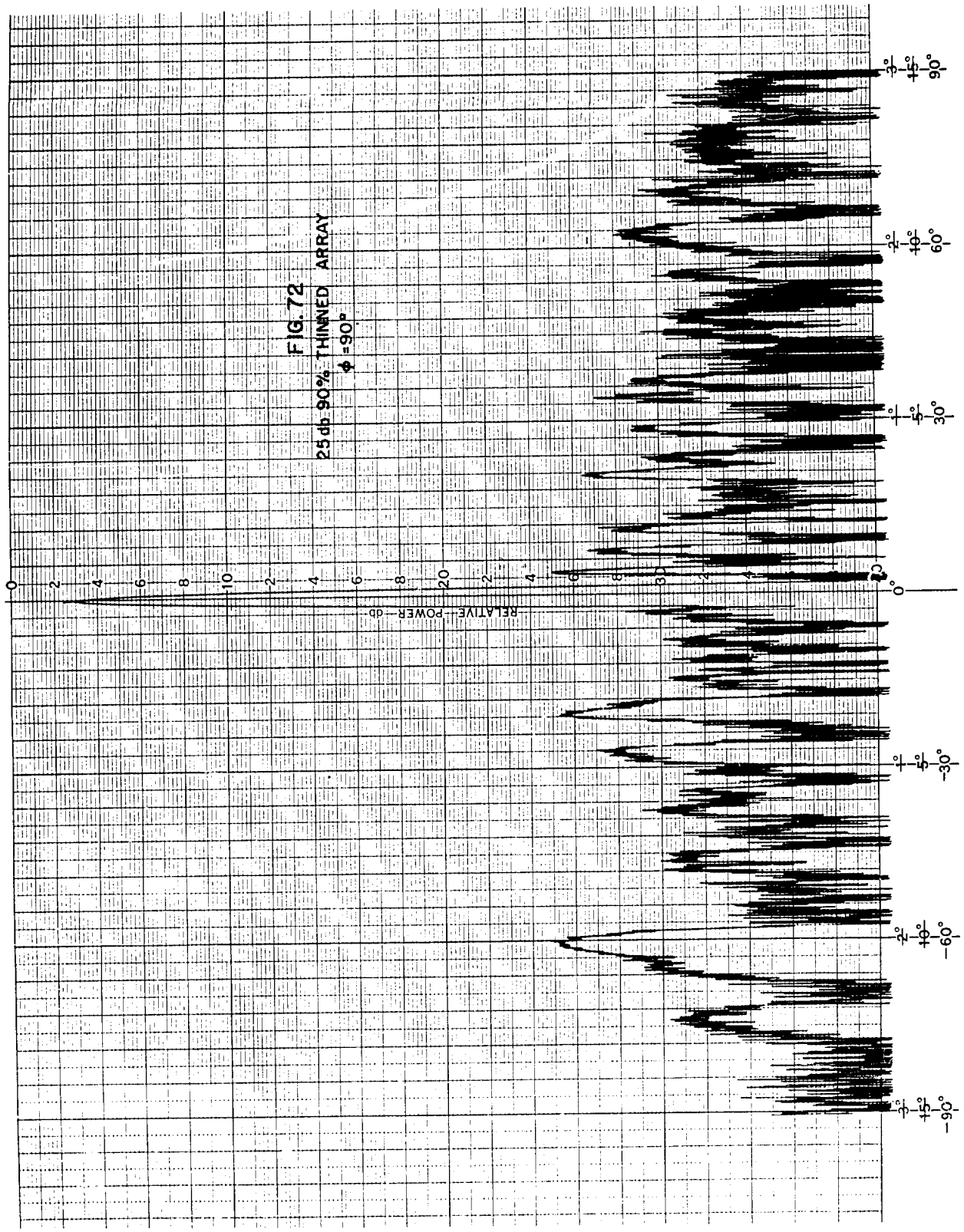
FIG. 72
25 db 90% THINNED ARRAY
ϕ = 90°
RELATIVE — POWER — db
0
2
4
6
8
10
20
30
90°
60°
30°
0°
-30°
-60°
-90°

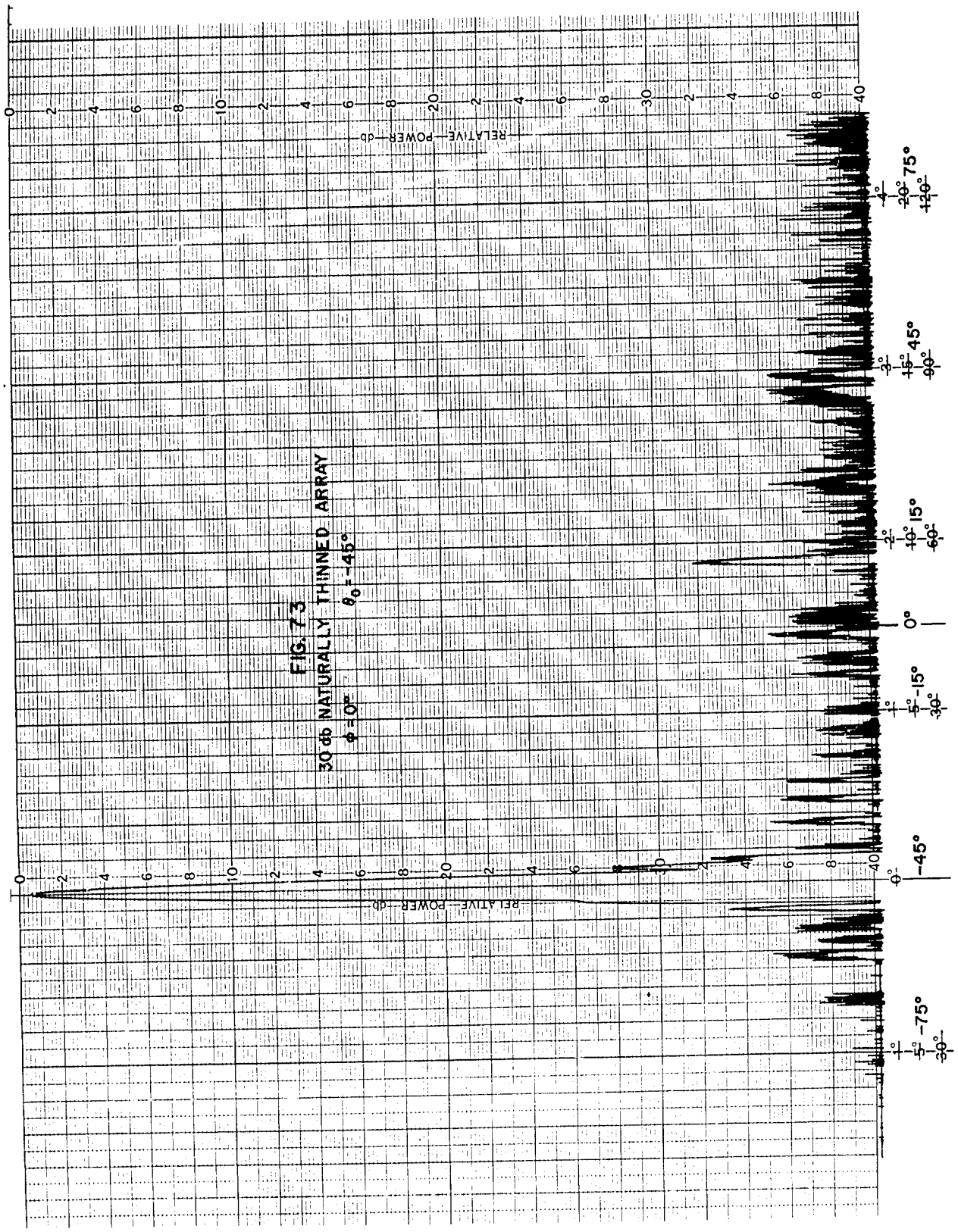
FIG. 73
30 db NATURALLY THINNED ARRAY
$\theta_0 = -45°$
$\phi = 0°$
RELATIVE POWER - db
RELATIVE POWER - db
0°
-45°
-75°
-15°
15°
45°
75°

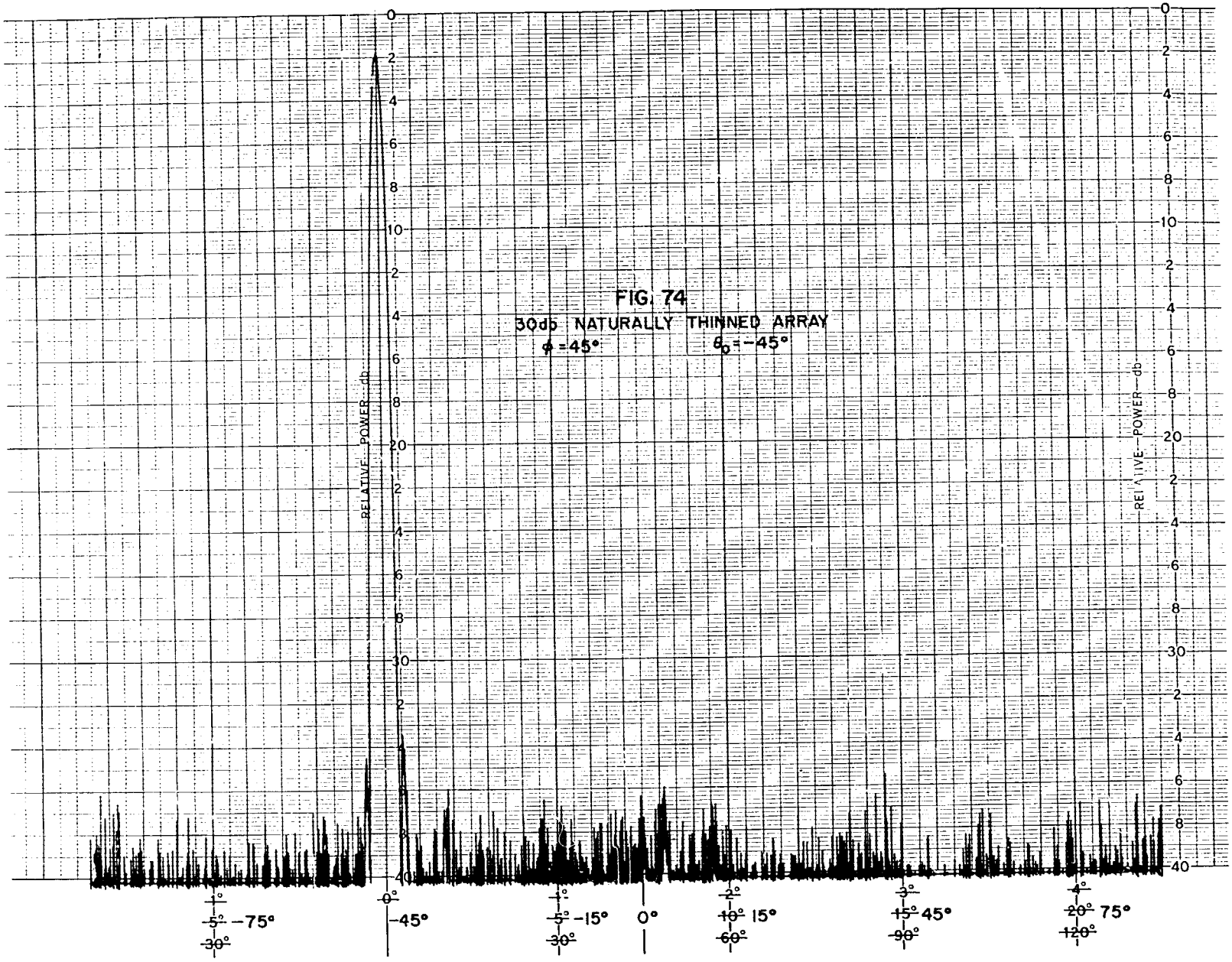
FIG. 74
30db NATURALLY THINNED ARRAY
ϕ =45° θ_0 =-45°
RELATIVE POWER—db
RELATIVE POWER—db
0
2
4
6
8
10
20
30
40
1°
5°
30°
-75°
0°
-45°
1°
5°
30°
-15°
0°
2°
10°
60°
15°
3°
15°
90°
45°
4°
20°
120°
75°

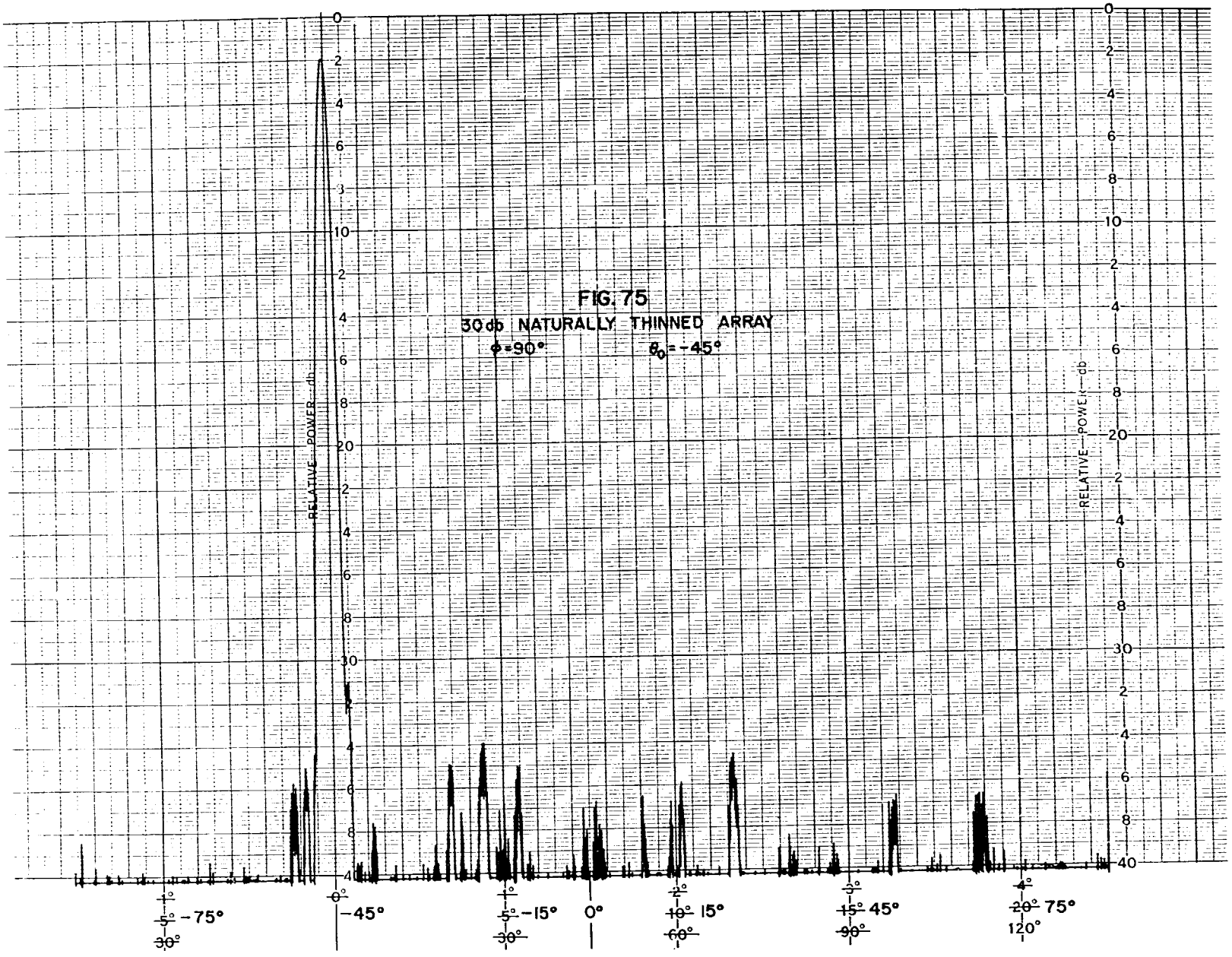
FIG. 75
30db NATURALLY THINNED ARRAY
φ=90°
θ0=-45°
RELATIVE POWER - db
RELATIVE POWER - db
-75°
-45°
-15°
0°
15°
45°
75°

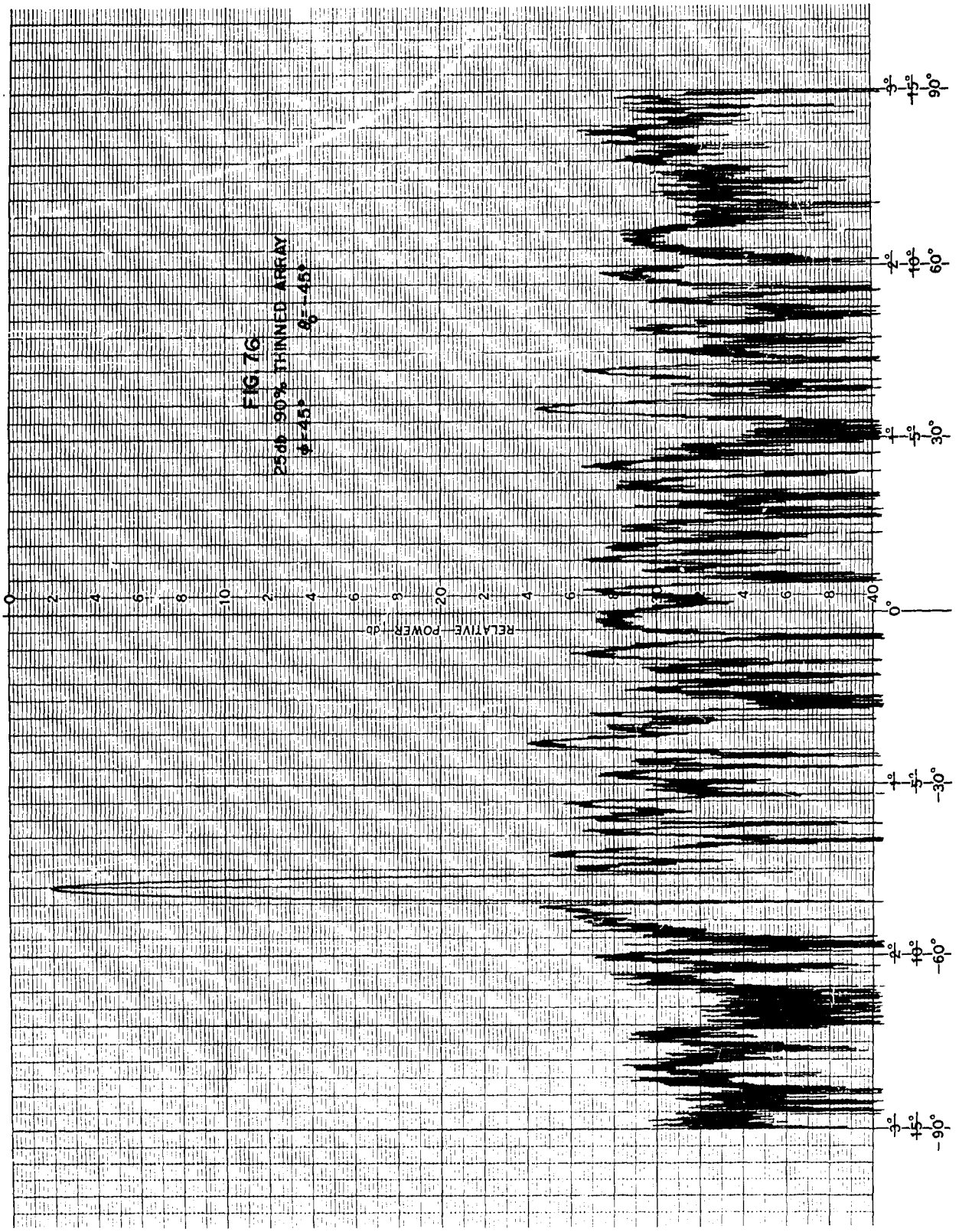
FIG. 76
25db 90% THINNED ARRAY
$\phi = 45°$
$\delta = -45°$
RELATIVE POWER db
0
2
4
6
8
10
20
40
0°
1° 5° 30°
2° 10° 60°
3° 15° 90°
-1° -5° -30°
-2° -10° -60°
-3° -15° -90°

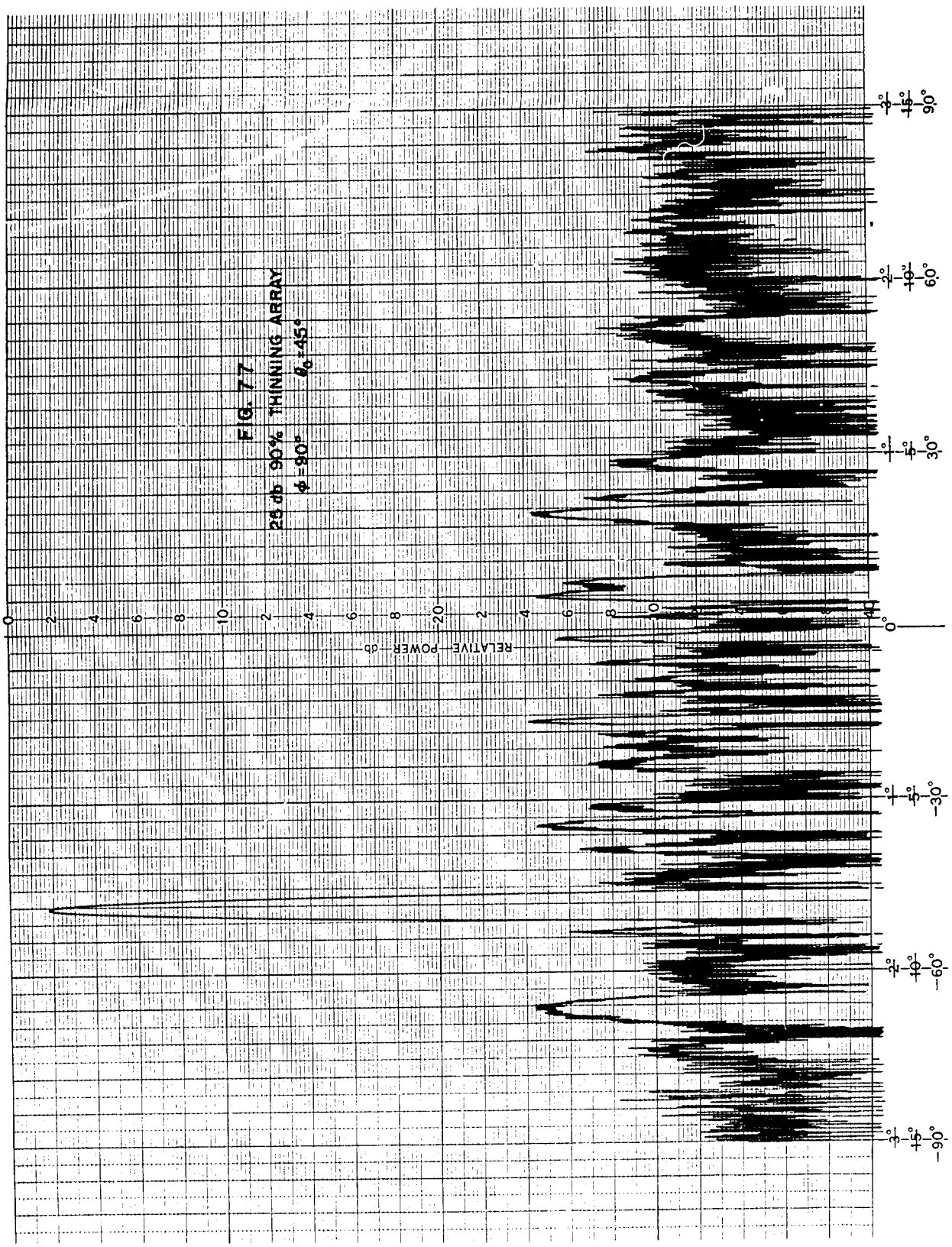
FIG. 7.7
25 db 90% THINNING ARRAY
ϕ=90° θ_0=45°
RELATIVE POWER—db
0
2
4
6
8
10
20
30°
60°
90°
-30°
-60°
-90°

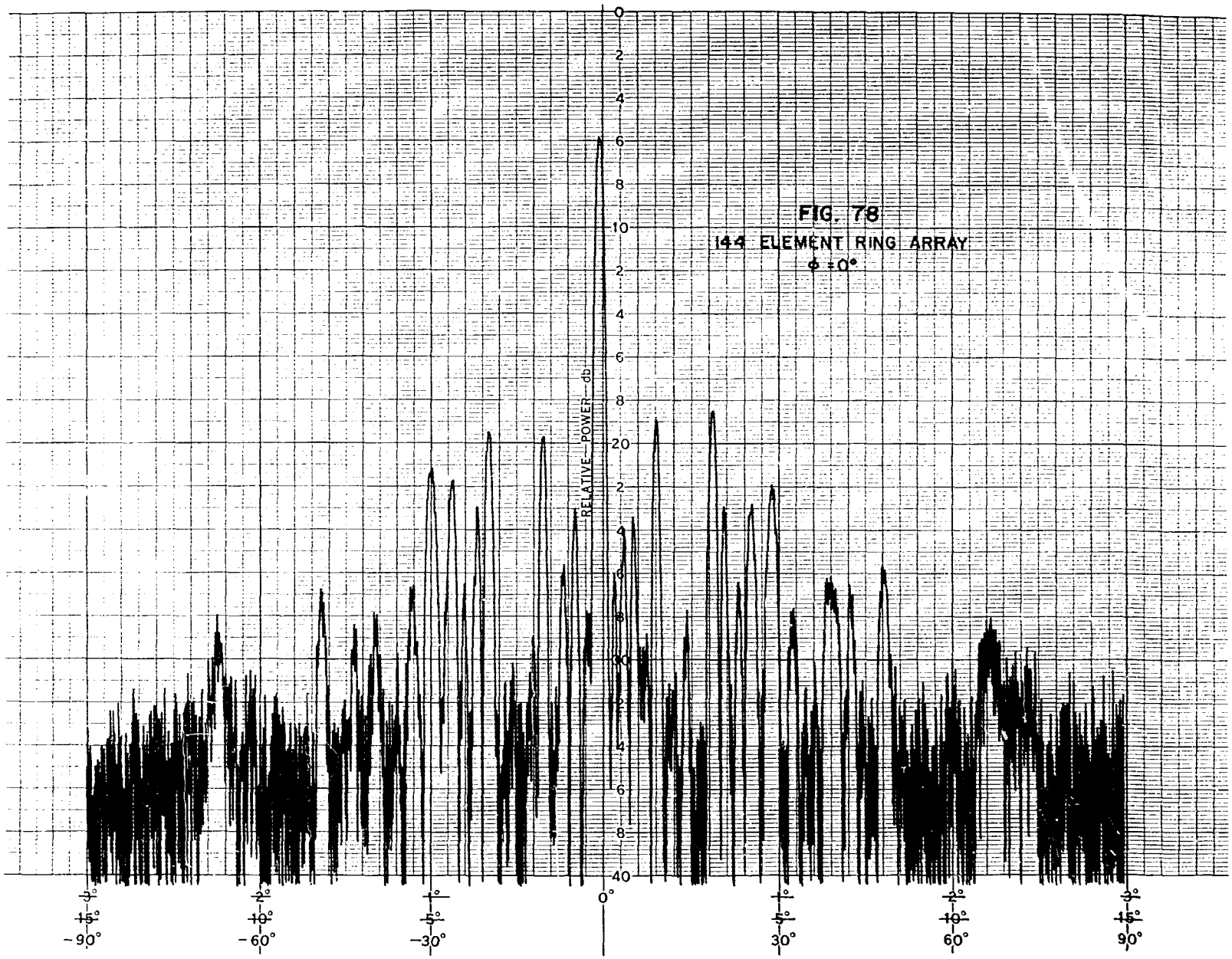

FIG. 78
144 ELEMENT RING ARRAY
$\phi = 0°$

considered test arrays, but is thinned 98.56%. Further pattern measurements indicate that all sidelobes throughout the hemisphere are below -12.5 db. The predicted average sidelobe level of Section 8 is -21.5 db and if it were possible to have this average as a pure two dimensional sine wave, the peak of the sidelobe would be -15.5 db. It is not possible to apply the statistical average of Section 3 to the ring array since the quantity

$$\sum_n A_n(1-A_n)$$

is unknown.

9.3 Conclusions

The test program using the breadboard models of the antenna arrays designed by the statistical or pseudo random technique is considered successful. The main beam performance has been evaluated, and acceptable sidelobe levels with good scanning capability achieved.

Several results achieved in Section 9.2.2 need further evaluation. First, the element factor, while unknown, seems to have minor effect. This statement is verified by an examination of the patterns when the main beam is steered. In the steered patterns the effect of the element factor should raise the sidelobes in the region $\theta^o = 0^o$ when $\theta_o = \pm 45^o$. For example a comparison may be made between Figure 72 and 77 the cases for $\theta_o = 0^o$ and $\theta_o = -45^o$, respectively, where $\phi = 90^o$ for both measurements. The large sidelobe at $\theta = 62^o$ in Figure 72 moves to $\theta = 19^o$ in Figure 77 as the result of steering the main beam to $\theta_o = -45^o$ (actually this sidelobe should move to $\theta = 17^o$ but this difference is well within experimental error). Since the peak value increases from -25.2 db to -24.4 db as result of steering, the element factor is such as to suppress the sidelobes by approximately one decibel at $\theta = 60^o$ in the unsteered case. If the element factor were cos θ the suppression of sidelobes in this region would be about 6 db.

Second, the element factor should cause no change in the relative values of sidelobes adjacent to the main beam when the array is steered. This is verified by again comparing Figures 72 and 77. Peak values of sidelobes remain the same adjacent to the main beam. However, while peak values are -22 db in both patterns, the peaks definitely do not occur for the same sidelobes. This suggests that there is another phenomena occurring to disturb the pattern, although the effect is not an adverse one. The phenomena is more pronounced if the larger array patterns are compared. Figures 65 and 73 are for the 30 db naturally thinned, density-tapered array with $\phi = 0^o$

(or 180°) for $\theta = 0^{\circ}$ and -45°, respectively. The effect of steering in this case is to raise the sidelobes adjacent to the main beam (as well as broaden the beam). Steering does slightly change the sidelobes for both test arrays.

It would be convenient to say that this is the effect of mutual coupling in the array. However, no such generality can be made because of the nature of the breadboard models for two reasons. First, these arrays are constructed by etching the copper from a copper-clad dielectric. It is known from experience that the dielectric can cause peculiar phenomena to occur due to surface waves on the dielectric. Second, the measured differences are well within experimental error. It appears that if mutual coupling causes pattern deterioration, it is only a minor effect.

REFERENCES

1. S. Silver, Microwave Antenna Theory and Design, MIT Rad. Lab. Series, Vol. 12, McGraw-Hill Book Co., New York; 1950.

2. J. Ruze, "Physical Limitations on Antennas," MIT Research Lab. Electronics Tech. Rept. 248; October 30, 1952.

3. C.L. Dolph, "A Current Distribution for Broadside Arrays which Optimizes the Relationship between Beamwidth and Side Lobe Level," Proc IRE, vol. 34, pp. 335-348; June 1946.

4. T.T. Taylor, "Design of Line-Source Antennas for Narrow Beamwidth and Low Sidelobes," IRE Trans, vol. AP-3, pp. 16-28; January 1955.

5. M.I. Skolnik, Introduction to Radar Systems, Sec. 7.8, McGraw-Hill Book Co., New York; 1962.

6. H. Unz, "Linear Arrays with Arbitrarily Distributed Elements," University of California, Institute of Engineering Research Series No. 60, Issue No. 172, December 19, 1956. See also IRE Trans. vol. AP-8, pp. 222-223; March 1960.

7. S.S. Sandler, "Some Equivalences Between Equally and Unequally Spaced Arrays," IRE Trans, vol. AP-8, pp. 496-500; Sept. 1960.

8. K. Baur, "Antennenzeilen mit gedampften Nebenzipfeln," Electronische Rundschau, vol. 14, pp. 217-222; June 1960.

9. D.D. King, R.F. Packard, and R.K. Thomas, "Unequally-Spaced Broadband Antenna Arrays," IRE Trans, vol. AP-8, pp. 380-384; July 1960.

10. R.F. Harrington, "Sidelobe Reduction by Non-Uniform Element Spacing," IRE Trans, vol. AP-9, pp. 187-192; March 1961.

11. M.G. Andreason, "Linear Arrays with Variable Interelement Spacings," IRE Trans, vol. AP-10, pp. 137-143; March 1962.

12. F.C. Ogg, "Steerable Array Radars," IRE Trans, vol. MIL-5, pp. 80-94; April 1961.

13. J.H. Best, "Space Tapered Antenna Arrays," paper presented at the 5th Mil-E-Con PGMIL National Convention, Washington, D.C.; June 26-28, 1961.

14. A.L. Maffett, "Array Factors with Non-Uniform Spacing Parameter," IRE Trans, vol. AP-10, pp. 131-136; March 1962.

15. Y.T. Lo, "A Spacing Weighted Antenna Array," IRE International Convention Record, vol. 10, Pt. 1, pp. 191-195; 1962.

16. R.E. Willey, "Space Tapering of Linear and Planar Arrays," IRE Trans, vol. AP-10, pp. 369-377; July 1962.

17. A. Ishimaru, "Theory of Unequally Spaced Arrays," IRE Trans, vol. AP-10, pp. 691-702; November 1962.

18. J.L. Allen, "Beam Shaping by Omission of Elements ('Space Tapering' or 'Density Tapering')" pp. 299-305 of Phased Array Radar Studies, MIT Lincoln Laboratory Technical Report No. 236; 13 November 1961.

19. S.J. Rabinowitz and R.F. Kolar, "Statistical Design of Space Tapered Arrays," paper presented at the 12th annual Symposium on USAF Antenna Research and Development Program, Univ. of Illinois; October 16-19, 1962.

20. W.B. Davenport, Jr. and W.L. Root, An Introduction to the Theory of Random Signals and Noise, McGraw-Hill Book Co., New York; 1958.

21. T.T. Taylor, "Design of Circular Apertures for Narrow Beamwidth and Low Sidelobes," IRE Trans, vol. AP-8, pp. 17-22; January 1960.

22. R.C. Hansen, "Table of Taylor Distributions for Circular Aperture Antennas," IRE Trans, vol. AP-8, pp. 23-26; January 1960.

23. W.H. Von Aulock, "Properties of Phased Arrays," Proc IRE, vol. 40, pp. 1715-1727; October 1960.

24. M.I. Skolnik, "A Method of Modeling Array Antennas," IRE Trans, vol. AP-11, pp. 97-98; January 1963.

25. M.I. Skolnik, J.W. Sherman, and G. Nemhauser, "Dynamic Programming Applied to Unequally Spaced Arrays," to be submitted for publication.

26. R.J. Spellmire, "Tables of Taylor Aperture Distributions," Hughes Technical Memorandum No. 581; October 1958.

27. M.I. Skolnik, "Resolution of Angular Ambiguities in Radar Array Antennas with Widely-Spaced Elements and Grating Lobes," IRE Trans, vol. AP-10, pp. 351-352; May 1962.

28. "Pseudo Random Array Investigation," Technical Note No. 2, on Contract AF 30(602)-2626, Electronic Communications, Inc., Timonium, Maryland; August 13, 1962.

29. R. Bellman, Dynamic Programming, Princeton University Press, Princeton, N.J.; 1957.

30. R. Bellman, Adaptive Control Processes, Princeton University Press Princeton, N.J.; 1961.

31. C.L. Shannon, "Communication in the Presence of Noise," Proc IRE, vol. 37, pp. 10-21; January 1949.

32. J.D. Kraus, Antennas, McGraw-Hill Book Co., New York; 1950.

33. R.V. Churchhill, Fourier Series and Boundary Value Problems, McGraw-Hill Book Co., New York, p. 32; 1941.

34. E.C. Titchmarch, "On Van der Corput's Method and the Zeta Function of Riemann," Quarterly Journal of Math., Vol. II, (Oxford Series), p. 161; 1931.

35. "Pseudo Random Array Investigation," Technical Note No. 3, on Contract AF 30(602)-2626, Electronic Communications, Inc., Timonium, Maryland, January 9, 1963.

36. Y.T. Lo, "A Probabilistic Approach to the Design of Large Antenna Arrays," IRE Trans, vol. AP-11, pp. 95-96; January 1963.

37. H.E. King, "Directivity of a Broadside Array of Isotropic Radiators," IRE Trans, vol. AP-7, pp. 197-198; April 1959.

38. S. Milazzo, and F. D'Angelo, "Spacing Phased Array Elements for Maximum Gain," Electronic Design, pp. 50-53; May 10, 1962.

39. R.F. Packard, "Technique for Measuring Radiation Patterns of Array Antennas," Final Report on Contract NObrs 85-127, Electronic Communications, Inc., Timonium, Md.; August 31, 1962.

40. On Contract AF 19(628)-398 "Adaptive Antennas For Communications" for Air Force Cambridge Research Labs.

APPENDIX I

Analysis of Statistical Density-Taper Array Patterns

The elements of the arrays under discussion are either removed or allowed to remain according to some statistical criterion. Thus the resulting radiation patterns must be described in statistical terms. In this appendix it is shown that the average radiation power pattern of a statistically designed density-taper array may be considered as the sum of two components, one of which is the pattern that would have been obtained had the equivalent amplitude taper been used and the other is an omni-directional random pattern.

Consider an array antenna with some arbitrary arrangement of N elements. The excitation at each element is assumed to be of equal amplitude. The field intensity pattern (array factor) assuming the elements to be isotropic radiators is

$$E(\theta, \phi) = \sum_{n=1}^{N} \exp j \psi_n , \qquad (A.1)$$

where θ and ϕ are angular coordinates describing the pattern and ψ_n is the phase of the signal at the nth element measured with respect to some reference. The phase ψ_n is a function of θ and ϕ and the location of the nth element on the aperture. The N elements may be located on any type of aperture.

If elements are removed from the array the field-intensity pattern may be written

$$E(\theta, \phi) = \sum_{n=1}^{N} F_n \exp j \psi_n , \qquad (A.2)$$

where F_n is either zero or unity according as the element is removed or left in place. The quantity F_n thus has only the values of 0 and 1. In a statistically designed array, F_n is selected randomly and independently from element to element by a random number generator in such a way that its average value (ensemble average over many selections) is

$$\overline{F_n} = A_n , \qquad (A.3)$$

where A_n is the amplitude of the excitation that would normally be applied to the nth element if it were designed with an amplitude taper across the aperture. The field-intensity of the equivalent amplitude-tapered array used as the model is

$$E_o(\theta, \phi) = \sum_{n=1}^{N} A_n \exp j \psi_n \qquad (A.4)$$

The radiation pattern of Equation A.2 is statistical since F_n is statistical. By the Central Limit Theorem of statistics, the distribution of the quantity $E(\theta, \phi)$ for a given θ and ϕ will be Gaussian. This theorem holds only approximately for finite N but will be sufficiently accurate if N is large.

The mean of the statistical pattern of Equation A.2 is found using the fact that the mean of the sum is the sum of the means,

$$\overline{E(\theta, \phi)} = \sum_{n=1}^{N} \overline{F_n} \exp j \psi_n = \sum_{n=1}^{N} A_n \exp j \psi_n = E_o(\theta, \phi). \qquad (A.5)$$

Thus the mean or average pattern is identical with the field-intensity pattern of the amplitude tapered array used as the model. This array factor (Equation A.4) will be referred to as the model array factor. The coefficients A_n are selected by standard design procedures[1-5] for amplitude-tapered arrays to obtain a desired mean pattern. Since the quantities A_n are the mean values of a random variable with values 0 and 1, we must always have $0 \leq A_n \leq 1$. This may be obtained by properly scaling the original amplitude taper of the model-array design.

The square of the field-intensity pattern is the power pattern and is written

$$|E(\theta, \phi)|^2 = E(\theta, \phi) \cdot E^*(\theta, \phi) =$$

$$\sum_m \sum_n F_m F_n \exp j(\psi_m - \psi_n), \qquad (A.6)$$

where $E^*(\theta, \phi)$ denotes the complex conjugate. There is a theorem[20] which states that the mean of a product of statistically independent random variables is equal to the product of the means of those random variables. The variables F_m and F_n in Equation A.6 are independent if and only if $m \neq n$. If $m=n$ they are of course identical. Therefore the double summation is separated into terms with $m=n$ and terms with $m \neq n$, and the average is taken as follows:

$$\overline{|E(\theta, \phi)|^2} = \sum_n \overline{F_n^2} + \sum_{\substack{m \\ (m \neq n)}} \sum_n \overline{F_m F_n \exp\left[j(\psi_m - \psi_n)\right]} \qquad (A.7)$$

Since the values of F_n are either 0 or 1, $F_n^2 = F_n$, and the first summation of Equation A.7 becomes

$$\overline{\sum_n F_n^2} = \sum_n \overline{F_n^2} = \sum_n \overline{F_n} = \sum_n A_n . \qquad (A.8)$$

Using the theorem mentioned above, the second summation of Equation A.7 involving terms with $m \neq n$ becomes

$$\overline{\sum_{\substack{m \\ (m \neq n)}} \sum_n F_m F_n \exp\left[j(\psi_m - \psi_n)\right]} =$$

$$\sum_{\substack{m \\ (m \neq n)}} \sum_n \overline{F_m}\,\overline{F_n} \exp\left[j(\psi_m - \psi_n)\right] =$$

$$\sum_{\substack{m \\ (m \neq n)}} \sum_n A_m A_n \exp\left[j(\psi_m - \psi_n)\right] \qquad (A.9)$$

This is simply the power pattern corresponding to the model-array pattern $E_o(\theta, \phi)$ of Equation A.4, except that the terms with $m = n$ are missing. When these terms are restored and subtracted from the result, the following is obtained

$$\overline{|E(\theta,\phi)|^2} = \sum_n A_n + |E_o(\theta,\phi)|^2 - \sum_n A_n^2 =$$

$$|E_o(\theta,\phi)|^2 + \sum_n A_n(1 - A_n) \qquad (A.10)$$

where $|E_o(\theta,\phi)|^2$ is the power pattern of the model-array with "equivalent" amplitude taper A_n applied to each element.

The fraction of elements removed is controlled by the amplitude taper chosen for the model array. The exact number of elements after the elimination procedure is

$$N_E = \sum_n F_n . \qquad (A.11)$$

On the average, the number of elements left in the array is

$$\overline{N_E} = \sum_n \overline{F_n} = \sum_{n=1}^{N} A_n = N\overline{A_n} \leq N. \tag{A.11}$$

and the variance is

$$\sigma_N^2 = \overline{N_E^2} - \overline{(N_E)}^2 = \sum_n A_n(1 - A_n). \tag{A.13}$$

Neglecting the effects of mutual coupling between elements, the gain of an average statistical array is

$$G_s = \overline{N_E} = \sum_{n=1}^{N} A_n \tag{A.14}$$

The gain of a conventional amplitude-tapered array, again neglecting the coupling between elements, is

$$G_a = \frac{\left(\sum_{n=1}^{N} A_n\right)^2}{\sum_{n=1}^{N} A_n^2} \tag{A.15}$$

The ratio of the gain of a statistically designed space-tapered array (Equation A.14) and the gain of an amplitude-tapered array (Equation A.15) is therefore

$$\frac{G_s}{G_a} = \frac{\sum_{n=1}^{N} A_n \sum_{n=1}^{N} A_n^2}{\left(\sum_{n=1}^{N} A_n\right)^2} = \frac{\sum_{n=1}^{N} A_n^2}{\sum_{n=1}^{N} A_n} \tag{A.16}$$

The radiation intensity or the power pattern is, from Equation A.10 the superposition of the power pattern of the model amplitude-tapered array plus an omnidirectional component which is the same as the variance of Equation A.12. If it is assumed that the degree of

element removal is such that the omnidirectional component of the power pattern (second term of Equation A.10) is larger than the sidelobes of the model amplitude-tapered array pattern, then the average value of the sidelobes is

$$\text{average statistical sidelobes} = \overline{SL} = \sum_n A_n - \sum_n A_n^2. \qquad (A.17)$$

Substituting $\overline{N_E}$ from Equation A.12 and using Equation A.15.

$$\overline{SL} = \overline{N_E} - \left(\overline{N_E}\right)^2 \Big/ G_a = \overline{N_E}\left(1 - \frac{\overline{N_E}}{N\rho_a}\right), \qquad (A.18)$$

where ρ_a is the aperture efficiency of the model amplitude taper given by A_n. Since ρ_a is of the order of unity, Equation A.18 states that the average sidelobe level approaches $\overline{N_E}$, the number of elements left within the array, when the fraction of elements removed $\left(1 - \frac{N_E}{N}\right)$ is large.

The average sidelobe level relative to the peak value of the main beam after the elimination of elements is

$$\text{average relative sidelobe level} = \rho \approx \frac{\sum_n A_n(1-A_n)}{\overline{|E(0,0)|^2}} \qquad (A.19)$$

From Equation A.10

$$\overline{|E(0,0)|^2} = \left(\sum_n A_n\right)^2 + \sum_n A_n(1 - A_n) \approx \left(\sum_n A_n\right)^2 \qquad (A.20)$$

Therefore, Equation A.19 becomes

$$\rho \approx \frac{\sum_n A_n(1 - A_n)}{\left(\sum_n A_n\right)^2} = \frac{1 - \frac{\sum A_n^2}{\sum A_n}}{\sum A_n} \qquad (A.21)$$

From Equations A. 15 and A. 14

$$\rho \approx \frac{1 - \frac{G_s}{G_a}}{G_s} = \frac{1 - \frac{\overline{N_E}}{N\rho_a}}{\overline{N_E}} \qquad (A.22)$$

and

$$\rho \approx \frac{1}{\overline{N_E}} \text{ for } \frac{\overline{N_E}}{N} \ll 1 , \qquad (A.23)$$

where G_a is the gain of the model amplitude-tapered array and G_s is the gain of the statistical designed spaced-tapered array.

If one starts with an N element array and removes elements according to the above statistical procedure, the average number of elements that remain $\overline{N_E}$ is given by Equation A. 12. The N-element array is said to be "thinned" and the degree of thinning, or percentage of elements removed is

$$\text{degree of thinning} = 100 \left(1 - \frac{\overline{N_E}}{N}\right) \text{percent.} \qquad (A.24)$$

A given amplitude taper therefore has a certain natural degree of thinning. If it is desired to remove more elements than the natural number, say $N_r = k\,\overline{N_E}$, where $k < 1$, an examination of Equation A. 12 shows that this may be accomplished by multiplying the amplitudes A_n by the factor k. Thus

$$N_r = k\,\overline{N_E} = \sum_{n=1}^{N} k\,A_n . \qquad (A.25)$$

The above analysis can be repeated and one would obtain for $N_r = k\,\overline{N_E}$ elements

$$\text{average field-intensity} = \overline{E'(\theta,\phi)} = k\,E_o(\theta,\phi) ; \qquad (A.5')$$

$$\text{power pattern} = \overline{|E'(\theta,\phi)|^2} = k^2\,|E_o(\theta,\phi)|^2 + \sum_{n=1}^{N} kA_n(1 - kA_n); \qquad (A.10')$$

$$\text{Gain} = G'_s = k \sum_{n=1}^{N} A_n = N_r \; ; \qquad \text{(A.14')}$$

$$\text{Gain Reduction} = \frac{G_s'}{G_a} = k \frac{G_s}{G_a} = \frac{k \sum_{n=1}^{N} A_n^2}{\sum_{n=1}^{N} A_n} \qquad \text{(A.16')}$$

$$\text{Side lobe ratio} = \rho' \approx \frac{1 - k \frac{\sum A_n^2}{\sum A_n}}{k \sum A_n} = \frac{1 - \frac{N_r}{N\rho_a}}{N_r} \qquad \text{(A.22')}$$

APPENDIX II

Brief Description of Dynamic Programming Applied to Array Design

The mathematical statement of the problem is to find the vector $x_n = (x_1, \ldots, x_j, \ldots, x_n)$, where x_n specifies the position of the nth element, such that the $\max_{0 < u \leq 2} E(X_n, u)$ is minimum.

$$E(X_n, u) = 1 + 2 \sum_{j=1}^{N} \cos 2\pi x_j u$$

The purpose of the dynamic programming analysis is to find the optimal X_n without searching over all feasible values of X_n. In fact, total search must be ruled out as a practical method, since even with an array of a few elements, the number of possible designs is enormous. For example, checking all possibilities for the 25-element symmetrical array where each element could be placed at any one of 20 positions, would involve examining approximately 4,000,000,000,000,000 designs. With dynamic programming under 5,000 designs are considered, which can be done in a fraction of a minute on a high-speed computer.

The basic concept underlying the dynamic programming is that if positions, $X^*_{n-1} = (x^*_1, \ldots, x^*_{n-1})$, have been determined for the first (n-1) elements as a function of the position x_n, of the nth element, such that

$$\max_u E(X_n, u) = \max_u \left[1 + 2 \sum_{j=1}^{n} \cos 2\pi x_j u \right]$$

is minimum for each feasible value of x_n, then $x^*_{n-1}(x_n)$ will be an optimum placement for the first (n-1) elements as a function of the position of the nth element regardless of the positions of the remaining (N-n) elements. Theoretically, this assumption is not quite correct for this problem and the dynamic programming analysis only leads to approximate solutions.

Applying this concept, an approximation to the optimal design can be calculated recursively. Suppose (1+2 cos $2\pi x_1 u$) is calculated for all values of x_1 and u. Now consider a particular value for x_2. For this value of x_2, the optimal value of x_1, x^*_1, is determined by solving

$$f_2(x_2) = \min_{x_1} \left[\max_u \left(1 + 2 \sum_{j=1}^{2} \cos 2\pi x_j u \right) \right]$$

This calculation is carried out for each value of x_2. Thus, for each value of x_2, we now have an optimal value of x_1, $x^*_1(x_2)$.

Proceeding one step further, we consider a particular value for x_3 and then calculate the optimal value of x_2 associated with it by solving

$$f_3(x_3) = \min_{x_2} \left[\max_{u} (2 \cos 2\pi x_3 u + f_2(x_2, u) \right]$$

This computation is done for every x_3. Consequently, we have determined $x^*_2(x_3)$ and since $x^*_1(x_2)$ is known, we now have $X^*_2(x_3)$, $X^*_2 = (x^*_1, x^*_2)$.

The general recursion equation to determine $X^*_{n-1}(x_n)$, $n=2, \ldots, N$ is

$$f_n(x_n) = \min_{x_n} \left[\max_{u} 2 \cos 2\pi x_n u + f_{n-1}(x_{n-1}, u) \right]$$

$$n = 2, \ldots, N$$

with $f_1(x_1, u) = 1 + 2 \cos 2\pi x_1 u$.

It should be noted that using dynamic programming, we calculate the optimal values of the variables one at a time and recursively as a function of the next variable. A particular combination of the variable $(x_1, \ldots x_{n-1}, x_n)$ will only be considered if $(x_1, \ldots, x_{n-2})$ is optimal for some value of x_{n-1}. This can be contrasted with a total search procedure in which one must consider all possible combinations of the variables.

APPENDIX III

Symmetry in the Radiation Pattern

The radiation pattern of the unequally spaced array symmetrically located about the center element is

$$E(u) = 1 + 2 \sum_{n=1}^{N} \cos 2\pi x_n u$$

where x_n is measured in wavelengths. If the pattern is to be symmetrical about some value of $u = u_o$, then

$$E(u_o + \Delta u) = E(u_o - \Delta u)$$

thus we must have

$$\cos 2\pi x_n (u_o + \Delta u) = \cos 2\pi x_n (u_o - \Delta u)$$

Expanding the cosine term on each side of the equation gives

$$\cos 2\pi x_n u_o \cos 2\pi x_n \Delta u - \sin 2\pi x_n u_o \sin 2\pi x_n \Delta u$$

$$= \cos 2\pi x_n u_o \cos 2\pi x_n \Delta u + \sin 2\pi x_n u_o \sin 2\pi x_n \Delta u$$

The equality will hold if $\sin 2\pi x_n u_o = 0$, or if

$$2\pi x_n u_o = \pi, 2\pi, \ldots, k\pi$$

or

$$x_n u_o = \frac{1}{2}, 1, \frac{3}{2}, \ldots, \frac{k}{2}$$

This is satisfied if $u_o = 1$ and x_n is some multiple of $1/2$. Thus the pattern need only be examined from $0 < u < 1$ to determine the behavior over the region $-2 < u < 2$ when the element spacing is quantized in half-wave increments.

APPENDIX IV

An Upper Bound For The Sidelobes Of An Unequally Spaced Array

If an unequally spaced linear array is symmetric about its center and contains 2N + 1 equally fed elements (one a center element), the far field is proportional to the following expression

$$E(u) = 1 + 2 \sum_{n=1}^{N} \cos 2\pi \frac{d_n}{\lambda} u \qquad \text{(IV-1)}$$

where $u = \sin\theta - \sin\theta_o$, and d_n = distance of the nth element from the center of the array. The length of the array is then $2d_N$.

Equation IV-1 for E(u) may be rewritten as

$$E(u) = 1 + \sum_{n=1}^{N} \left[e^{2\pi i \frac{d_n}{\lambda} u} + e^{-2\pi i \frac{d_n}{\lambda} u} \right] \qquad \text{(IV-2)}$$

It follows that

$$|E(u)| \leq 1 + 2 \left| \sum_{n=1}^{N} e^{2\pi i \frac{d_n}{\lambda} u} \right| \qquad \text{(IV-3)}$$

In continuing a sequence of inequalities utilizing Equation IV-3, two lemmas will prove useful and are given below:

Lemma 1. Let f(x) be a real differentiable function in (a, b) where f'(x) is monotonic and $|f'(x)| < 1/2$. Then

$$\left| \sum_{a \leq n \leq b} e^{2\pi i f(n)} - \int_a^b e^{2\pi i f(x)} dx \right| < 1 + 3/\pi \qquad \text{(IV-4)}$$

Proof: Look at the function

$$\chi(x) = -1/\pi \sum_{\nu=1}^{\infty} \frac{\sin 2\nu\pi x}{\nu} \qquad \text{(IV-5)}$$

{$\chi(x) = x - [x] - 1/2$ if x is <u>not</u> an integer. The symbol [x] means the closest integer to x.}

Consider

$$2\pi i \int_a^b \chi(x)\, e^{2\pi i f(x)}\, f'(x)dx = -\sum_{\nu=1}^{\infty} \frac{2i}{\nu} \int_a^b \sin(2\nu\pi x)\, e^{2\pi i f(x)} f'(x)\, dx$$

$$= \frac{-1}{2\pi i} \sum_{\nu=1}^{\infty} \frac{1}{\nu} \int_a^b \left[\frac{f'(x)}{f'(x)+\nu} d\left(e^{2\pi i [f(x)+\nu x]}\right) - \frac{f'(x)}{f'(x)-\nu} d\left(e^{2\pi i [f(x)-\nu x]}\right) \right] \tag{IV-6}$$

Each of the functions $\frac{f'(x)}{f'(x) \pm \nu}$ is monotonic and does not exceed $1/(2\nu-1)$ in absolute value. From the second mean value theorem of calculus, it is possible to write

$$\left| \int F(x)\, G(x)\, dx \right| \leq F(b) \left[\max \int_{\bar{a}}^{\bar{b}} G(x)\, dx \right] \tag{IV-7}$$

where $(\bar{a}, \bar{b})$ is some subinterval, $F(x)$ is monotonic and bounded, and $G(x)$ is bounded. Using Equation IV-7 and IV-6

$$\left| 2\pi i \int_a^b \chi(x)\, e^{2\pi i f(x)}\, f'(x)\, dx \right| \leq \frac{1}{2\pi} \sum_{\nu=1}^{\infty} \frac{4}{\nu(2\nu-1)} \leq \frac{3}{\pi} \tag{IV-8}$$

since

$$\sum_{\nu=1}^{\infty} \frac{1}{\nu(2\nu-1)} = 1 + \sum_{\nu=2}^{\infty} \frac{1}{\nu(2\nu-1)} < 1 + \frac{1}{2} \sum_{\nu=2}^{\infty} \frac{1}{\nu(\nu-1)} = \frac{3}{2}$$

By using $\chi(x) = x - [x] - \frac{1}{2}$, the integral in Equation IV-6 may also be written exactly as

$$2\pi i \int_a^b \chi(x)\, e^{2\pi i f(x)}\, f'(x)\, dx = \sum_{n=a}^{b} e^{2\pi i f(n)} - \int_a^b e^{2\pi i f(x)} dx - \frac{1}{2}\left(e^{2\pi i f(b)} + e^{2\pi i f(a)}\right) \tag{IV-9}$$

Since $\left|\frac{1}{2}\left(e^{2\pi i f(b)} + e^{2\pi i f(a)}\right)\right| \leq 1$, Equation IV-8 and IV-9 may be combined to yield Lemma 1.

Lemma 2. Let f(x) and its first and second derivatives be continuous in (a, b), and $f''(x) \geq \gamma > 0$ (or ≤ 0) throughout (a, b).
Then

$$\left| \int_a^b e^{2\pi i f(x)} \, dx \right| < \frac{4}{\sqrt{\pi\gamma}} \qquad \text{(IV-10)}$$

Proof: Suppose $f'(c) = 0$ is the only zero of $f'(x)$ in (a, b). Then

$$\int_a^b e^{2\pi i f(x)} dx = \int_a^{c-\delta} \frac{d(e^{2\pi i f'(x)})}{2\pi i f'(x)} + \int_{c-\delta}^{c-\delta} e^{2\pi i f(x)} \, dx + \int_{c+\delta}^{b} \frac{d(e^{2\pi i f(x)})}{2\pi i f'(x)} \qquad \text{(IV-11)}$$

Employing Equation IV-7

$$\left| \int_a^b e^{2\pi i f(x)} \, dx \right| \leq \frac{1}{\pi \left| f'(c-\delta) \right|} + 2\delta + \frac{1}{\pi \left| f'(c+\delta) \right|} . \qquad \text{(IV-12)}$$

Since $|f'(c \pm \delta)| = \left| \int_c^{c \pm \delta} f''(x) \, dx \right|$, the following is true:

$$|f'(c \pm \delta)| > \delta\gamma \quad \text{or} \quad \left| \frac{1}{f'(c \pm \delta)} \right| < \frac{1}{\delta\gamma} .$$

Then

$$\left| \int_a^b e^{2\pi i f(x)} \, dx \right| < \frac{2}{\pi\delta\gamma} + 2\delta \qquad \text{(IV-13)}$$

To minimize the right side of Equation IV-13, set $\delta = \frac{1}{\sqrt{\pi\gamma}}$. Then

$$\left| \int_a^b e^{2\pi i f(x)} \, dx \right| < \frac{4}{\sqrt{\pi\gamma}} . \quad \text{(Lemma 2.)} \qquad \text{(IV-10)}$$

Using Lemmas 1 and 2, the following theorem, due originally to Van der Corput but modified here, is easily proved:

Theorem. Let f(x) be real and continuous and have continuous first and second derivatives. Furthermore, let f'(x) be monotonic and $f''(x) \geq \gamma$ (or $\leq -\gamma$ for $\gamma > 0$) throughout (a, b), then

$$\left| \sum_{a \le n \le b} e^{2\pi i f(n)} \right| < (2 + |f'(b) - f'(a)|)\left(1 + \frac{3}{\pi} + \frac{4}{\sqrt{\pi\gamma}}\right) \qquad \text{(IV-14)}$$

[If $\gamma \ge 1$, the result is not very good since $|f'(b) - f'(a)| = \int_a^b f''(x)dx \ge \gamma(b-a)$.]

Proof: Divide the range of variation of $f'(x)$ into intervals $\nu - \frac{1}{2} \le f'(x) < \nu + \frac{1}{2}$, where ν is an integer. Let (a_ν, b_ν) be the corresponding x-interval.

Then

$$\sum_{a_\nu \le n \le b_\nu} e^{2\pi i f(n)} = \sum_{a_\nu \le n \le b_\nu} e^{2\pi i [f(n) - \nu n]} \qquad \text{(IV-15)}$$

From Lemma 1,

$$\left| \sum_{a_\nu \le n \le b_\nu} e^{2\pi i g(n)} - \int_{a_\nu}^{b_\nu} e^{2\pi i g(x)} dx \right| < 1 + \frac{3}{\pi}$$

where $g(x) = f(x) - \nu x$. From this, one can write

$$\left| \sum_{a_\nu \le n \le b_\nu} e^{2\pi i g(n)} \right| < 1 + \frac{3}{\pi} + \left| \int_{a_\nu}^{b_\nu} e^{2\pi i g(x)} dx \right| \qquad \text{(IV-16)}$$

and from Lemma 2.

$$\left| \int_{a_\nu}^{b_\nu} e^{2\pi i g(x)} dx \right| < \frac{4}{\sqrt{\pi\gamma}} \qquad \text{(IV-17)}$$

where $f''(x) = g''(x) \ge \gamma > 0$ throughout (a_ν, b_ν).

Then

$$\left| \sum_{a_\nu \le n \le b_\nu} e^{2\pi i f(n)} \right| < 1 + \frac{3}{\pi} + \frac{4}{\sqrt{\pi\gamma}} \qquad \text{(IV-18)}$$

The number of intervals cannot be greater than $2 + |f'(b) - f'(a)|$, thus the theorem follows.

To apply Equation IV-14 to the case of the non-uniform array, let a = 1, b = N, or

$$|E(u)| \leq 1 + 2\,[2 + |f'(N) - f'(1)|]\,\left[1 + \frac{3}{\pi} + \frac{4}{\sqrt{\pi\gamma}}\right] \qquad \text{(IV-19)}$$

DISTRIBUTION LIST

	No. of Copies
RADC RALTM, Attn: Mr. Potenza Griffiss AFB, New York	3
RADC Attn: RAAPT Griffiss AFB, NY	1
RADC Attn: RAALD Griffiss AFB, NY	1
GEEIA Attn: ROZMCAT Griffiss AFB, NY	1
RADC Attn: RAIS. Mr. Malloy Griffiss AFB, NY	1
US Army Electronics R and D Labs Liaison Officer RADC Griffiss AFB, NY	1
AUL (3T) Maxwell AFB, Ala.	1
ASD Attn: ASAPRD Wright-Patterson AFB, Ohio	1
Chief, Naval Research Lab. Attn: Code 2027 Washington 25, DC	1
Air Force Field Representative Naval Research Lab. Attn: Code 1010 Washington 25, DC	1
Commanding Officer US Army Electronics R and D Labs Attn: SELRA/SL-ADT Ft. Monmouth, NJ	1
US Strike Command Attn: STRJ5-OR MacDill AFB, Florida	1

DISTRIBUTION LIST (Continued)

	No. of Copies
AFSC Attn: SCSE Andrews AFB Washington 25, DC	1
Commanding General US Army Electronics Proving Ground Attn: Technical Documents Library Ft. Huachuca, Arizona	1
ASTIA Attn: TISIA-2) Arlington Hall Station Arlington 12, Va.	10
Chief, Bureau of Ships Attn: Code 213 Main Navy Bldg. Washington 25, DC	1
AFPRO GE Co Lockland Br PO Box 91 Cincinnati 15, Ohio	1
Airborne Instruments Laboratory Dept. of Radar Systems Attn: L.K. DeSize Deer Park, LI, NY	1
Syracuse University Dept. of Electrical Engineering Attn: Dr. Cheng Syracuse 10, NY	1
AFSWC Attn: SWOI Kirtland AFB, N. Mex.	1
RADC Attn: RALSS, Mr. Diab Griffiss AFB, NY	1
RADC Attn: RAUER, Mr. Waters Griffiss AFB, NY	1
RADC Attn: RAWED, Mr. Blymiller Griffiss AFB, NY	1